



DTIC
ELECTE
JAN 05 1995
S G D

INVESTIGATION OF TENSION-COMPRESSION
FATIGUE BEHAVIOR OF A UNIDIRECTIONAL
METAL MATRIX COMPOSITE AT ELEVATED
TEMPERATURE

THESIS

Darren L. Kraabel, 2nd Lieutenant, USAF

AFIT/GAE/ENY/94D-6

19950103 011

DEPARTMENT OF THE AIR FORCE
AIR UNIVERSITY

AIR FORCE INSTITUTE OF TECHNOLOGY

Wright-Patterson Air Force Base, Ohio

DISTRIBUTION STATEMENT A

Approved for public release;

Accession For	
NTIS CRA&I	<input checked="" type="checkbox"/>
DTIC TAB	<input type="checkbox"/>
Unannounced	<input type="checkbox"/>
Justification _____	
By _____	
Distribution /	
Availability Codes	
Dist	Avail and/or Special
A-1	



INVESTIGATION OF TENSION-COMPRESSION
FATIGUE BEHAVIOR OF A UNIDIRECTIONAL
METAL MATRIX COMPOSITE AT ELEVATED
TEMPERATURE

THESIS

Darren L. Kraabel, 2nd Lieutenant, USAF

AFIT/GAE/ENY/94D-6

DTIC QUALITY INSPECTED 3

Approved for public release; distribution unlimited

REPORT DOCUMENTATION PAGE			Form Approved OMB No. 0704-0188	
Public reporting burden for this collection of information is estimated to average 1 hour per response, including the time for reviewing instructions, searching existing data sources, gathering and maintaining the data needed, and completing and reviewing the collection of information. Send comments regarding this burden estimate or any other aspect of this collection of information, including suggestions for reducing this burden, to Washington Headquarters Services, Directorate for Information Operations and Reports, 1215 Jefferson Davis Highway, Suite 1204, Arlington, VA 22202-4302, and to the Office of Management and Budget, Paperwork Reduction Project (0704-0188), Washington, DC 20503.				
1. AGENCY USE ONLY (Leave blank)		2. REPORT DATE December 1994		3. REPORT TYPE AND DATES COVERED Master's Thesis
4. TITLE AND SUBTITLE INVESTIGATION OF TENSION-COMPRESSION FATIGUE BEHAVIOR OF A UNIDIRECTIONAL METAL MATRIX COMPOSITE AT ELEVATED TEMPERATURE			5. FUNDING NUMBERS	
6. AUTHOR(S) 2nd LT Darren L. Kraabel				
7. PERFORMING ORGANIZATION NAME(S) AND ADDRESS(ES) Air Force Institute of Technology Wright-Patterson AFB, OH 45433-6583			8. PERFORMING ORGANIZATION REPORT NUMBER AFIT/GAE/ENY/94D-6	
9. SPONSORING/MONITORING AGENCY NAME(S) AND ADDRESS(ES) Dr. Walter Jones AFOSR/NA Wright-Patterson AFB, OH 45433			10. SPONSORING/MONITORING AGENCY REPORT NUMBER	
11. SUPPLEMENTARY NOTES				
12a. DISTRIBUTION/AVAILABILITY STATEMENT Approved for public release; distribution unlimited			12b. DISTRIBUTION CODE	
13. ABSTRACT (Maximum 200 words) This study investigated the fatigue behavior in a unidirectional metal matrix composite under tension-compression loading conditions. Stress-strain responses, modulus and strain trends were monitored to characterize damage. Fractography and microscopy were used to characterize failure modes. Fatigue life curves were plotted based on different parameters such as stress and strain. Tension-compression fatigue life was shorter than tha obtained under tension-tension fatigue cycling. Creep, observed in tension-tension fatigue cycling, and the effects of the compressive load on the plastic zone around the crack tip explain shorter life under tension-compression fatigue loading.				
14. SUBJECT TERMS metal matrix composite (MMC), creep, fiber bridging			15. NUMBER OF PAGES 99	
			16. PRICE CODE	
17. SECURITY CLASSIFICATION OF REPORT Unclassified	18. SECURITY CLASSIFICATION OF THIS PAGE Unclassified	19. SECURITY CLASSIFICATION OF ABSTRACT Unclassified	20. LIMITATION OF ABSTRACT UL	

INVESTIGATION OF TENSION-COMPRESSION FATIGUE BEHAVIOR IN A
UNIDIRECTIONAL METAL MATRIX COMPOSITE AT ELEVATED
TEMPERATURE

THESIS

Presented to the Faculty of the School of Engineering
of the Air Force Institute of Technology

Air University

In Partial Fulfillment of the
Requirements for the Degree of
Master of Science in Aeronautical Engineering

Darren L. Kraabel, B.S.

Second Lieutenant, USAF

December, 1994

Approved for public release; distribution unlimited

Acknowledgements

Many people aided me in completion of this project. First and foremost I would like to thank my wife, Diane, who encouraged and supported me throughout all of my research. None of this research would have been possible without the guidance of my advisor, Dr. Shankar Mall and the frequent consultations of Dr. Brian Sanders. I would also like to thank Dr. Walter Jones, AFOSR/NA, for sponsoring this research. Many thanks go out to the AFIT lab technicians, especially Mr. Mark Derisso, for having the patience to teach and demonstrate many of the techniques I employed in my research and a great sense of humor to ease my frustrations. To the guys over at the Met Lab, thanks for all the guidance and helpful hints. If it wasn't for you, I would still be polishing those dogbone specimens.

Table of Contents

ACKNOWLEDGEMENTS.....	ii
LIST OF FIGURES	v
LIST OF TABLES	viii
ABSTRACT	ix
1. INTRODUCTION.....	1
2. PREVIOUS WORKS.....	5
2.1 FUNDAMENTALS OF MACRO-MECHANICAL BEHAVIOR	5
2.2 FUNDAMENTALS OF MICRO-MECHANICAL BEHAVIOR.....	8
2.3 PREVIOUS WORKS	11
2.3.1 Tension-Tension Tests.....	11
2.3.2 Tension-Compression Tests.....	14
2.3.3 Analysis Tools	15
3. EXPERIMENTAL SET-UP AND PROCEDURE	17
3.1 MATERIAL.....	17
3.2 SPECIMEN DESIGN & PREPARATION	18
3.3 TEST SETUP	20
3.3.1 Buckling Guide Design.....	22
3.4 TESTS/PROCEDURES	23
3.4.1 Edge Replicas.....	25
3.5 POST-FAILURE ANALYSIS.....	25
4. RESULTS AND DISCUSSION.....	27
4.1 OVERVIEW OF TEST DATA	27

4.2 FREQUENCY EFFECTS	29
4.3 MACRO-MECHANICAL BEHAVIOR.....	30
4.3.1 Group 1 Data.....	31
4.3.2 Group 2 Data	33
4.3.3 Group 3 Data	38
4.3.4 Tension-Tension Test Data	39
4.3.5 Summary of Macro-mechanical Behavior	45
4.4 MICRO-MECHANICAL BEHAVIOR.....	46
4.4.1 Fracture Surfaces.....	47
4.4.2 Specimen Sectioning.....	54
4.4.3 Matrix Plasticity.....	62
4.4.4 Summary of Micro-mechanical Behavior	63
5. FATIGUE LIFE.....	65
5.1 TENSION-COMPRESSION FATIGUE LIFE.....	65
5.2 TC VS. TT FATIGUE LIFE COMPARISON	66
5.2.1 Maximum Stress/Strain Basis.....	67
5.2.2 Stress/Strain Range Basis	70
5.3 [0] ₈ VS. [0/90] _{2s} FATIGUE LIFE COMPARISON	71
5.4 0° FIBER STRESS ANALYSIS.....	72
5.5 0° PLY STRESS ANALYSIS	76
6. CONCLUSIONS.....	78
APPENDIX A: LISOL ANALYSIS.....	82
0° FIBER STRESS RESULTS	82
MATRIX STRESS RESULTS.....	83
7. BIBLIOGRAPHY.....	85

List of Figures

FIGURE 1. TENSION-TENSION LOAD-TIME RELATIONSHIP, $R=0.1$	3
FIGURE 2. TENSION-COMPRESSION LOAD-TIME RELATIONSHIP, $R=-1$	3
FIGURE 3. BOYUM'S MODEL FOR REGIMES OF CROSS-PLY LAMINATE S-N CURVE	7
FIGURE 4. SANDERS' MODEL FOR REGIMES OF $[0]_8$ LAMINATE	7
FIGURE 5. DAMAGE MECHANISMS	9
FIGURE 6. REPRESENTATIVE UNIT CELL	16
FIGURE 7. UNIDIRECTIONAL METAL MATRIX COMPOSITE $[0]_8$	18
FIGURE 8. DOGBONE SPECIMEN GEOMETRY	19
FIGURE 9. TEST SETUP.....	21
FIGURE 10. BUCKLING GUIDE MODIFICATIONS	23
FIGURE 11. EXCESSIVE BUCKLING.....	24
FIGURE 12. SPECIMEN SECTIONING.....	26
FIGURE 13. INITIAL STRESS-STRAIN CURVE, 800 MPA.....	29
FIGURE 14. GROUP 1 NORMALIZED MODULUS TRENDS.....	31
FIGURE 15. GROUP 1 STRAIN TRENDS	33
FIGURE 16. GROUP 2 NORMALIZED MODULUS TRENDS.....	34
FIGURE 17. GROUP 2 MODULUS TRENDS.....	35
FIGURE 18. GROUP 2 STRAIN TRENDS	36
FIGURE 19. MODULUS, STRAIN RANGE DATA FOR 625 MPA, $T=427^{\circ}\text{C}$	37
FIGURE 20. STRESS-STRAIN RESPONSE AT 625 MPA, $T=427^{\circ}\text{C}$	37
FIGURE 21. MODULUS VS FATIGUE LIFE FOR GROUP 3 TESTS.....	38
FIGURE 22. GROUP 3 STRAIN TRENDS	39
FIGURE 23. NORMALIZED MODULUS VS FATIGUE LIFE	41
FIGURE 24. MAX, MIN AND AVG STRAIN, TT HT.....	42
FIGURE 25. TT HT STRAIN TRENDS (LINEAR SCALE)	42
FIGURE 26. MODULUS AND STRAIN RANGE, 800 MPA, TT HT	43

FIGURE 27. TT VS. TC STRAIN TRENDS, 427 ° C	44
FIGURE 28. FRACTURE SURFACE AT 800 MPA, TC HT	48
FIGURE 29. FRACTURE SURFACE AT 700 MPA, TC HT	48
FIGURE 30. FRACTURE SURFACE AT 625 MPA, TC HT	49
FIGURE 31. FRACTURE SURFACE AT 425 MPA, TC HT	49
FIGURE 32. MATRIX NECKING, 800 MPA, TC HT	50
FIGURE 33. DUCTILE VOID COALESCENCE, 800 MPA, TC HT	51
FIGURE 34. FATIGUE STRIATIONS, INTACT FIBERS, 700 MPA, TC HT	52
FIGURE 35. FATIGUE STRIATIONS, 425 MPA, TC HT	53
FIGURE 36. FRACTURE SURFACE, 800 MPA, TT HT	54
FIGURE 37. MATRIX AND FIBER CRACKING, 800 MPA, TC HT	55
FIGURE 38. 625 MPA FIBER BRIDGING	56
FIGURE 39. 500 MPA FIBER BRIDGING, TC HT	57
FIGURE 40. 425 MPA FIBER BRIDGING AND MOLYWEAVE	57
FIGURE 41. EDGE CRACK INITIATION, 625 MPA, TC HT	58
FIGURE 42. CRACK INITIATION WITHIN SPECIMEN, 500 MPA, TC HT	59
FIGURE 43. TRANSGRANULAR CRACK GROWTH, 425 MPA, TC HT	60
FIGURE 44. SLIP BANDS AROUND CRACK, 425 MPA, TC HT	60
FIGURE 45. FACE SECTION, 375 MPA, TC HT	61
FIGURE 46. FIBER FRACTURE, 800 MPA, TT HT	62
FIGURE 47. ETCHED FACE SPECIMEN, 800 MPA	63
FIGURE 48. $[0]_8$ TENSION-COMPRESSION FATIGUE LIFE CURVE	66
FIGURE 49. MAXIMUM STRESS FATIGUE LIFE CURVE	69
FIGURE 50. MAXIMUM STRAIN FATIGUE LIFE CURVE	69
FIGURE 51. STRESS RANGE FATIGUE LIFE CURVE	70
FIGURE 52. STRAIN RANGE FATIGUE LIFE CURVE	71
FIGURE 53. $[0]_8$ VS. $[0/90]_{2s}$ FATIGUE LIFE COMPARISON	72

FIGURE 54. 0° FIBER STRESS FATIUGE LIFE CURVE, R = 0.1 (29)	73
FIGURE 55. 0° FIBER STRESS FATIGUE LIFE CURVE, R = -1	74
FIGURE 56. MAXIMUM 0° FIBER STRESS FATIGUE LIFE CURVE, R = -1.....	75
FIGURE 56. 0° PLY STRESS FATIGUE LIFE CURVE.....	76
FIGURE 57. 0° FIBER STRESS CORRELATION BETWEEN LISOL AND APPROXIMATE VALUES.....	83

List of Tables

TABLE 1. FIBER AND MATRIX PROPERTIES	17
TABLE 2. TC HT MATERIAL DATA.....	28
TABLE 3. LISOL FIBER STRESS CALCULATIONS.....	83
TABLE 4. LISOL MATRIX STRESSES	84

Abstract

The fatigue characteristics of a unidirectional, [0]_s, metal matrix composite (MMC), SCS-6/Ti-15-3, were investigated under tension-compression (TC) fatigue at elevated temperature. Several fatigue tests were conducted at various load levels to establish fatigue life diagrams (S-N curves). Stress-strain data was used to evaluate the macro-mechanic behavior of the material and microscopic evaluation was performed to characterize the damage on a micro-mechanic level. Also, some high temperature tension-tension fatigue tests were performed to compare damage mechanisms and fatigue lives with that of similar specimens tested at 427 °C under tension-compression loading conditions.

This investigation shows that the fatigue life diagram for the unidirectional metal matrix composite studied can be broken up into three regions based on the observed failure mechanisms. Region I is dominated by fiber failure with very little matrix cracking. Region II contains matrix cracking, fiber bridging and minimal fiber cracking. Region III contains specimens that fall below the fatigue limit of the matrix material resulting in fatigue lives greater than one million cycles.

Based on maximum stress or maximum strain, the fatigue life under fully-reversed, tension-compression cycling is less than that for fatigue loading under tension-tension cycling. But when compared on the basis of stress or strain range, the tension-compression fatigue life actually increases, exceeding that obtained under tension-tension loading conditions.

INVESTIGATION OF TENSION-COMPRESSION FATIGUE BEHAVIOR OF A UNIDIRECTIONAL METAL MATRIX COMPOSITE AT ELEVATED TEMPERATURE

1. Introduction

Advances in aircraft technology have increased the demand for lightweight materials that exhibit high stiffness and strength at elevated temperatures. The monolithic alloys previously used for these applications cannot meet the stiffness and strength requirements, especially at high temperatures. Thus, new materials must be employed. Metal matrix composites (MMCs), metal alloys reinforced with ceramic fibers, are the latest class of materials showing the potential to satisfy these demands.

MMCs exhibit high stiffness and strength as well as good toughness and impact properties. They also maintain good properties at elevated temperature and resist thermal shock. Additionally, their sensitivity to surface flaws is greatly diminished when compared to monolithic alloys (39:3). These qualities make MMCs the leading candidates for future aircraft applications. One particular MMC, a titanium alloy reinforced with silicon carbide fibers (SCS-6/Ti-15-3), is the focus of this research because it is a good model material in titanium matrix composites, and has been used extensively in previous studies.

Before MMCs can be used in real applications, the deformation and failure mechanisms in the environment in which the MMC will operate must be fully characterized. For aircraft applications, this routinely includes fatigue loading. Aircraft

wings are constantly subjected to fatigue due to the bending moments caused by changes in lift and gravitational forces encountered in aircraft maneuvers. These fatigue loads sometimes include compressive loads. For example, cracks were found in an F-15 at the inboard end of the intermediate spar (31:243). Since the maximum tensile loads were only 26% of the maximum compressive loads, the structure was thought to be resistant to fatigue cracking. But the compressive loads exceeded the compressive yield limit and caused residual tensile stresses after unloading. Fatigue cracks were detected after only 1000-1500 hours of operation. Future aircraft will be expected to fly and maneuver faster. These increased performance standards will create larger forces and higher temperatures applied to the wings. Thus, the need for the characterization of MMCs under fatigue loading, which includes fully-reversed cycling, at elevated temperatures is essential for future aircraft design.

While MMCs have been characterized for both monotonic tension and compression loading conditions (20,23), very little is known about their response to fatigue loading. Also, most published metals fatigue data is based on fully-reversed loading (3:9). It is therefore necessary to obtain similar fatigue data for MMCs.

Some research has been conducted in the area of tension-tension fatigue loading of MMCs (6,9,11,18,21,22,25,26,33), but there is an extreme lack of research in the area of tension-compression fatigue loading. The MMC laminates available are usually thin, i.e. about 3 mm (8 plies). The inability to prevent excessive buckling while forcing the thin specimen from these laminates to fail in the gage length has long been the cause for this lack of research. However, recent developments in specimen geometry and the design of a buckling guide (4) have opened the door for research in this direction.

This research investigates the behavior of the [0]8, unidirectional laminate of SCS-6/Ti-15-3, MMC in tension-compression fatigue loading. High temperature (427 °C), fully reversed, load controlled fatigue tests (TC HT) were performed to obtain fatigue life data. Tension-tension fatigue tests (TT HT) at 427 °C were also performed to verify testing techniques and material properties. Tests were performed at a frequency of 10 Hz, with the exception of the high stress tests which were conducted at 1 Hz. The tension-compression tests had a load ratio (minimum load/maximum load) of $R=-1$, while $R=0.1$ for the tension-tension tests. These load-time relationships are shown in Figures 1 and 2.

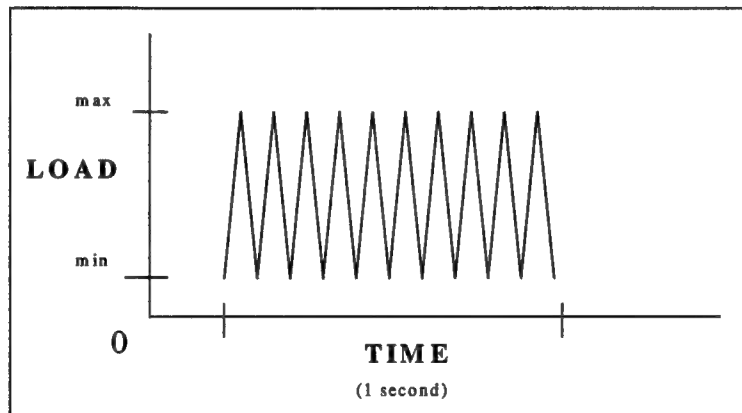


Figure 1. Tension-Tension Load-Time Relationship, $R=0.1$

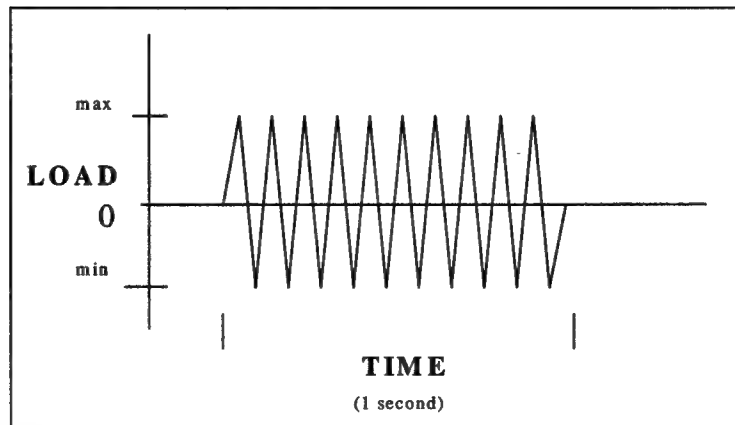


Figure 2. Tension-Compression Load-Time Relationship, $R=-1$

Eight tests at several load levels were performed under TC HT conditions. For each case, edge replicas were periodically taken to document the progression of damage. Stress range and strain range data, as well as the modulus, were plotted against fatigue cycles for each specimen. Fatigue life diagrams were developed for tension-compression fatigue testing based on either maximum value or range value of both applied stress and strain.

Two high temperature tension-tension tests were performed at different stress levels. Additionally, a monotonic tension test was performed at high temperature (427 °C). Similar data analysis was conducted as for the fully-reversed tests described above.

Micromechanical behavior was analyzed through microscopic examination of edge replicas, the specimen edge and fracture surfaces, and specimen sectioning. The specimen sections were also etched which enabled observation of plastic deformation, if present. This combined approach involving macro-mechanical and micro-mechanical evaluation provided the complete picture of the fatigue behavior of a unidirectional metal matrix composite subjected to fully-reversed tension-compression cycling.

2. Previous Work

In order to fully understand the material presented in this study, it is necessary to have an understanding of the fundamentals of macro-mechanical and micro-mechanical behavior. This chapter briefly reviews some important fundamentals that are pertinent to this study. This chapter also outlines previous works concerning characterization of MMCs under fatigue loading conditions that form the basis upon which the current study can be conducted. A brief summary of these works is important to understand the direction of the current research as well as appreciate any results. The previous works are separated into three sections: tension-tension and tension-compression fatigue loading and analysis.

2.1 Fundamentals of Macro-mechanical Behavior

The macro-mechanical behavior of the unidirectional composite includes the fatigue life, modulus degradation, and strain response. The fatigue life is often characterized by the Wholer, or S-N, diagram where the applied maximum stress or stress range is plotted against the number of cycles throughout the life of the material. For all materials, to include ploymers, homogenous metals, and composites, the slope of the S-N curve is negative, i.e. the fatigue life decreases as the applied stress or stress range increases (1:297). Factors which influence this trend for composite materials include ply orientation, loading type, mean stress, environment, fiber volume fraction, and interface properties. In this study, two of these factors have been altered; loading type and mean

stress. The loading type varied between tension-compression and tension-tension (Figures 1 and 2), thereby also altering the mean stress. During tension-compression testing, the mean stress is 0 while it depends on a positive load ratio (R) for the tension-tension loading condition. For the tension-tension tests in this study, $R=0.1$. While all of these factors do influence the fatigue life of the material in this study, frequency does not at this temperature. Discussion of the effects of frequency is found in Appendix A.

For composite materials, fatigue life diagrams are often broken into regimes consisting of varying failure mechanisms. Following Taljera's approach (38), many researchers have broken the fatigue life of a MMC into three distinct regimes: Regime 1, 2 and 3. Specifically, Majumdar and Lerch have separated the S-N curve for the unidirectional SCS-6/Ti-15-3 laminate, tested in tension-tension at an R-ratio of 0.1, into Regime 1, which is dominated by fiber failure, Regime 2, which is dominated by matrix failure, and Regime 3, which consists of specimens that did not fail and fall below the fatigue limit of the material (21). Between these regimes, the authors found the failure modes to be complex, consisting of combinations of failure modes. Boyum, who tested a cross-ply laminate under tension-compression conditions, elaborated upon Taljera's approach by breaking Regime 2 into two separate qualitative regimes, Regime 2a and Regime 2 (4). In Regime 2a, the higher range of applied stress, failure was caused by a combination of fiber and matrix cracking while Regime 2 consisted solely of matrix cracking. Boyum's regimes are shown in Figure 3.

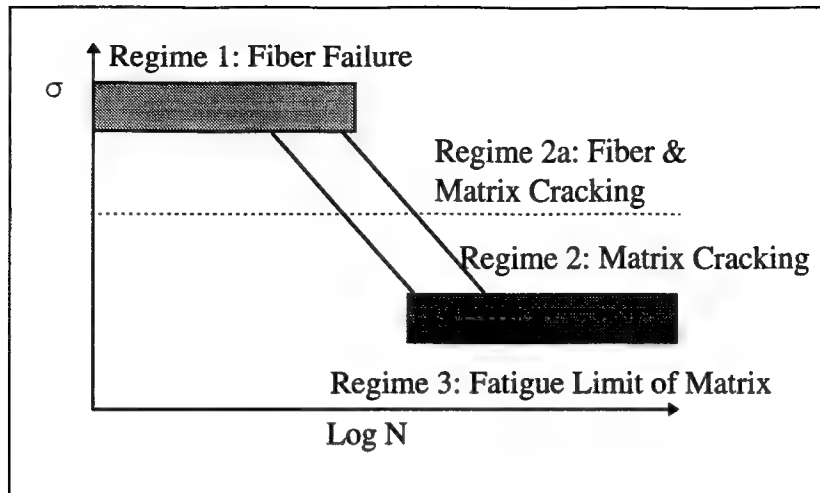


Figure 3. Boyum's Model for Regimes of Cross-Ply Laminate S-N Curve

The macroscopic response of a composite can also be separated into regions defining various behavior. Sanders analyzed fatigue life data for strain-controlled fatigue by breaking the σ - ϵ response over time into two stages (32). Stage I is dominated by matrix creep and can be broken into two sub-stages, Ia and Ib. Stage Ia consists of creep deformation of the matrix resulting in a relaxation of the lamina stress. Stage Ib represents the region where the maximum applied stress remains constant. Stage II is defined by a reduction in the maximum stress. These stages are schematically shown in Figure 4.

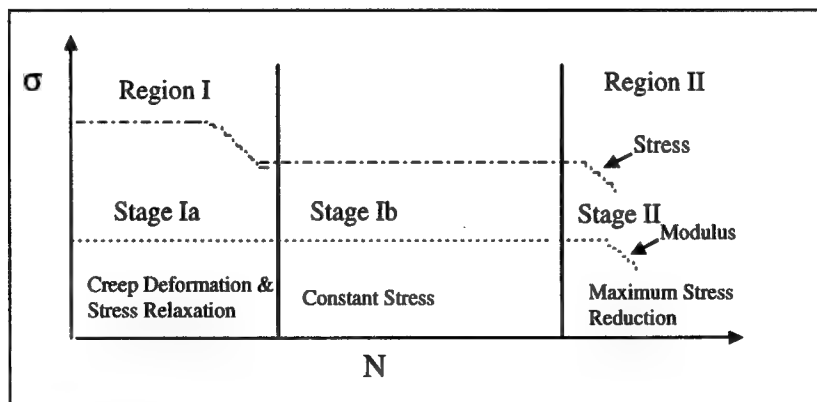


Figure 4. Sanders' Model for Regimes of $[0]_8$ Laminate

In addition to fatigue life, the macro-mechanical behavior of a failed specimen can be based on modulus degradation. Modulus (E), or stiffness, is defined as the slope of the elastic stress-strain curve. Analytically, it is represented by the equation shown below.

$$E = \frac{\sigma}{\epsilon_{elastic}} \quad (1)$$

Since the applied stress remains constant for load control testing conditions, any change in modulus results in a change in strain. As the number of cycles increase, damage occurs resulting in an increase in strain range. The nature of this damage may be debonding, matrix and /or fiber cracking or matrix plasticity. Although fatigue life and modulus degradation are strong indicators that damage has occurred, the exact nature of the damage can only be determined by micro-mechanical analysis.

2.2 Fundamentals of Micro-mechanical Behavior

Micro-mechanical analysis in the current study is broken into two separate groups, damage and plasticity. Damage mechanisms include matrix cracks, fiber breaks, and fiber-matrix debonding. Plasticity includes slip band formation, crack nucleation and fatigue striations, which are similar to slip bands. The type of damage in each specimen is dependent upon the applied stress level. Figure 5 illustrates the damage mechanisms as they pertain to a unidirectional laminate.

Damage is defined by the creation of new free surfaces from fiber and matrix crack growth. Cracks may originate within the fiber and matrix itself or they may originate from fiber-matrix interfaces. Fiber cracks may cause debonding between the fiber and matrix. This debonding prevents the fibers from transferring any load to the

matrix. Debonding may also occur from low interface strength caused by poor material processing. Debonding of this nature provides numerous crack initiation sites within the matrix. The two types of debonding are important in determining what causes failure. Extreme necking around fibers shows a great deal of debonding which is caused by fiber overload, i.e. fiber cracks. Debonding that shows less necking indicates destruction of the fiber-matrix interface due to low interface strength. Matrix cracks are likely to originate from this region whereas fiber cracks may be nonexistent.

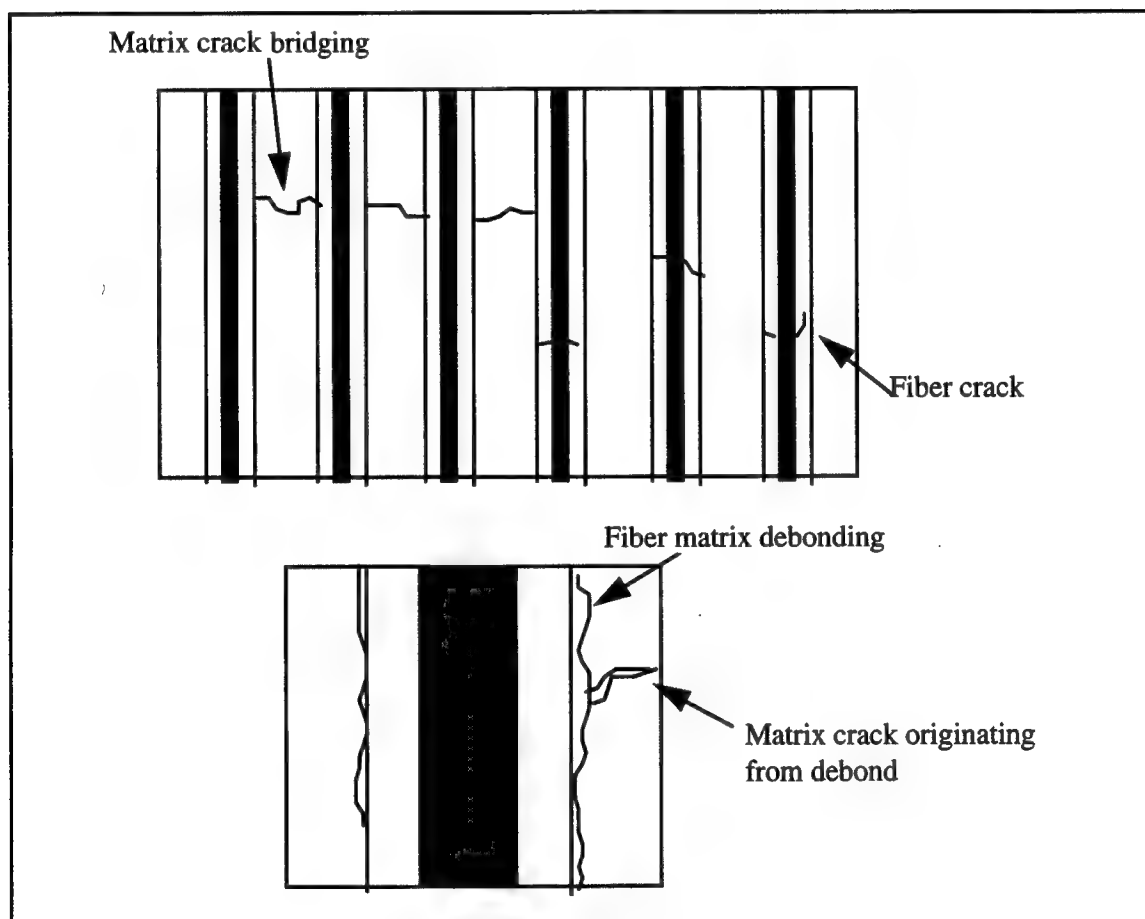


Figure 5. Damage Mechanisms

Plasticity includes the formation of slip bands and fatigue striations as well as microvoid coalescence. Slip bands are caused by deformation of atoms along closely-packed crystallographic planes called slip planes (7:13-55). The ridges or steps formed by slip bands are seen as parallel lines on the surface and remain after unloading. Slip bands created by fatigue are called fatigue striations. The striations run parallel to the crack growth direction, thereby indicating where cracks originated and in what direction they were moving (12:530-537). Each striation represents the incremental advance of the crack front as a result of one cycle. The extent of the advancement varies with stress range, i.e. higher stress ranges result in larger spaces between striations.

Microvoid coalescence also indicates plastic behavior (12:254-257). Furthermore, it indicates ductile failure. This behavior is most easily found in regions containing high concentrations of matrix necking. Microvoid coalescence appears as a dull, dimpled surface and is caused by necking of the matrix material around tiny voids created in material processing (12:257-258).

In composite materials, the damage mechanisms and plastic behavior may be interdependent. Pre-existing matrix cracks will result in the plastic deformation of the material just ahead of the crack tip, thereby creating slip bands or fatigue striations. Alternatively, the formation of slip bands in composites may cause cracks. Debonding may also lead to the formation of matrix cracks. In strong, complex alloys, planar slip is prevalent and surface nucleation of cracks by slip processes is retarded. In these materials, the stress concentration produced by the interaction between slip bands and second phase particles, i.e. inclusions or precipitates, can crack or debond the particle and

produce internal fatigue cracks (36:141). Similar behavior may be expected in a MMC, treating the fibers as the interspersed precipitate. Hence, debonding between the fiber and matrix may cause internal cracks. This will be shown later in the discussion of the micro-mechanic behavior of the tested material.

2.3 Previous Work

2.3.1 Tension-Tension Tests

Johnson, Mirdamadi and Bakuckas investigated $[0]_8$, $[0_2/\pm 45]_s$, $[0/90]_s$, $[0/90/0]$, and $[0/\pm 45/90]_s$ SCS-6/Ti-15-3 laminates under tension-tension load-controlled fatigue mode at room temperature (15). They noticed that laminates containing off-axis plies lost stiffness very early in the fatigue life due to the fiber/matrix interface failure. After a few cycles, the stiffness stabilized and the strain range was obtained. The strain range and fiber modulus were used to determine the unidirectional fiber stress. They found that when compared on a maximum stress basis, the fatigue life decreased as the number of unidirectional fibers decreased (i.e. $[0]_8 > [0/90]_s > [0_2/\pm 45]_s$). A comparison of fatigue life based on stress within the unidirectional fibers showed that the data collapsed onto a single S-N curve.

In the same study, the authors conducted the same tests at 650 °C. For high maximum strains, damage initiated in the fibers and the composite exhibited a shorter fatigue life than the Ti-15-3 matrix alone. For low strains, damage initiated in the matrix and the composite had a longer fatigue life than the matrix material alone. This

comparison enables us to predict strain levels at which matrix cracking will precede fiber breaks and when fiber breaks will precede matrix cracking.

Majumdar and Newaz investigated the fatigue response of a $[0]_8$ SCS-6/Ti-15-3 laminate at room temperature and at 538 °C (22). Three different fiber volume fraction laminates were tested (41, 35, and 15%). Data from these tests showed that strain range controls the fatigue life of MMCs in Regime II (Figure), the matrix dominated failure region. It is well established that the fatigue life of metals are strain-range dependent: thus, the analysis included a search for classical fatigue mechanisms in tests falling within Regime II. The observation of persistent slip bands and matrix crack growth led to the conclusion that such fatigue mechanisms are present in Regime II. It was also determined that reaction zone cracks are important crack initiation sites and allow slip bands to form more easily.

At high maximum strains, the dominant failure mode was observed to be fiber failure caused by fiber-matrix debonding. This debonding leads to rubbing induced damage of the fibers. Matrix cracking was not observed at high strain ranges. Also noted is that the fatigue life is affected by the fiber volume fraction. Low fiber volume fractions may lead to early fiber failure.

Pollock and Johnson characterized unnotched SCS-6/Ti-15-3 MMCs at 650 °C (29). Four different laminates were considered, all of which contained 0° plies. All tests were conducted under load control at a frequency of 10 Hz and a load ratio of 0.1. Evidence of the time-dependent deformation of the matrix material was produced by heating a specimen of matrix material to various temperatures and holding for one hour.

Up to 480 °C, no time-dependent deformation was observed. At 650 °C, however, the specimen continued to deform well past the one hour holding period. Thus, any analytical model wishing to predict fatigue life at 650 °C must account for this behavior.

Of all the laminates tested, the $[0]_8$ laminate had the longest fatigue life.

Fractography revealed that failure in high strain tests was again caused by fiber failure and at low strains, failure was caused by matrix cracking. The data from these tests were plotted against room temperature data obtained from other sources. It was noted that the strain range decreased at high temperatures during the first 10 cycles and then stabilized. This is opposite of the room temperature results. Also, the high temperature data is more scattered when compared on a stress range basis, but when compared on a strain range basis, there was no significant difference in fatigue life between room and elevated temperature. The explanation stems from monotonic tension tests conducted by Bhatt on free fibers, i.e. fibers not bonded by a matrix material. Bhatt showed that fiber strength is not affected by temperature up to 1100 °C. This study once again indicates that stress in the 0° fibers may be the controlling factor in fatigue life.

Bhatt also examined the matrix material in monotonic tension tests. These tests revealed that the matrix material is extremely weak at elevated temperature. Thus, fiber strength contributes more to monotonic strength and fatigue endurance of the laminate at elevated temperatures than at room temperature.

Sanders and Mall investigated a unidirectional SCS-6/Ti-15-3 laminate with 36% fiber volume fraction at 427 °C (33). Test specimens were heat treated at 700 °C for 24 hours to stabilize the microstructure of the matrix material. All experiments were

conducted under strain-controlled conditions. Such a loading condition requires that a compressive load be introduced to the specimen to bring the residual strain back to zero. Efforts to use a buckling guide resulted in specimen failure at the grips of the testing machine. Thus, a hybrid strain-controlled program was developed. This program increased to minimum strain when the load reached zero, thereby preventing the specimen from buckling under a compressive load.

In the fiber dominated failure region, modulus remained constant throughout the fatigue life while the maximum stress dropped slightly. It was verified that matrix creep during cycling caused the drop in maximum stress. The stress-strain response was separated into three segments: Stages Ia, Ib, and II. As a whole, Stage I was dominated by matrix creep. In segment Ia, matrix creep deformation resulted in a relaxation of the lamina stress while the modulus remained constant. In segment Ib, the maximum stress remained constant since matrix creep in tension was exactly balanced by that occurring in compression. Stage II revealed a reduction in maximum stress and modulus which indicates matrix cracking.

2.3.2 Tension-Compression Tests

Lerch, Verrilli, and Halford conducted fully-reversed, strain-controlled fatigue tests on a $[\pm 30]_{8s}$ titanium metal matrix composite at 427 °C (19). Load-controlled, zero-tension ($R = 0.05$) fatigue tests were performed as well. The thick plate material, 32 plies, allowed compression without causing buckling. Fully reversed tests had longer fatigue lives based on strain range than zero-tension tests. For a given strain range, the

fully-reversed fatigue lives were comparable to, but slightly less than, that observed in the matrix alone. Damage mechanisms were limited to long, isolated matrix cracks.

Boyum investigated a cross-ply SCS-6/Ti-15-3 laminate under tension-compression (TC) loading conditions (4). The study included data from room temperature tests and an elevated temperature of 427 °C. Development of the AFIT buckling guide and the dogbone specimen enabled the completion of the first fully-reversed load-controlled fatigue test. Also, some tension-tension (TT) tests, $R=0.1$, were conducted at room temperature. The results indicate that when based on a maximum stress basis, the TC fatigue life was less than the TT fatigue life. The decrease in fatigue life is caused by additional damage and plasticity sites created by the loading conditions. On a stress range basis, however, the life of the TC specimen increased compared to the TT specimen. The cause of the extended life is related to the mean tensile stress associated with a tension-tension test where $R=0.1$.

Comparison of room temperature data and data from tests conducted at 427 °C yielded some interesting results. For the fiber dominated failure region, fatigue life was generally identical, but in Regime II, the fatigue life at 427 °C was actually longer than at room temperature. The cause of the increased fatigue life is the increased ductility of the fiber-matrix reaction zone which delayed the onset of matrix cracking.

2.3.3 Analysis Tools

There are several micro-mechanically-based tools available for predicting fiber and matrix stress (METCAN, VISCOPLY, LISOL) under a variety of loading conditions. The computer program, LISOL, developed by Robertson and Mall (32), is based on the

tenet that classical laminated plate (CLP) theory assumptions on the strain variation apply to the non-linear laminate formulation. It also incorporates a unified viscoplastic theory for the inelastic matrix behavior. This theory is based on combining plastic and viscoplastic strain into a single term. The advantages of this model over others is that it more closely models laminates containing off-axis plies. All calculations are made using the unit cell as illustrated in Figure 6. This cell models one quarter of the fiber and surrounding matrix, employing symmetry and equivalent boundary conditions.

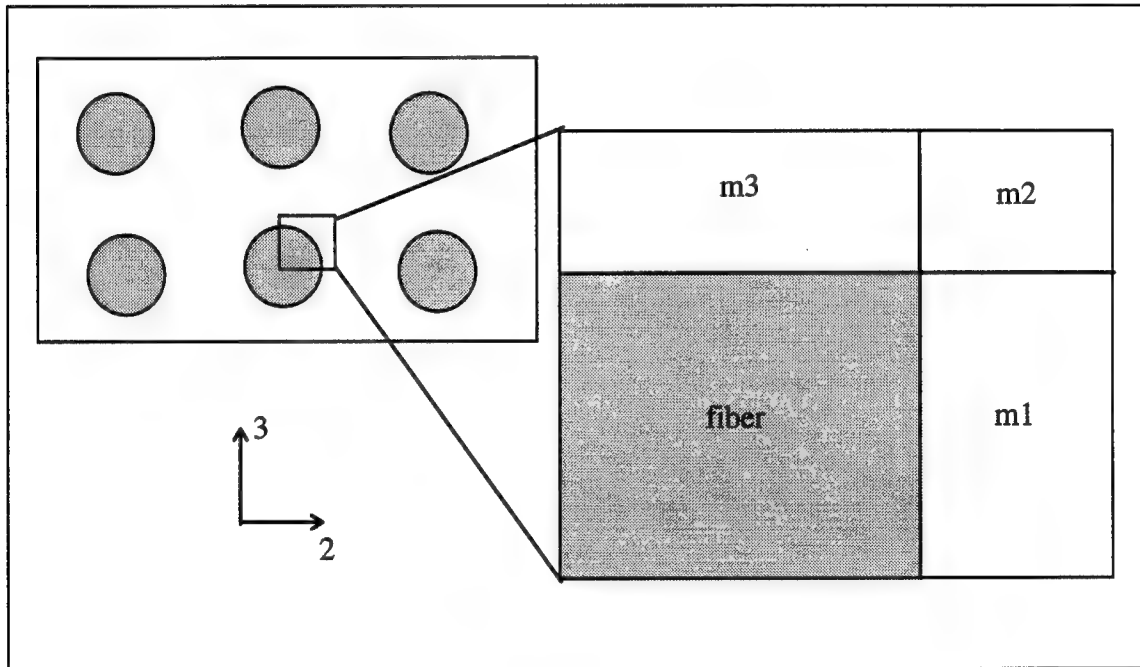


Figure 6. Representative Unit Cell

3. Experimental Set-up and Procedure

An essential part of any experimental research is a complete understanding of how the study was conducted. This chapter describes the equipment and procedures used to gather and analyze the data in this study. Descriptions of the material, test specimen design and specimen preparation are included.

3.1 Material

The material investigated in this study is SCS-6/Ti-15-3, a fiber reinforced, unidirectional metal matrix composite (Figure 7). The fiber volume fraction is 36%. Table 1 contains the fiber and matrix properties. Silicon carbide fibers, SCS-6, are embedded within a titanium matrix to provide increased strength in only the fiber direction. The panel used in this study was fabricated by Textron Specialty Materials Inc. using their patented Hot ISO static pressing (HIP) method. The fiber layers are held together with a molybdenum weave, that is woven through, and perpendicular to the fibers. The matrix layers are thin, cold-rolled sheets of titanium foil. After the fibers and sheets are properly arranged, the system is heated to a temperature of approximately 815 °C and held there at a pressure of 35 MPa.

Table 1. Fiber and Matrix Properties at Room Temperature

	Fiber	Matrix
E (GPa)	400	82
α (10^{-6} mm/mm/C)	4.9	10
ν	0.25	0.36
σ_{ult} (MPa)	3550	865
σ_{ys} (MPa)	-	865

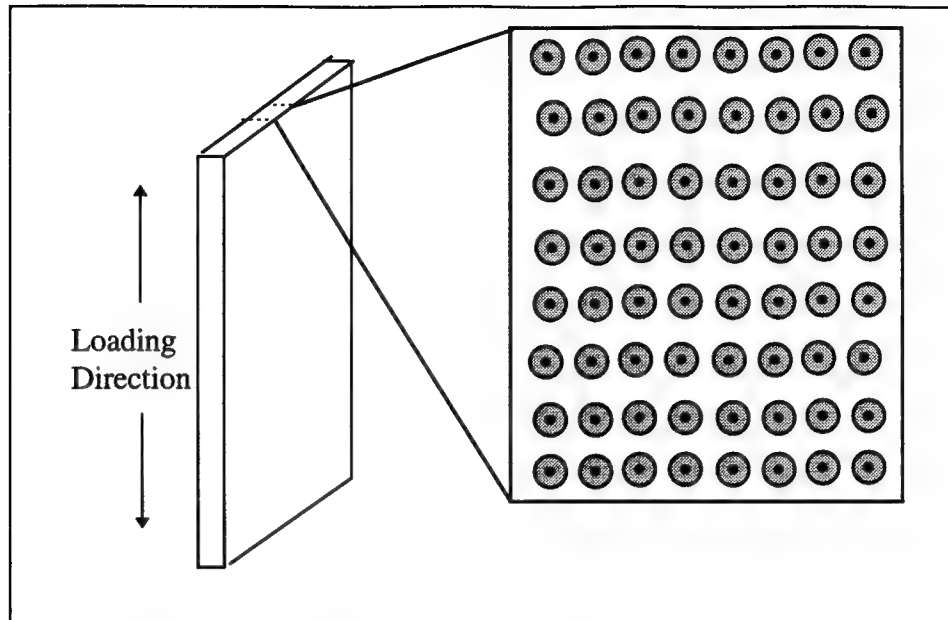


Figure 7. Unidirectional Metal Matrix Composite [0]₈

3.2 Specimen Design & Preparation

A dogbone specimen was used for all fatigue tests. The key to designing the dogbone specimen is to achieve maximum reduction in area within the gage length while maintaining a large enough radius of curvature so that failure does not occur in the shoulder region due to high shear stresses. As the shoulder radius decreases, the shear stress increases, thereby increasing the chance of failure outside the gage length.

Majumdar and Newaz used a finite element analysis (FEA), developed by Worthem (40), to determine the shoulder shear stress for varying radii of curvature (22). The goal was to obtain a shear stress not exceeding 0.06 times the nominal tension stress. This value was determined through previous experience with notched MMCs and observed locations of fatigue cracks in previous experiments. The FEA results showed that a radius greater

than 31.75 cm would produce a small enough shear stress. A conservative radius of 35.56 cm was used to further reduce the shear stress in the shoulder region. Consistent failures within the gage length indicate that the specimen design works well for fatigue testing. Thus, the specimen design used for this study is identical to the one used by Majumdar and Newaz. The specimen geometry is shown in Figure 8.

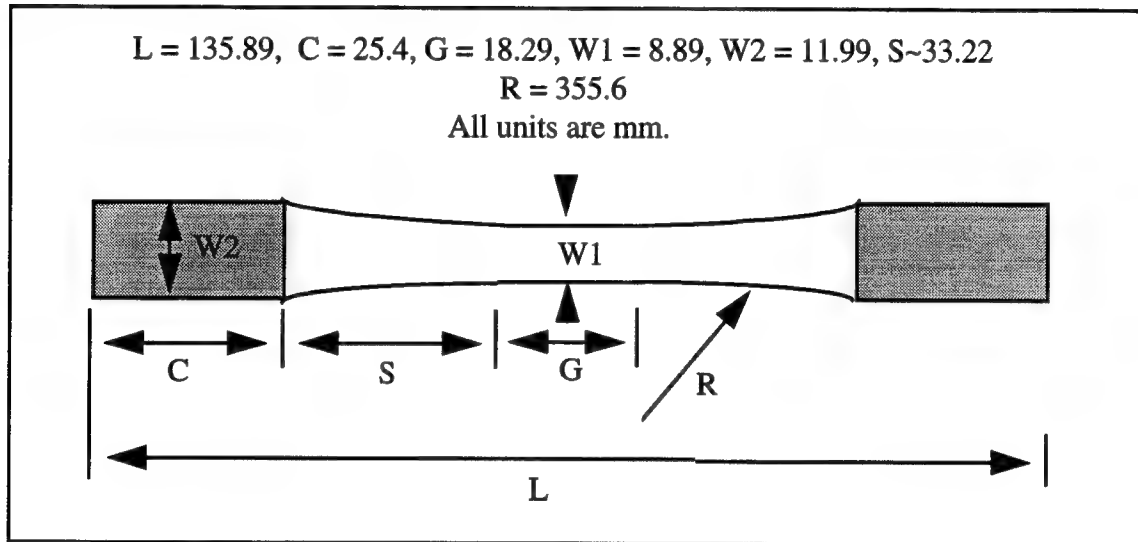


Figure 8. Dogbone Specimen Geometry

Specimens were initially cut into rectangular strips. The dogbone shape was then machined using a diamond encrusted blade. Once cut to the final dimensions, all specimens were wrapped in tantalum foil and heat treated at 700 °C for 24 hours in an argon atmosphere.

Polishing of the curved edges on the dogbone specimen required the development of a hand polishing technique. Several specimens could be polished simultaneously by gluing them together. Dummy specimens were glued to the outside to prevent edge rounding. Fragments accumulated during the machining process on both edges were

eliminated by using boron carbide powder, low grit silicon carbide paper, and a hand-held rotary tool. Once these fragments were removed, a nylon pad was used in conjunction with diamond paste and slurry (45, 15, and 3 μm) to achieve a smooth surface. The final polishing step consisted of using Mastermet and a neoprene pad to produce a mirror-like finish. The last two steps were applied only to one edge for the purpose of taking edge replicas. Tabs were applied using a high temperature application epoxy. Once in position, the tabs were clamped and placed in a furnace at 57 °C for one hour.

3.3 Test Setup

All elevated temperature tests were conducted on a servo-hydraulic test stand (Material Test System 810) equipped with a 22 kip load cell. The test profile was loaded from a Zenith 386 computer using a program called LOADTEST developed by Sanders (33). User entered information included the maximum desired stress, load ratio (R), specimen area, temperature, and testing frequency. The program also inquires as to the calibrations of the load and strain cards inserted into the test stand. All specifications were then sent to the micro-profiler which ultimately drives the load cell. The test apparatus is shown in Figure 9.

The data acquisition system can also be controlled in the program. The user may specify a cycle interval at the end of which data is to be taken. The data is written to a file in the computer with the cycle number as the filename and the extension “.dat”. Approximately 500 pairs of data are taken during the cycle. Also, every time data is taken, the maximum and minimum stress and strain, modulus, and temperature for the corresponding cycle are written to a file called “minmax.dat”.

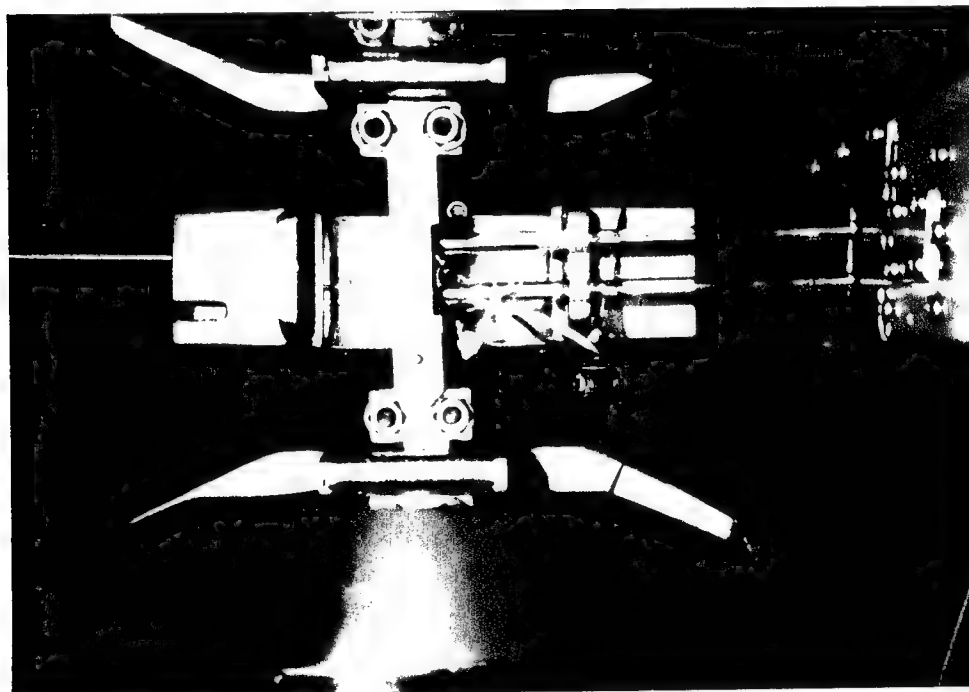
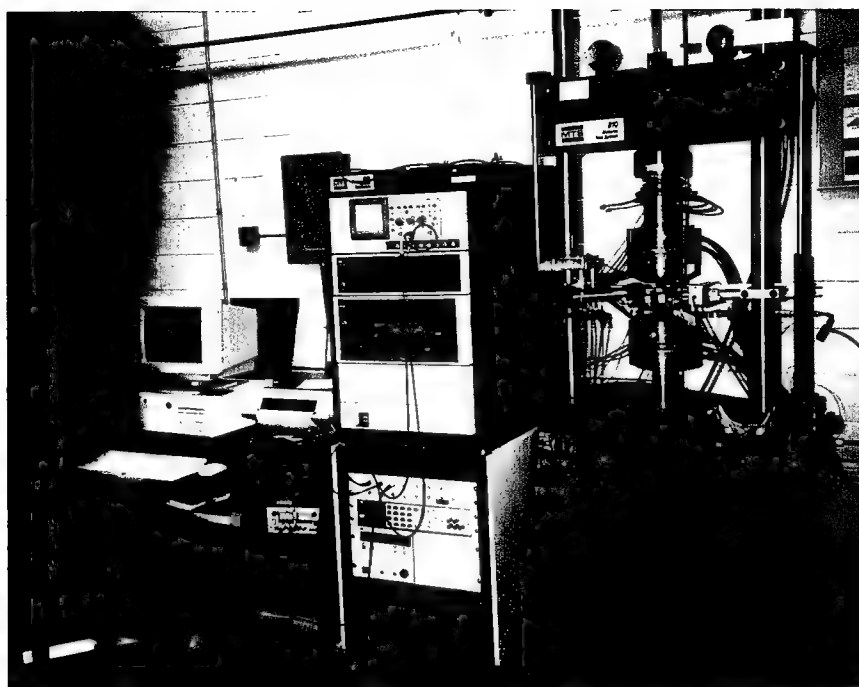


Figure 9. Test Setup

Three thermocouples were spot welded to the outside of the buckling guide; two were used to control temperature generated by parabolic lamps and one to relay temperature data back to the computer. The lamps were attached to the test stand, one in front and one behind. A temperature ramp-up time of 40-45 minutes was used to allow the temperature to diffuse through the buckling guide. Preliminary testing of temperature differences between the outside of the buckling guide and the specimen at the end of the ramp-up time showed the temperature had reached equilibrium in the specimen. The test stand must be protected from the high temperatures produced by the lamps. Thus, circulating cold water cooled the load cell, grips, and lamps.

Strain data was measured with a 0.5 in gage length, high temperature quartz rod extensometer (MTS model 632.50b-04). This device was placed on the specimen edge. Rods were changed periodically due to dulling or chipping. Each time rods were replaced, the extensometer was recalibrated to ensure accurate strain measurements.

3.3.1 Buckling Guide Design

Use of a buckling guide is necessary in this study since the specimen thickness is thin enough that buckling would occur during compressive loading. Boyum designed and built the original AFIT buckling guide specifically for use with dogbone specimens (4). The guide consists of two separate pieces connected through a sliding mechanism. The sliding mechanism allows the guide to expand and contract with the specimen. A very small amount of buckling is allowed but excessive out of plane motion is restricted by the locknut and washer assembly which only allows the guide to move axially.

The guide, as designed by Boyum, would not fit the dogbone specimen used for this study. Also, initial testing indicated that the diameter of the locknut screws was too small to withstand the large forces generated by buckling of the specimen during high stress tests. Thus, the overall length of the guide was shortened and the smaller half modified to withstand the increased loads. The modifications consisted of providing additional support to the locknut screw as shown in Figure 10.

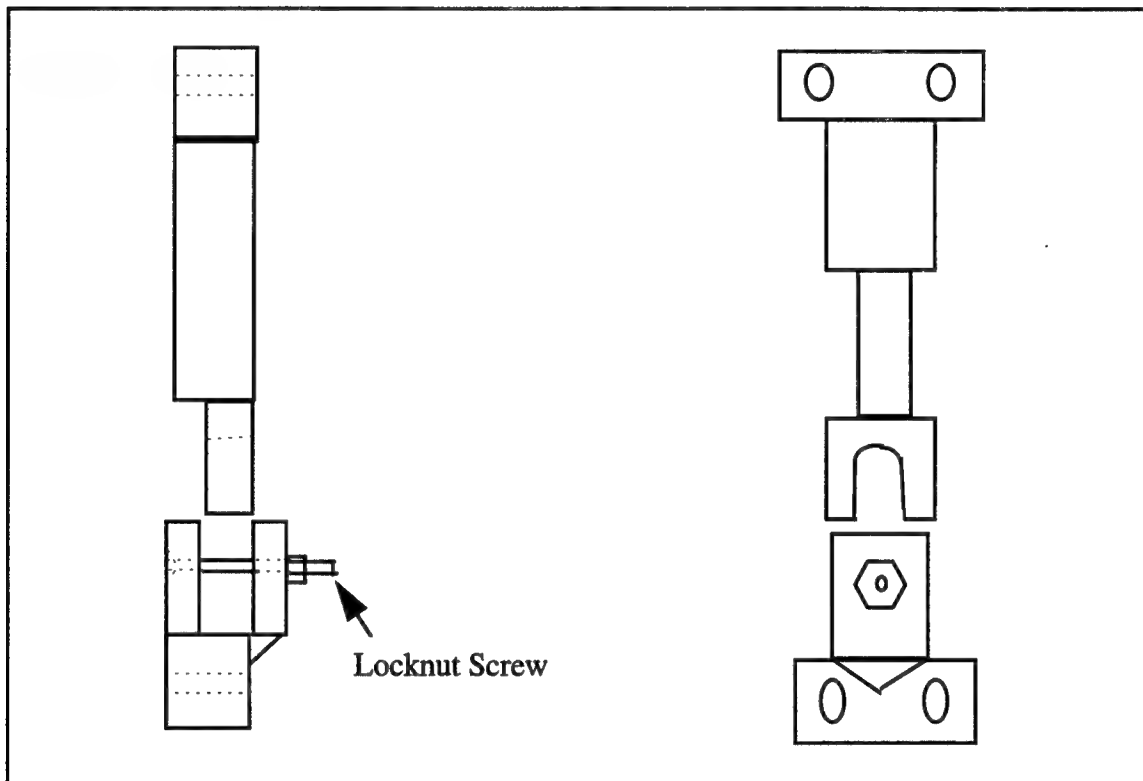


Figure 10. Buckling Guide Modifications

3.4 Tests/Procedures

The buckling guide was carefully attached to the specimen ensuring that the guide and the specimen were aligned properly. Improper alignment often resulted in excessive buckling which could be determined from the initial stress-strain response. Specimens

were then mounted perpendicular to the test stand grips using a small level. Once mounted, the specimen temperature was raised to 427 °C over a period of 40-45 minutes. When the temperature had reached equilibrium the thermal strain was measured. The initial cycle was controlled by hand to determine the initial modulus and to check for excessive buckling. Excessive buckling was observed by a cusp in the compression region as shown in Figure 11. To correct this situation, the specimen was realigned with the buckling guide. Additionally, the guide and specimen were realigned in the test stand.

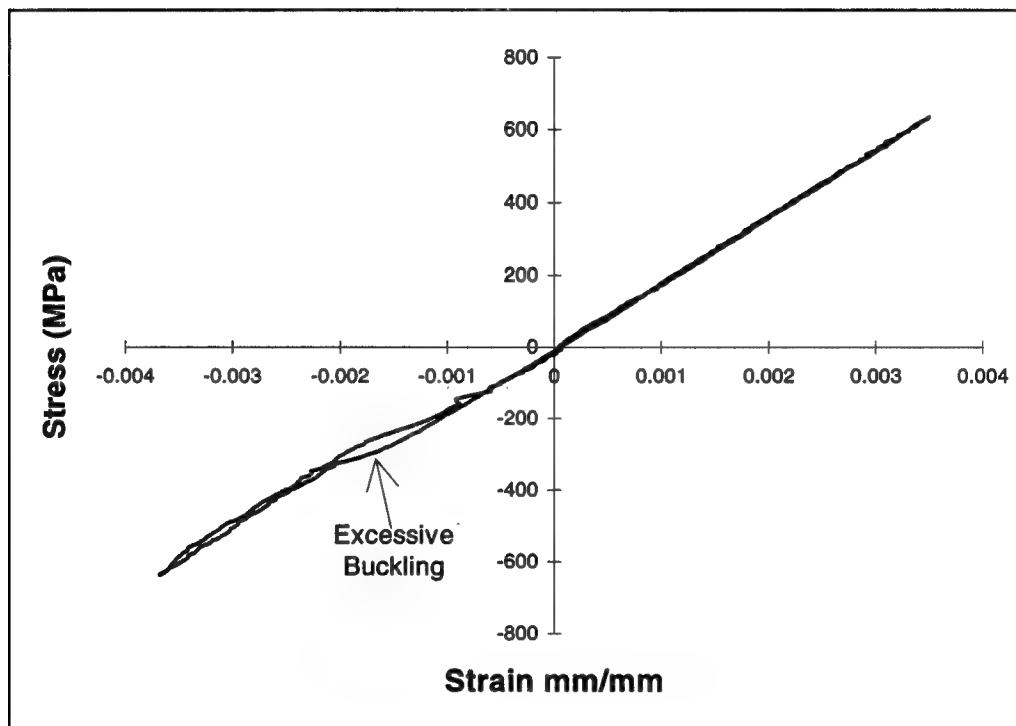


Figure 11. Excessive Buckling

The first few cycles during any start-up portion of a test were run at 1 Hz so that the computer could take data. Subsequent cycles were then run at 10 Hz but slowed down to 1 Hz every time the test reached a data acquisition interval.

3.4.1 Edge Replicas

Edge replicas were taken to trace the development of fiber and matrix cracks during fatigue life. Replicas were taken approximately every decade of the test. Fifty percent of the test load was applied to the specimen for all replicas with the exception of the initial replica where no load was applied. The applied load opens the cracks which would otherwise close under no load. Acetate strips were then dowsed with acetone and held on the polished edge for 50-60 seconds. To prevent the replicas from curling, they were placed in an oven at 57 °C for one hour.

3.5 Post-Failure Analysis

Post-failure analysis consisted of the sectioning of several tested specimens, fine polishing, examination under both optical and scanning electron microscopes (SEM), and etching the specimens in an acid solution. Fracture surfaces were also examined under the SEM. All tested specimens were post-heat treated at 427 °C for 24 hours to aid in the detection of slip bands after etching (20).

Selected specimens were sectioned to reveal one longitudinal, one transverse, and one face section. The location of these three sections is shown in Figure 12. These sections were mounted in Buehler Konductomet, a black conductive mounting compound. The Konductomet surrounds the section and allows for automated polishing.

The initial polishing stage was completed using a 45 µm diamond slurry and a number 8 platten. This rough polishing is then followed by smaller diamond slurries (9,3, and 1 µm). At this point, any remaining scratches are removed using 3 and 1 µm Permats. Final polishing is conducted on a Beuhler Vibromet. Specimens are placed in a

1 μm solution Vibromet and polished for approximately 24 hours. The specimens are then moved to a 1/2 μm solution Virbomet for approximately 8 hours. Lastly, the specimens are placed in a mastermet solution Vibromet for 20 minutes.

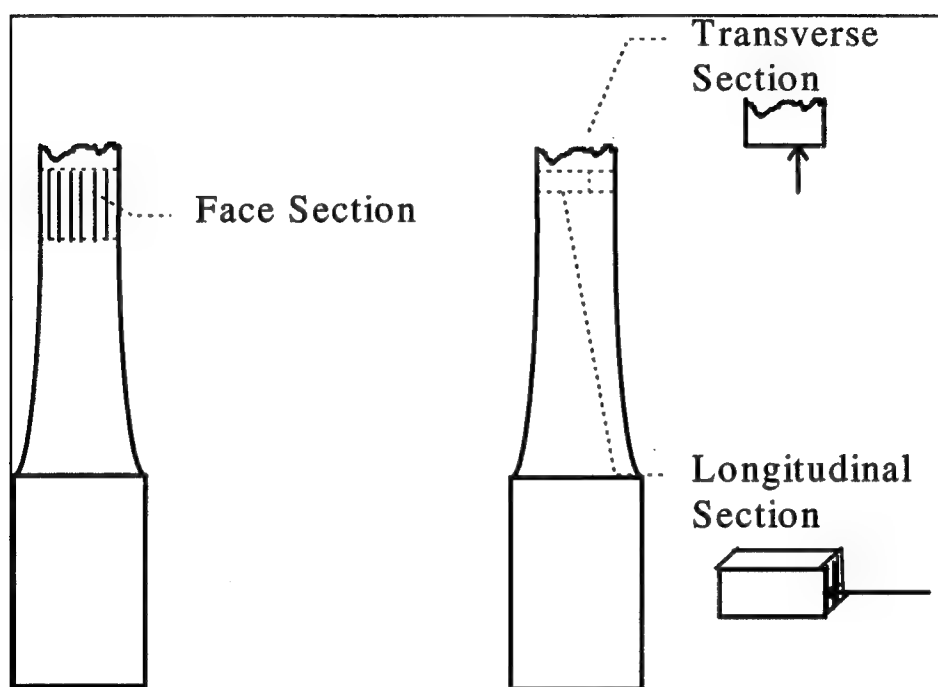


Figure 12. Specimen Sectioning

Following final polishing, selected specimens were etched. A three percent solution of Ammonium Flouride and Hydroflouric Acid ($\text{NH}_4\text{F}+\text{HF}$) is applied to the specimen. This solution attacks the alpha phase precipitates which enables one to more easily observe slip bands, matrix plasticity, and grain boundaries.

4. Results and Discussion

A complete investigation of the fatigue life of any material must consist of both macro-mechanical analysis and a microscopic evaluation. The purpose of this chapter is to present the results and related discussion based on these two topics. The results of the fatigue lives are discussed in the next chapter. Results of the macro-mechanical behavior of the tested material includes observations concerning trends in the modulus, maximum and minimum strains, and strain ranges during cycling. Microscopic evaluation includes examination of the fracture surfaces and sectioning of the specimens to reveal internal damage.

4.1 Overview of Test Data

It has been shown by Majumdar and Newaz that the σ - ϵ response for the tested material remains linear up to more than 900 MPa (0.55% strain) (23). In addition, they showed that slip bands in the matrix material of the unidirectional SCS-6/Ti-15-3 MMC initiate at the same strain level. Slip bands indicate plastic deformation which stem from yielding of the matrix material and would result in a knee in the stress-strain curve. In the current study, the maximum applied stress of 800 MPa (0.425% strain) is well below the tensile yield limit, therefore no nonlinearity or knee in the tensile region of the stress-strain (σ - ϵ) curves were observed in the fatigue tests of this study. The initial modulus (based on tension) ranged from 180-197 GPa with an average value of 189 GPa.

With proper application of the buckling guide, the compressive modulus is completely linear and matches the tensile modulus. Boyum showed that the σ - ϵ curve in

compression was linear for a $[0/90]_{2s}$ laminate while the tensile σ - ϵ curve exhibited a knee around 180 MPa (4). Such behavior was noted at all stress levels investigated. This indicates that the cross-ply laminate is at least as stiff in compression as it is in tension. Therefore, since no nonlinearity was observed in the tensile region for the unidirectional material tests in this investigation, complete linearity was expected in the compression region as well. As shown in Figure 13, the initial compressive and tensile moduli were identical. Table 2 shows various data and failure modes for all TC HT fatigue tests.

Table 2. Summary of TC HT Fatigue Tests

Stress, MPa	Initial * Modulus (GPa)	Max ** Strain (%)	Strain ** Range (%)	Cycles to	Failure Mode
800	184	0.424	0.850	23658	mc,ff
700	195	0.381	0.746	33870	mc,ff
675	180	0.349	0.708	56216	mc,ff
625	197	0.342	0.699	100186	mc,fb
500	188	0.283	0.572	163000	mc,fb
425	188	0.238	0.469	355499	mc,fb
375	190	0.223	0.445	$>10^6$	N/A
340	195	0.195	0.390	$>10^6$	N/A

* based on tension and compression

** values at half life

mc - matrix cracking

ff - fiber failure directly behind crack tip

fb - fiber bridging

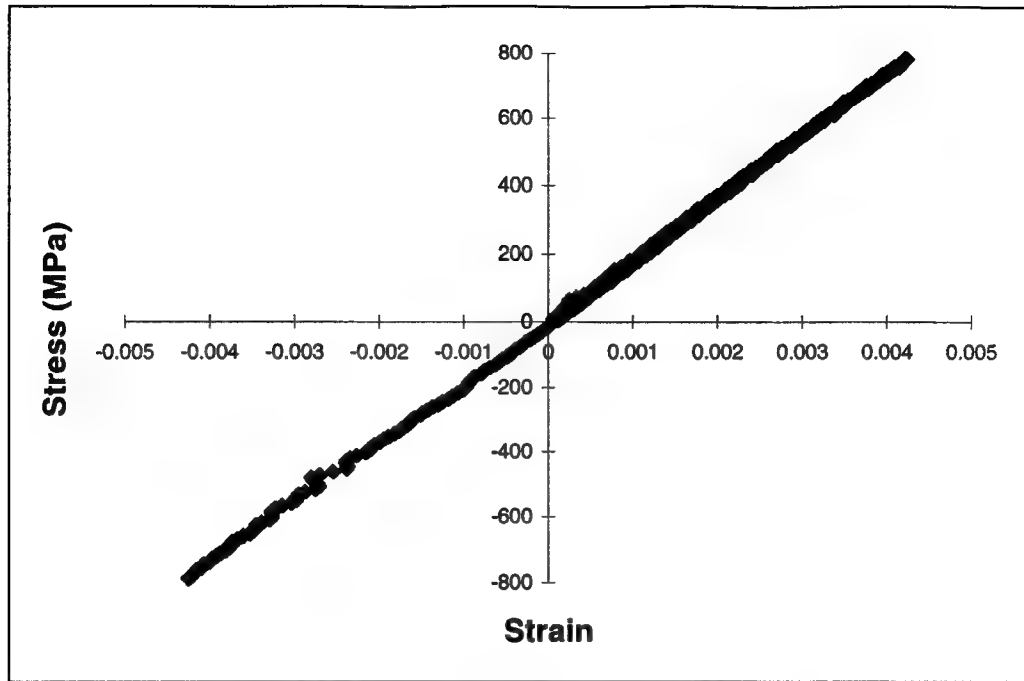


Figure 13. Initial stress-strain curve, 800 MPa

4.2 Frequency Effects

While most of the fatigue tests in this study were conducted at a loading frequency of 10 Hz, problems encountered with slipping of the extensometer rods forced the tests at 700 and 800 MPa to be run at 1 Hz. The change in frequency did not alter the fatigue life curve but a brief investigation was conducted to determine the effects of frequency.

The effects of frequency (or strain rate) are well documented for most alloys. As the strain rate increases, the yield point increases. However, within the elastic region, all strain rates yield similar results. Also, macroscopic results only show a noticeable difference at very high strain rates, e.g. 10^{-5} to 10^{-6} . At low strain rates, 10^0 to 10^{-1} , there is no appreciable difference in behavior.

Although the frequency response of alloys is well documented, the response of composites is not yet fully understood. To better understand this behavior, Portner compared several tension-tension fatigue tests on a unidirectional MMC at varying frequencies (30). The test frequencies varied between 0.02 and 2 Hz. There was no appreciable difference in the σ - ϵ response between the two test frequencies. Since the frequencies differed by a factor of 100 and the current study contains frequencies that differ only by a factor of 10, no appreciable difference is expected in the current study as well.

To provide further evidence that the current range of frequencies did not skew the data, micro-mechanical analysis using LISOL (32) was performed to predict fiber and matrix stresses for the two high stress tests conducted at 1 Hz (reference Appendix A). To accomplish this, tests at 700 and 800 MPa were run at two frequencies, 1 Hz and 10 Hz. After 10 cycles, the stresses had stabilized and showed no difference between the two test frequencies. This data, combined with the above discussion indicates that the change in frequency from 1 Hz to 10 Hz did not alter the experimental data.

4.3 Macro-mechanical Behavior

The fully-reversed fatigue tests performed in this study can be separated into three groups: Group 1 which includes tests at stress levels from 675-800 MPa inclusively, Group 2 which includes those tests performed between 425 and 625 MPa, and Group 3 which includes tests conducted at 340 and 375 MPa. Group 1 and 2 behavior, as will be discussed later, both were dominated by matrix failure, however, the distinction between groups 1 and 2 arises from the nature of progression of matrix cracking throughout the specimen. Group 3 contains specimens that were cycled below the fatigue limit of the

material and lasted at least 3 million cycles. Specimens lasting more than 1 million cycles are generally classified below the fatigue limit (24). These groups will be discussed separately followed by discussion of the tension-tension test results.

4.3.1 Group 1 Data

4.3.1.1 Modulus Trends

Trends in the modulus during cycling are extremely helpful in determining the initiation of damage and the rate of damage progression throughout the fatigue life of the specimen. Generally, any degradation in the modulus indicates damage. Figure 14 shows the trends in the normalized modulus for all tests in Group 1. The normalized modulus is calculated by dividing the current modulus by the initial modulus. Likewise, the normalized fatigue life is calculated by dividing the current cycle by the number of cycles at failure.

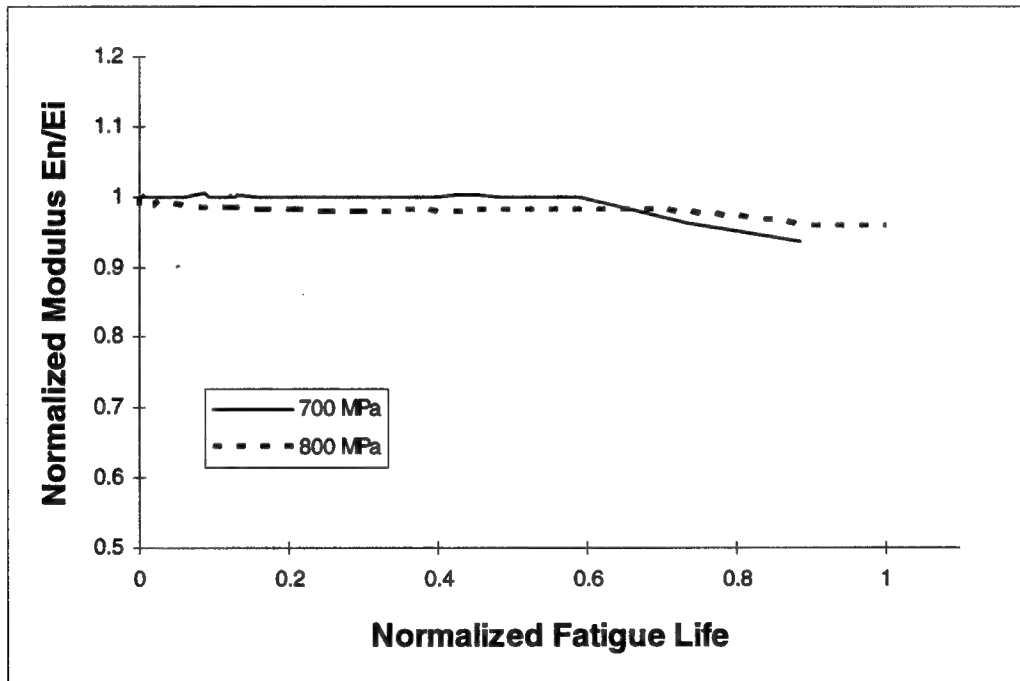


Figure 14. Group 1 Normalized Modulus Trends

The modulus remained constant for approximately 60 % of the fatigue life and then began to decrease. Modulus degradation is usually attributed to matrix cracking rather than fiber cracking. Nicholas and Ahmad showed that fiber cracking will not result in a drop in modulus unless the crack opening displacement (COD) is on the order of a few fiber diameters (27:13). Even though edge replicas indicated some fiber cracking after about 100 cycles, the cracks did not grow in number or size with additional cycles.

Additionally, edge fiber cracking is not indicative of damage inside the specimen.

Evidence to support this statement will be discussed later during examination of the face sections where no fiber cracking was observed. It will be shown later that the modulus degradation is attributed to matrix cracking for specimens contained in Group 1.

4.3.1.2 Strain Trends

Figure 15 shows the maximum tensile, minimum compressive and mean strains for the fatigue tests in Group 1. For all fatigue tests conducted in this group, the mean strain over the first few fatigue cycles remains constant providing no evidence of creep as commonly observed in tension-tension fatigue tests. Creep is indicated by a slight rise in mean strain over the first few loading cycles. Also, the mean strain is approximately zero for all tests indicating that there are no residual strains after unloading. Further examination of the strain data shows that a decrease in modulus, as shown in Figure 14, was the result of an increase in the maximum strain and, hence, an increase in the strain range while minimum strain remained constant. Therefore, modulus degradation can be attributed to a loss of tensile stiffness while the compressive stiffness maintains its initial

value. An example of this behavior will be shown in the σ - ϵ curves for specimens in Group 2 where tensile modulus degradation is more noticeable.

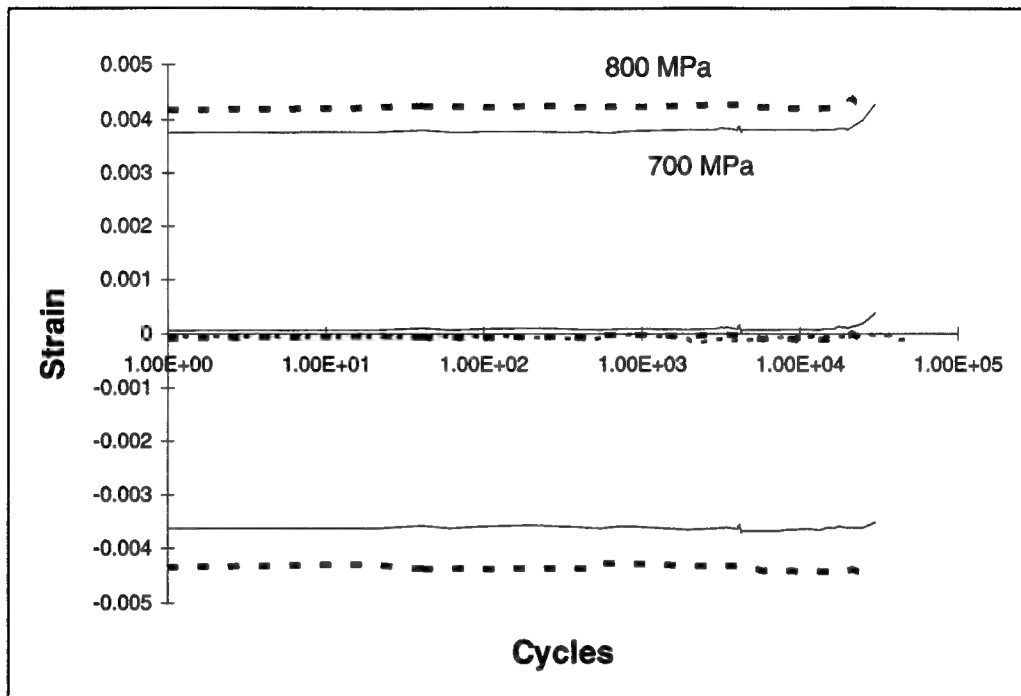


Figure 15. Group 1 Strain Trends

4.3.2 Group 2 Data

4.3.2.1 Modulus Trends

The specimens in Group 2 include those cycled between 425 and 625 MPa inclusively. The microscopic evaluation will reveal that Group 2 is dominated by matrix cracking, just as Group 1. However, the nature of progression of matrix cracking in Group 2 is quite different from that observed in Group 1 and the modulus trends reflect those differences.

Figure 16 shows the modulus trends for those specimens in Group 2. Upon initial inspection, the 425 MPa specimen shows a trend similar to that seen in Group 1, but microscopic evaluation and further macroscopic analysis show that this specimen exhibits behavior consistent with other specimens in Group 2. Whereas the modulus remained constant for approximately 60% of the fatigue life in Group 1, modulus degradation began after as little as 20-40% of the fatigue life in Group 2. Percentage of fatigue life should not be confused with actual cycle number. Simple calculations show that the modulus degradation in Group 2 began at later cycle counts than in Group 1, even though the corresponding fatigue life percentage is less for Group 2. Although modulus degradation at 425 MPa is not obvious in Figure 16, a plot of the actual modulus versus cycle count in Figure 17 shows a more dramatic reduction.

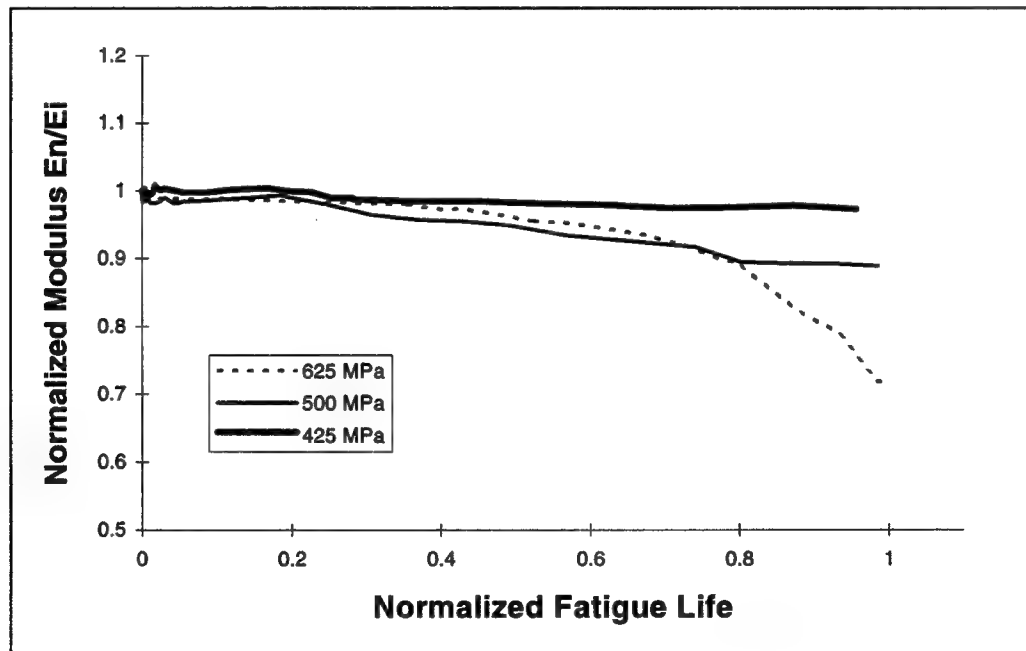


Figure 16. Group 2 Normalized Modulus Trends

The amount of modulus degradation in Group 2 also varies with the applied stress, as shown in Figure 17. As the applied stress increases, the amount of modulus degradation increases. This indicates that more matrix cracking occurs at higher stresses. Microscopy will show that the crack density increased with the increasing stress in Group 2.

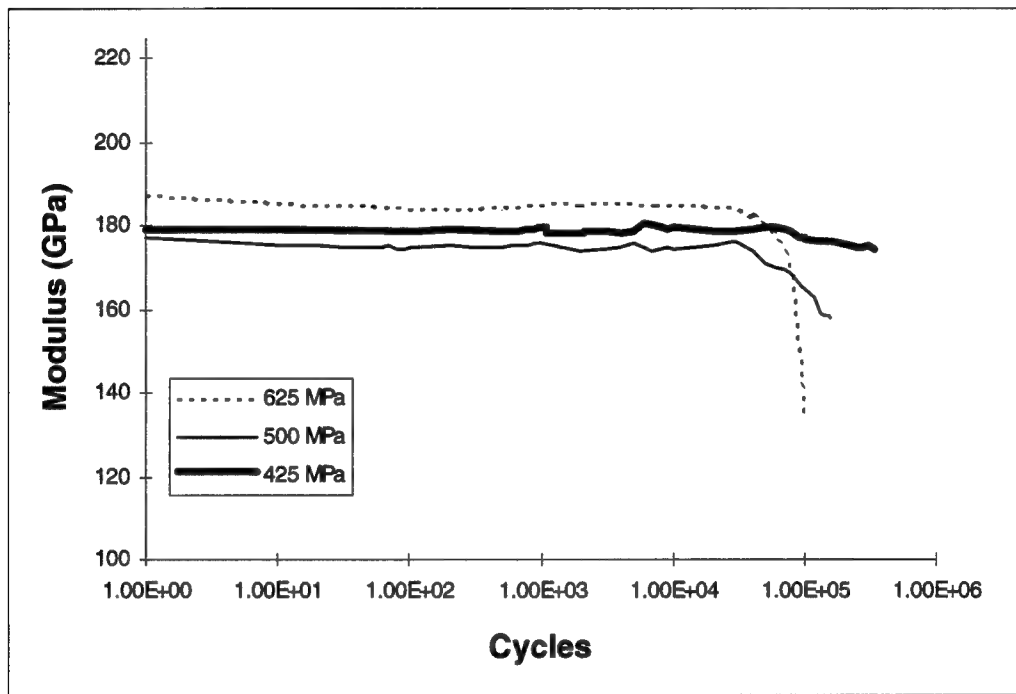


Figure 17. Group 2 Modulus Trends

4.3.2.2 Strain Trends

The maximum and minimum strain trends for Group 2 are plotted in Figure 18. As observed in Group 1, there is no evidence of creep as the mean strain remains constant at zero during the initial cycles. The increase in strain at the end of the fatigue life is the result of damage, which manifests itself in a decrease in stiffness. Very little stiffness

reduction was observed in the specimen cycled at 425 MPa, thereby explaining the lack of increase in maximum strain near the end of the fatigue life. Also, the decrease in modulus causes an increase in the strain range. This relationship can be shown by comparing the change in modulus versus the change in strain range as shown in Figure 19 where modulus and strain range data for the 625 MPa fatigue test are plotted against the fatigue life. The increase in strain range is caused by an increase in the tensile strain while compressive strain remains constant. To better illustrate the rise in strain range caused by an increase in the tensile strain, it is helpful to look at the stress-strain response.

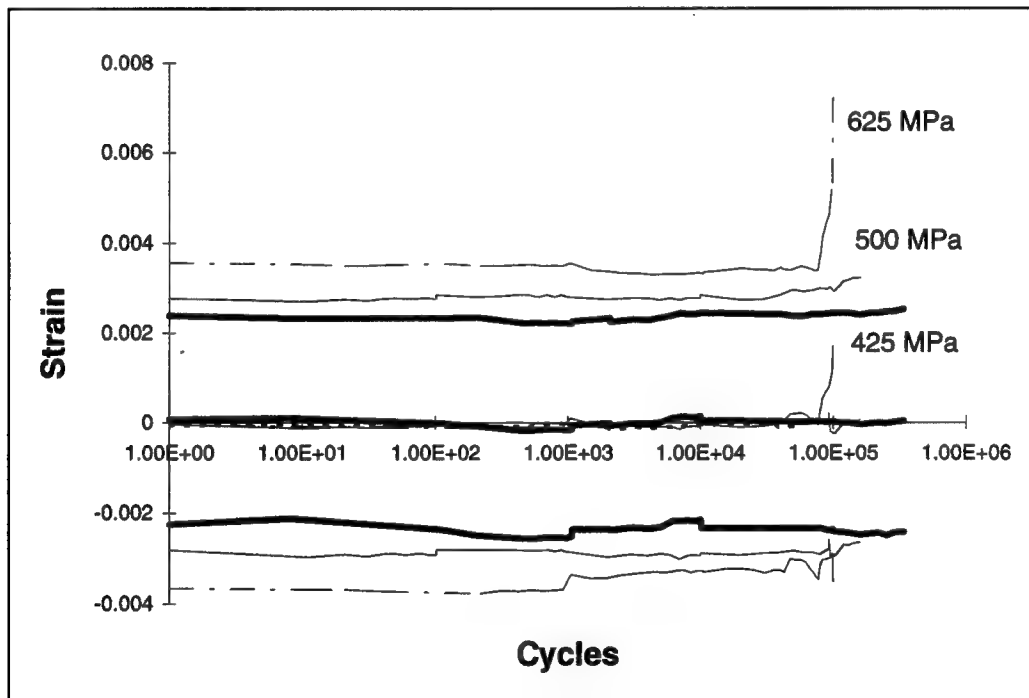


Figure 18. Group 2 Strain Trends

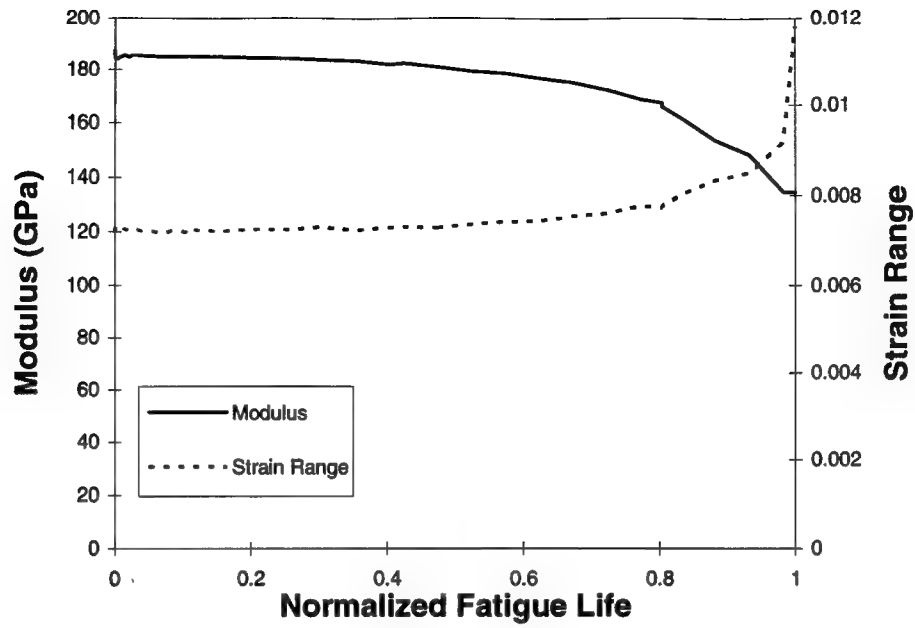


Figure 19. Modulus, Strain Range Data for 625 MPa, T=427 ° C

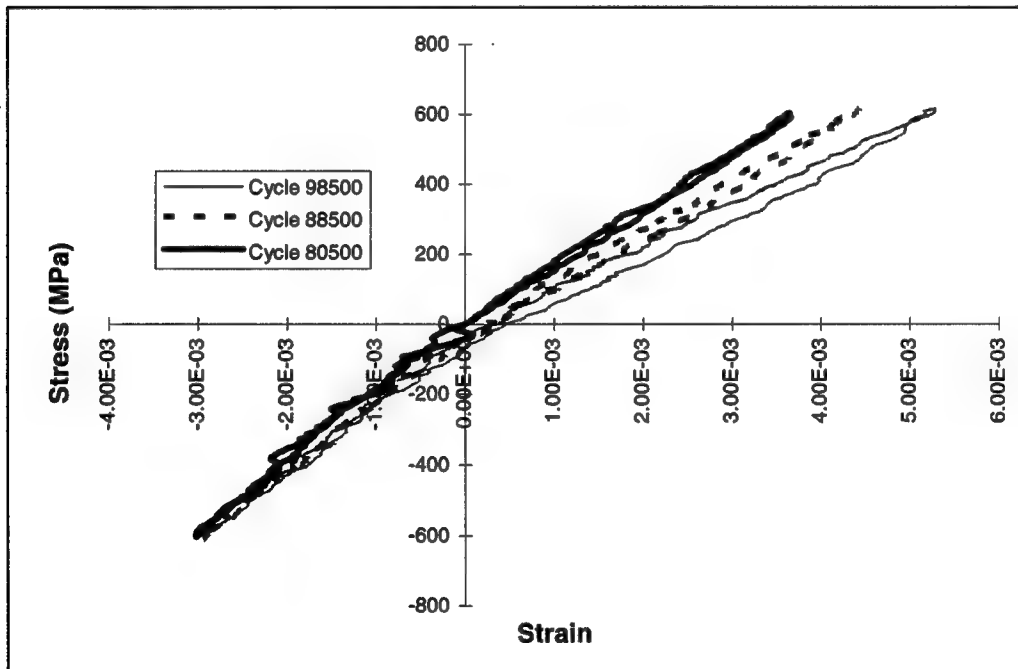


Figure 20. Stress-Strain Response at 625 MPa, T=427 ° C

The stress-strain responses for various cycles at 625 MPa are shown in Figure 20. It is easily seen that the compressive strain and modulus are constant over time while the tensile modulus decreases as the tensile strain increases. Additionally, the hysteresis in the σ - ϵ response increases with increasing cycles further indicating damage progression.

4.3.3 Group 3 Data

4.3.3.1 Modulus Trends

Figure 21 shows the modulus trends for specimens in Group 3. The modulus remained constant throughout the test showing no indication of damage. Edge replicas showed some fiber cracking after 100,000 cycles and their number did not increase with subsequent cycles, but as mentioned before, this is not indicative of the rest of the specimen. Edge replicas also showed that some matrix cracking developed from the debonding between the fibers and the matrix where the fibers had already cracked. Also, once matrix cracks were detected in edge replicas, they did not increase in number or size. Analysis of the modulus trends indicates that the existing matrix cracks had no effect on the material stiffness and probably did not progress throughout the laminate.

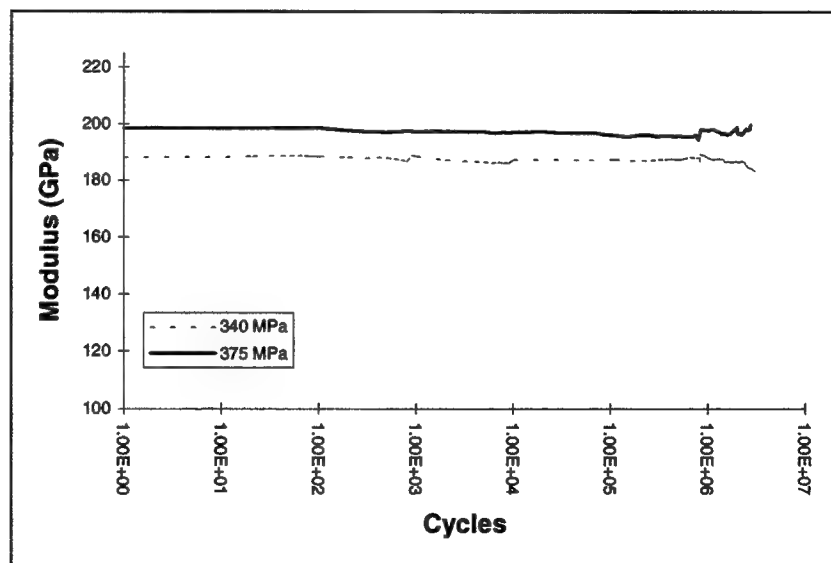


Figure 21. Modulus vs Fatigue Life for Group 3 Tests

4.3.3.2 Strain Trends

Figure 22 shows the strain trends for Group 3. Once again the trends show no evidence of creep. Also, since there was no change in modulus, there is no increase in maximum strain or strain range. Thus, it appears that damage observed in edge replicas has not progressed throughout the composite and that these specimens were cycled below the fatigue limit of the matrix material.

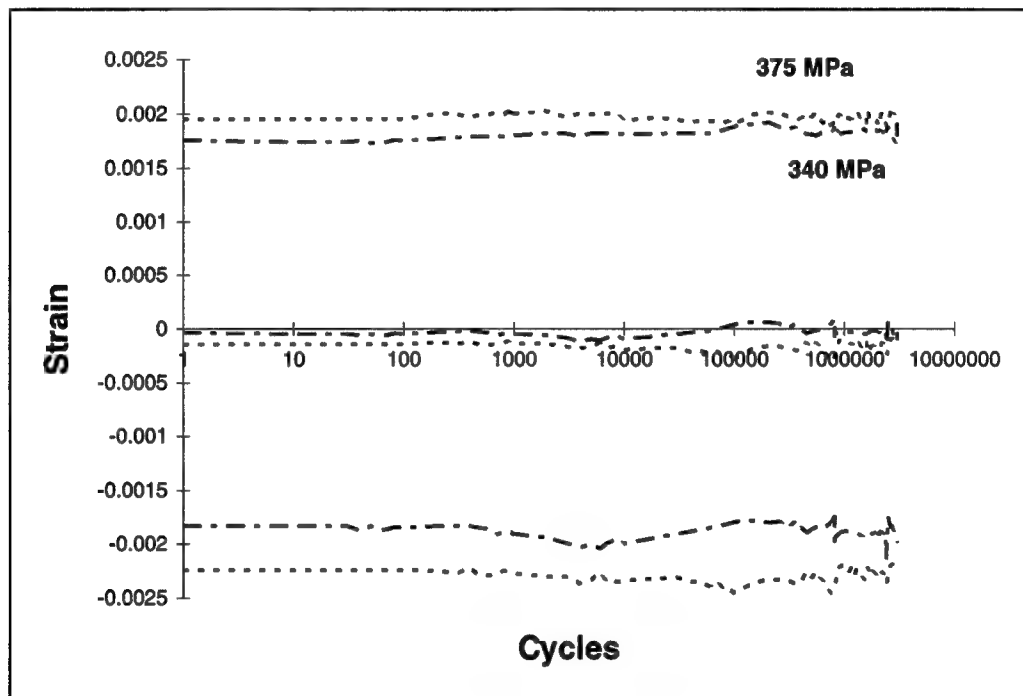


Figure 22. Group 3 Strain Trends

4.3.4 Tension-Tension Test Data

Two tension-tension fatigue tests were performed. The purpose of these tests was 1) to show that the response of the present material corresponded with fatigue life data of the previous studies and 2) to provide baseline data for comparison of failure mechanisms between tension-tension and tension-compression fatigue loading conditions. As will be

illustrated in Chapter 5, the tension-tension specimens failed in accordance with previous tests data obtained from various sources (22,29,33). Comparison of failure mechanisms can be found at the end of this chapter.

4.3.4.1 Modulus Trends

Different modulus trends were observed for each test performed. Figure 23 illustrates the modulus trends described here. At 1000 MPa, the modulus remained constant for a large portion of the fatigue life while the specimen cycled at 800 MPa exhibited modulus degradation much earlier. This difference stems from the type of failure. At 800 MPa, failure was dominated by a mixture of fiber and matrix cracking as will be discussed later. At 1000 MPa, failure was primarily associated with fiber failure which, as previously discussed, may not result in a loss of stiffness.

Also shown in Figure 23 is the modulus trend for the fully-reversed specimen cycled at 800 MPa. Modulus degradation under tension-tension fatigue occurred over a small number of cycles, spanning only over the end of the fatigue life, while tension-compression fatigue produced damage much earlier in the fatigue life. Once again, the percentage of fatigue life where damage initiates should not be confused with actual cycle number. Strain trends will show that damage initiated at approximately the same cycle count for both loading conditions but progressed at greatly different rates through the composite.

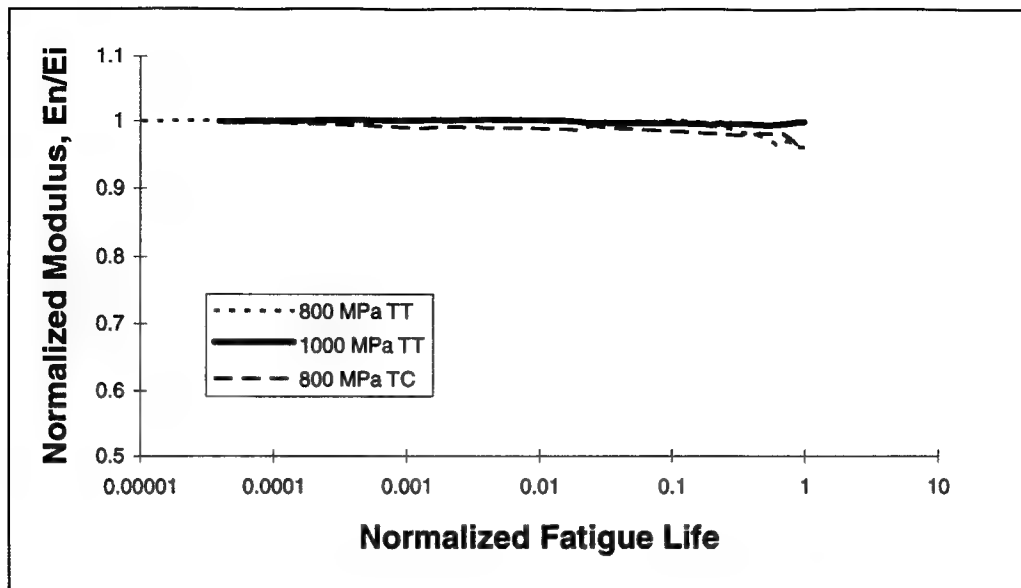


Figure 23. Normalized Modulus vs Fatigue Life

4.3.4.2 Strain Trends

The maximum and minimum strain trends are once again important in identifying creep behavior. Figure 24 shows the strain trends for the tension-tension tests conducted in this study. The initiation of damage is seen as a pronounced rise in both maximum and minimum strains at the end of the fatigue life. Unlike the strain trends in tension-compression loading, those for tension-tension loading show evidence of creep behavior. As shown in Figure 25, the maximum and minimum strains begin to rise after approximately 10,000 cycles. To determine whether this increase is a result of damage or creep, the modulus and strain range must be analyzed. Figure 26 shows that the modulus and strain range remain constant for more than 20,000 cycles indicating that the increase in strain between 10,000 and 20,000 cycles is a result of creep and not damage.

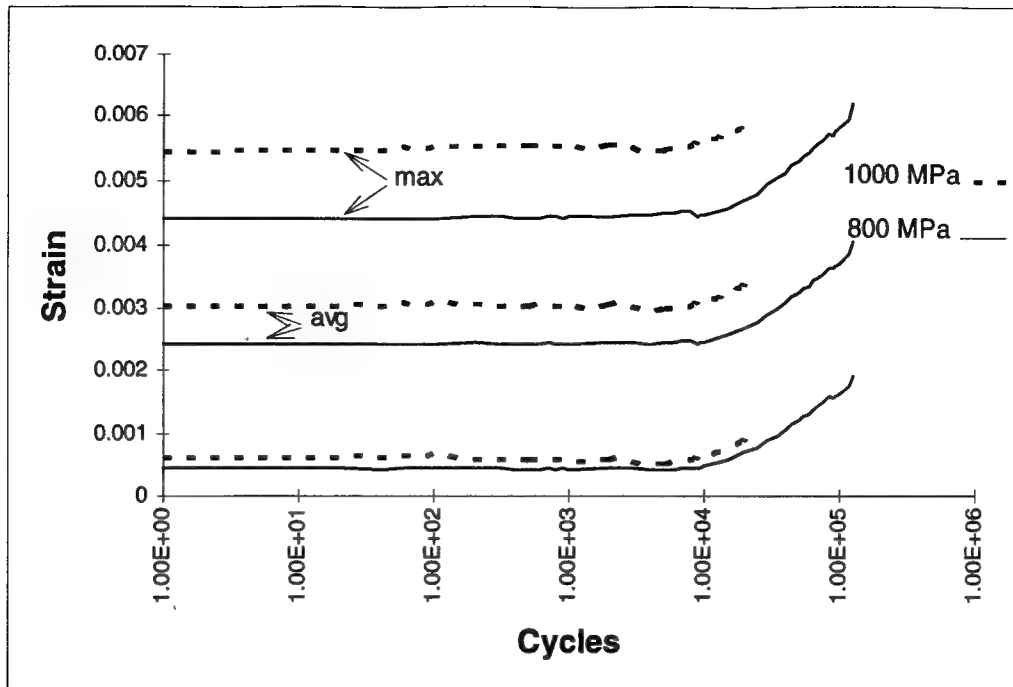


Figure 24. Max, Min and Avg strain, TT HT

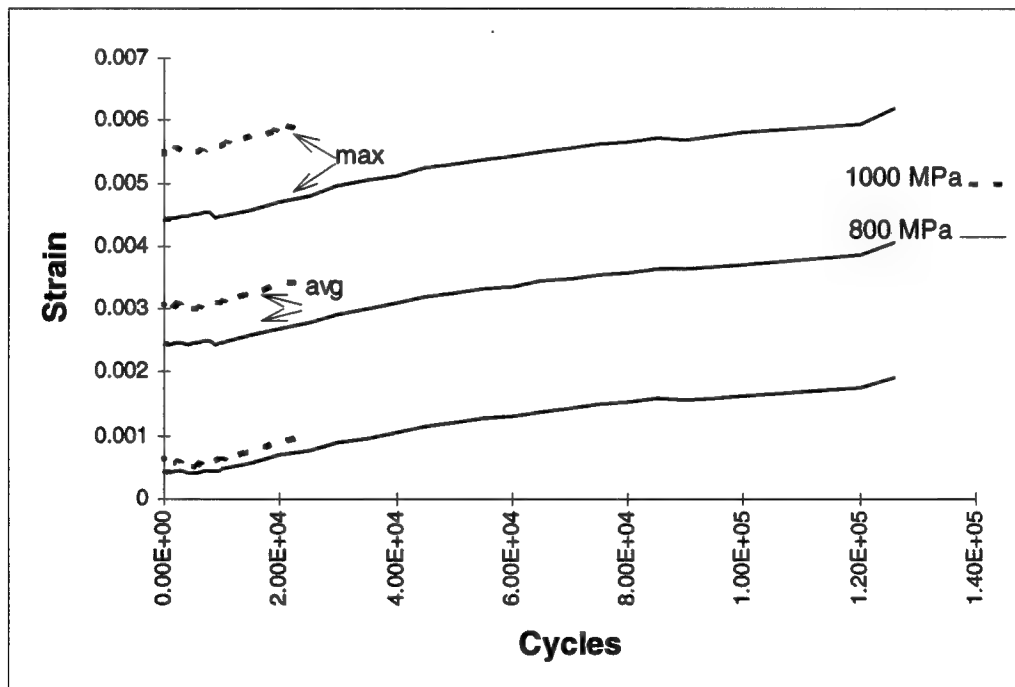


Figure 25. TT HT Strain Trends (Linear Scale)

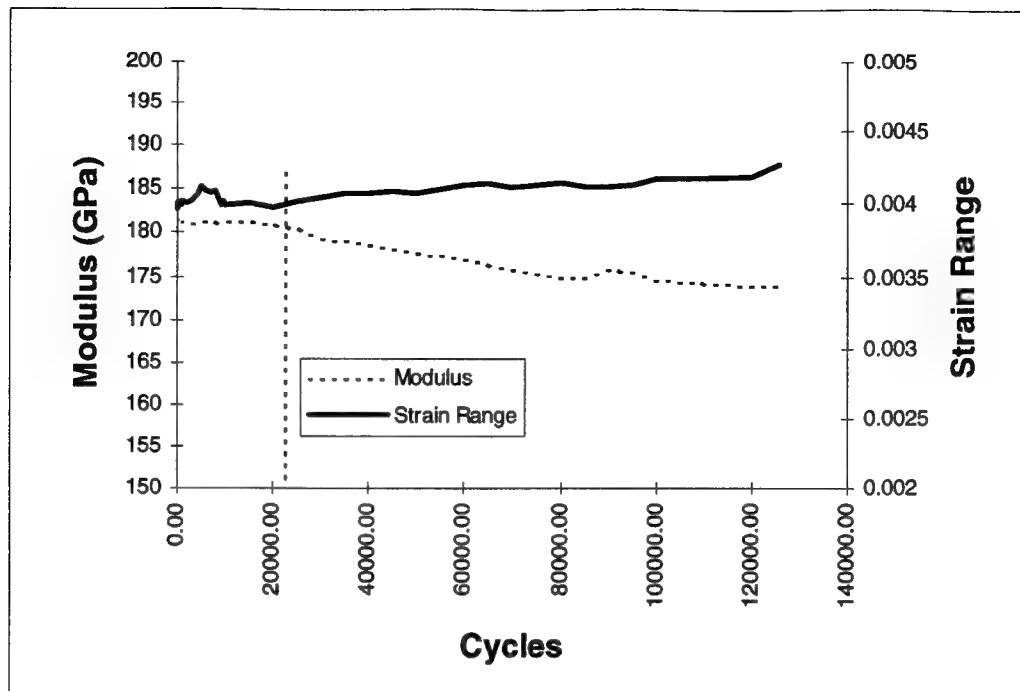


Figure 26. Modulus and Strain Range, 800 MPa, TT HT

Figures 25 and 26 also show that, under tension-tension cycling, the material creeps after the initiation of damage. During these cycles, the remaining undamaged material experiences a greater effective stress and therefore greater plastic (creep) strain accumulation. Under tension-compression cycling, however, creep is prevented by the compressive load which may plastically deform the specimen in compression. As will be discussed in Chapter 5, creep plays an important role in extending fatigue life under tension-tension cycling over fatigue life under tension-compression cycling.

The effects of mean strain become important in tension-tension loading and help to explain the differences between tension-tension and tension-compression testing. As seen in Figure 24, the mean strain is no longer zero as was observed in the tension-

compression testing. Thus, residual tensile strains are present after unloading. The effect of residual tensile strains has been documented by several authors including Boyum who concluded that since cracks only grow in tension, a residual tensile strain allows more time for cracks to grow, thereby reducing fatigue life based on stress range (4).

Figure 27 plots the maximum strains for fatigue tests conducted at 800 MPa in both tension-tension and tension-compression loading conditions. Although damage initiated at approximately the same cycle count, the number of cycles to failure is much greater under tension-tension fatigue. Thus, once damage occurred under tension-compression fatigue, it progressed faster through the composite than under tension-compression fatigue, it progressed faster through the composite than under tension-tension fatigue.

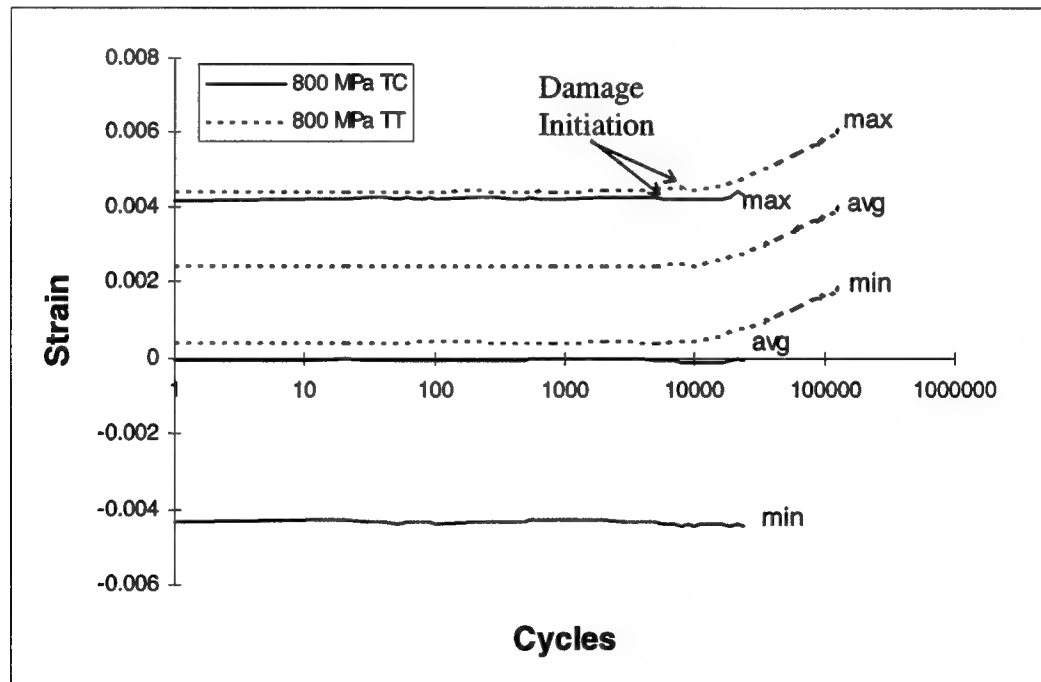


Figure 27. TT vs. TC Strain Trends, 427° C

4.3.5 Summary of Macro-mechanical Behavior

4.3.5.1 Tension-Compression Fatigue Loading

The fully-reversed fatigue tests in this study were separated into three groups based on the macro-mechanical behavior. Group 1 consisted of tests conducted between 675 and 800 MPa inclusively, Group 2 consisted of those tests cycled between 425 and 625 MPa, and Group 3 consisted of two fatigue tests cycled below the fatigue limit of the material. Failure modes of Groups 1 and 2 were dominated by matrix cracking which will be explained in the next section. The differences in modulus trends between these two groups can be explained by the progression of matrix cracks.

The σ - ϵ response was linear over the full range of applied stresses as expected from previous studies. Also, the compressive modulus was shown to be identical to the undamaged tensile modulus. Modulus degradation initiated at different points in the fatigue life and varied with the applied stress (i.e., the modulus remained constant for a greater percentage of the fatigue life with increasing applied stresses). The point at which modulus degradation begins is of great importance since it indicates the onset of damage. Thus, once damage initiated, the rate of progression depended on the applied stress. As the stress increased, the cracks advanced more rapidly throughout the specimen.

Strain data showed no evidence of creep in all groups. In addition, the mean strain was approximately zero for all fatigue tests indicating that no residual strains were present in the material after unloading. Any decrease in modulus was a result of an increase in strain range. Furthermore, the increase in strain range was completely attributed to a loss of tensile stiffness while the compressive stiffness remained constant.

4.3.5.2 Tension-Tension Fatigue Loading

The two tension-tension fatigue tests were not separated into groups even though they exhibit different modulus trends. Very little loss of stiffness was observed at 1000 MPa whereas the specimen at 800 MPa showed much more stiffness loss. This difference can be attributed to failure modes. Previous research has shown that the specimen at 1000 MPa was dominated by fiber failure while the specimen at 800 MPa was dominated by a combination of fiber and matrix failure (29:11). Strains were constant until the initiation of damage near the end of the fatigue life. No creep was observed in the strain trends due to the short duration of the test. Strain comparison between tension-tension and tension-compression show that damage initiated at the same time but progressed faster under tension-compression fatigue.

Micro-mechanical results are presented in the next section and will provide the documentary evidence of the type of failure observed in all fatigue tests. These failure modes can once again be separated into three groups as previously described.

4.4 Micro-mechanical Behavior

The micro-mechanical analysis in the current study consists primarily of fracture surface examination and sectioning of the specimens as described in Chapter 3 (Figure 12). Examination of the fracture surfaces identifies the mode of failure at fracture and sectioning identifies overall damage mechanisms. As the following results will show, all of the fatigue tests in Group 1 and 2 are dominated by matrix cracking. Failure dominated by fiber fracture was not observed. Previous research has concluded that maximum stress levels of approximately 950 MPa in tension-tension testing are necessary

to observe any fiber cracking at all (29). Also, Sanders found that fiber dominated failure occurred above 0.73% maximum strain. (33). Since the maximum applied stress is only 800 MPa (0.43% maximum strain) in the current study, no fiber cracking was observed in sectioned specimens (i.e. inside the specimen).

4.4.1 Fracture Surfaces

4.4.1.1 Tension-Compression Fatigue Specimens

Thus far the results of this study have been broken into three groups depending on the progression of matrix cracking and the resulting macroscopic trends. But for fracture surface evaluation, it is helpful to examine all fracture surfaces together since they possess similar characteristics that indicate matrix dominated failure. An overview of each fracture surface is shown in Figures 28-31. All four stress levels indicate similar behavior in that part of the fracture surface is flat like matrix dominated failures and part is cluttered with fibers that have pulled out of the matrix. The relative amounts of the two regions is dependent on the applied stress level. As the stress level increases, the amount of fiber pull-out increases and the amount of flat, matrix dominated area decreases. Yet even the test cycled at 800 MPa, the maximum for this study, showed some flat area.

Figure 31 shows many levels of flat area while Figure 28 shows a single level. This indicates that many cracks were progressing through the composite at low stress. As the stress level increases, one crack tends to dominate resulting in a single level of flat fracture surface area.

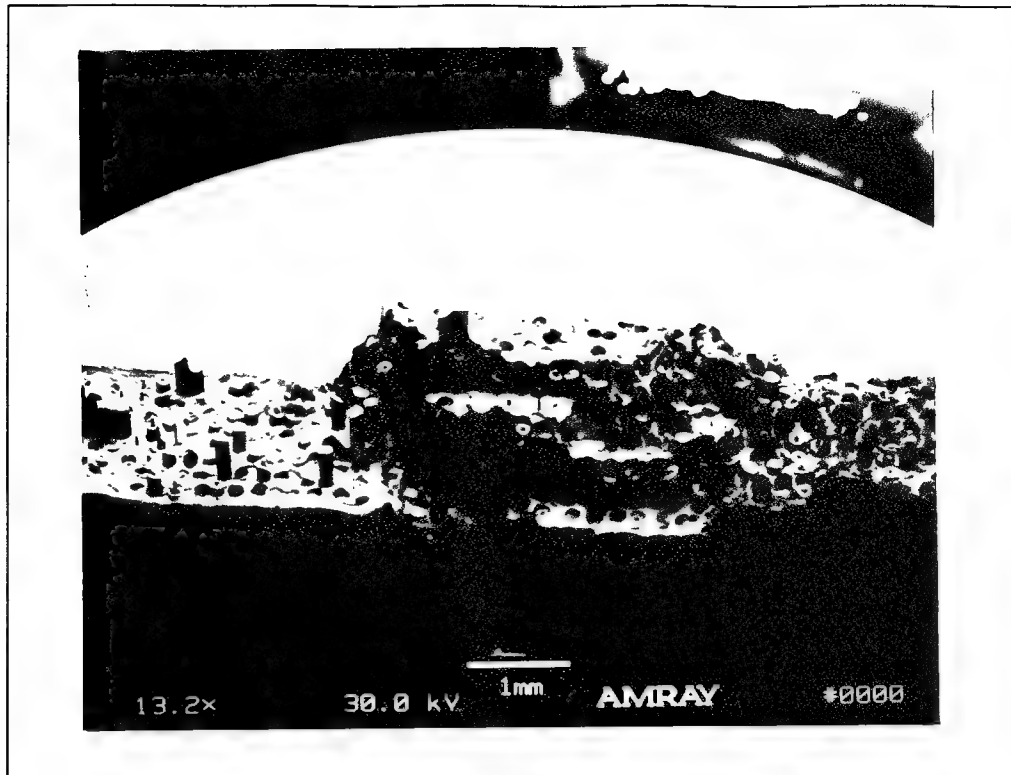


Figure 28. Fracture Surface at 800 MPa, TC HT

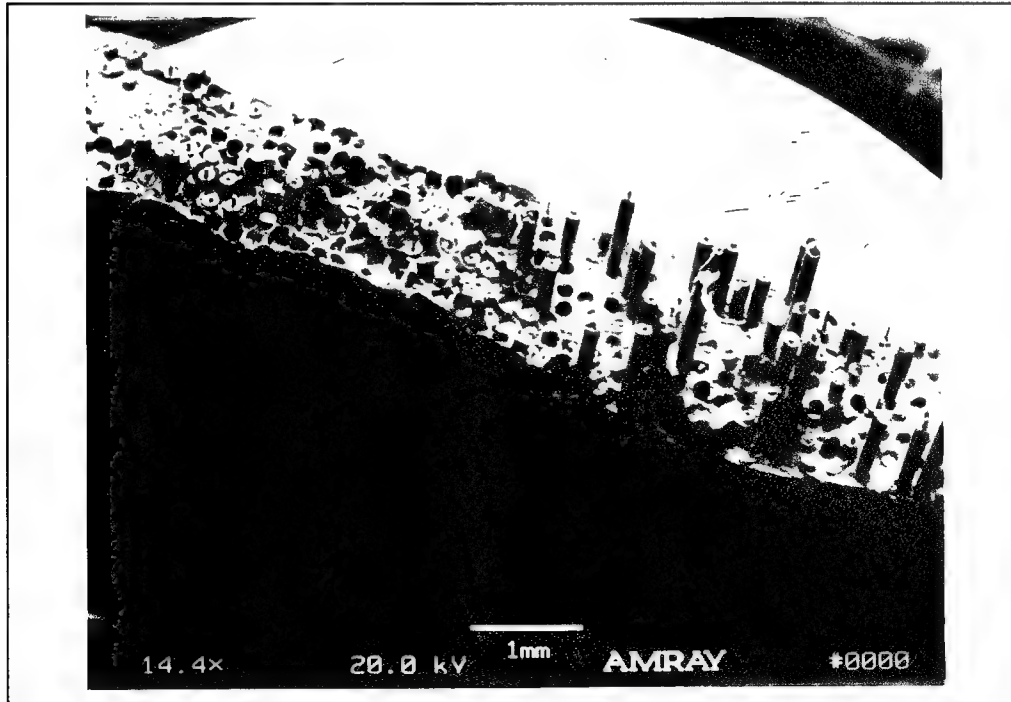


Figure 29. Fracture Surface at 700 MPa, TC HT

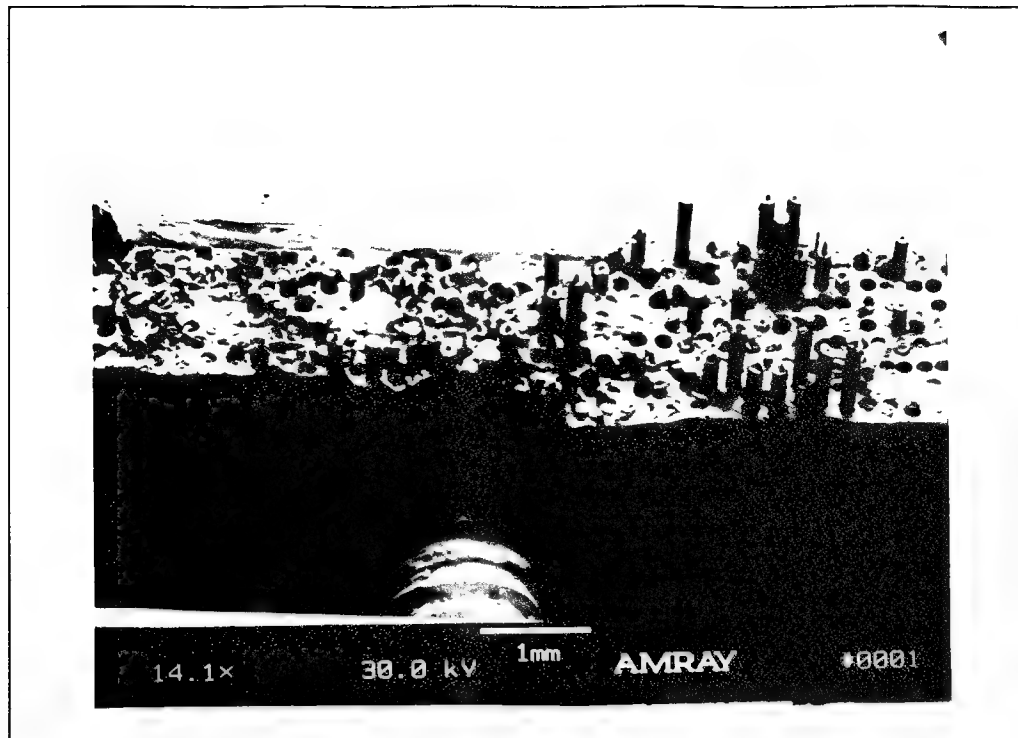


Figure 30. Fracture Surface at 625 MPa, TC HT

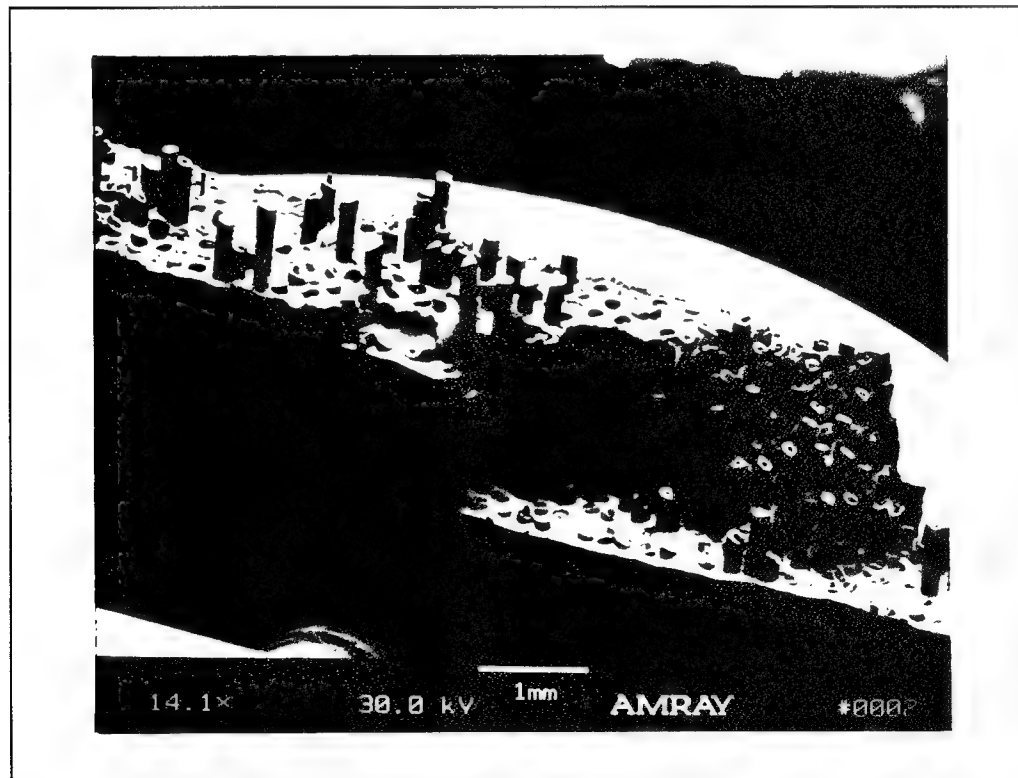


Figure 31. Fracture Surface at 425 MPa, TC HT

While all specimens show some flat area where the fibers remain intact, there also exists an area of fiber pull-out in each case where extensive matrix necking has occurred. Figure 32 shows extensive fiber-matrix debonding in the necked portion of the 800 MPa fracture surface. A closer examination of necked region of the 800 MPa specimen shows ductile void coalescence which is seen as dimples in Figure 33. This indicates that the fibers failed first followed by matrix failure caused by overload in tension. The overload resulted from a smaller amount of fibers carrying the same applied stress. The fibers in the necked region were carrying all the load since the other fibers had already fractured behind the advancing matrix crack tip.

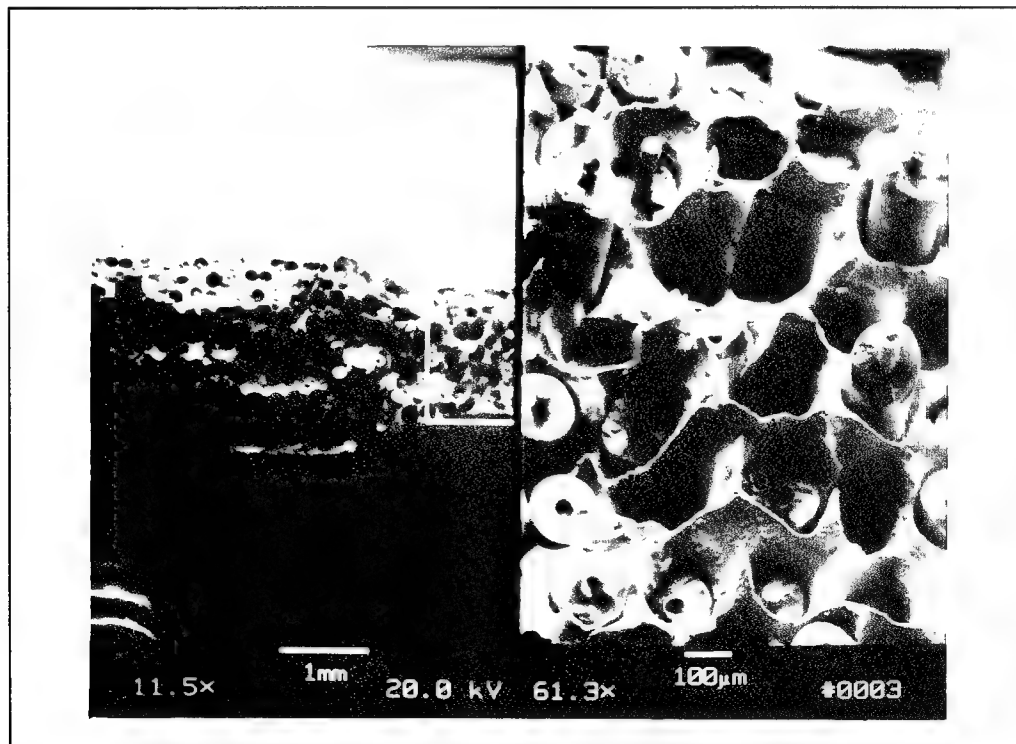


Figure 32. Matrix necking, 800 MPa, TC HT

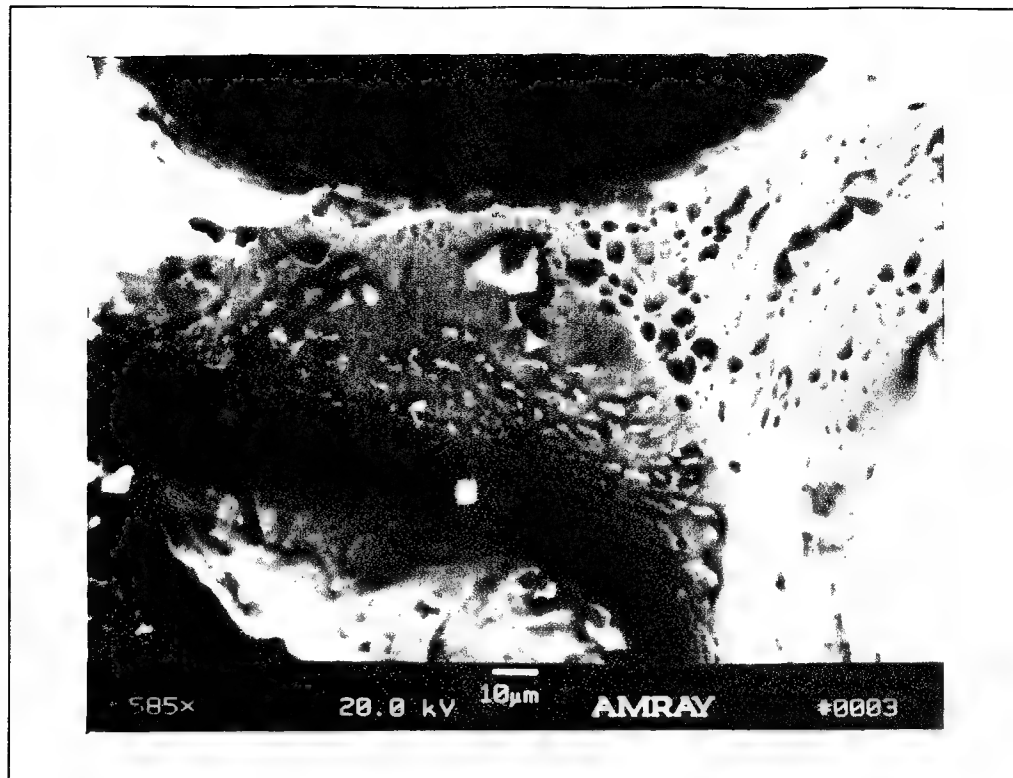


Figure 33. Ductile void coalescence, 800 MPa, TC HT

Examination of the flat portions of the fracture surface provide strong evidence of matrix fatigue crack growth caused by cycling. Figure 34 shows the flat area of the fracture surface at 700 MPa. It consists mainly of fibers that have remained intact. The fibers that appear to have pulled out of the matrix material in the flat region of the fracture surface are caused by random fiber failure as the matrix crack progresses throughout the specimen. Additionally, very little fiber-matrix debonding has occurred. Closer examination yields the presence of fatigue striations in the matrix caused by fatigue cracking. The striations grow parallel to the direction of the crack growth. In Figure 34, cracks can be seen growing from a few different directions.



Figure 34. Fatigue Striations, Intact Fibers, 700 MPa, TC HT

Whereas fatigue striations are present at 700 MPa, they are also found at lower stresses including the specimen cycled at 425 MPa. Recalling that as the surfaces at 800, 700, and 625 MPa contained areas of matrix necking and fiber pull-out, the surface of the 425 MPa specimen is completely flat. All the fibers appear to be intact with little or no fiber-matrix debonding. Initially it may appear that a different failure mechanism is occurring at lower stresses but the presence of fatigue striations, shown in Figure 35, across the entire surface describe numerous matrix cracks growing from different directions. Thus, failure is dominated by matrix cracking at low stresses as well as higher stresses. The progression of matrix cracking, however, requires the previously described group separation. Specimen sectioning clearly illustrates the difference in matrix crack growth between groups 1 and 2.

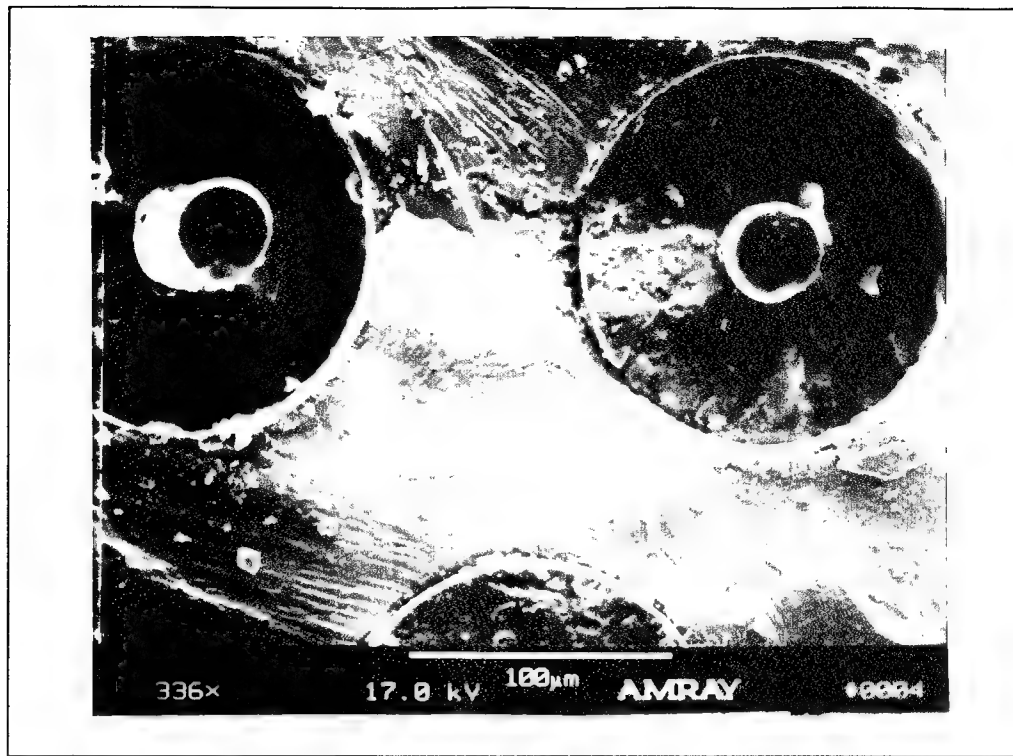


Figure 35. Fatigue Striations, 425 MPa, TC HT

4.4.1.2 Tension-Tension Fatigue Specimens

The examination of the micro-mechanical behavior of tension-tension fatigue loading was limited to the specimen cycled at 800 MPa since it was the only one used for comparison of failure mechanisms. The fracture surface shown in Figure 36 consisted of a small flat portion and a much larger, uneven area where fibers pulled out of the matrix. This is similar to the fracture surface at 800 MPa under tension-compression loading conditions. The flat region indicated matrix cracking while the uneven region once again indicated failure by tensile overload. The only difference between tension-tension and tension-compression loading is the amount of flat area. For the tension-tension loading case, the flat region is much smaller indicating that more of the surface was dominated by fiber pull-out.

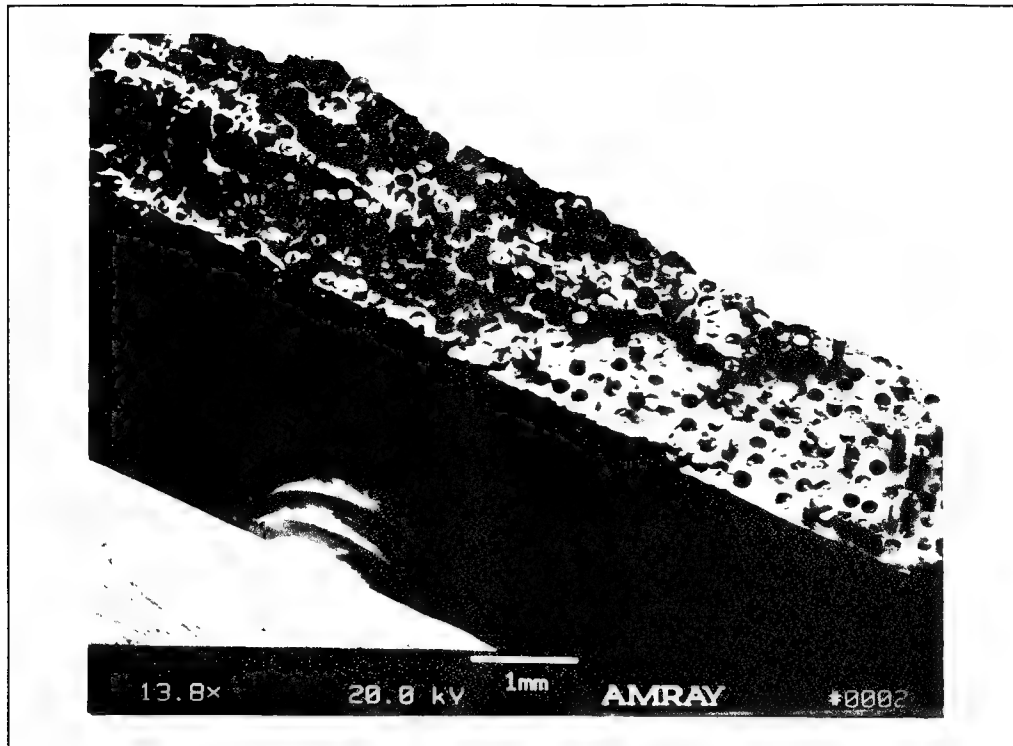


Figure 36. Fracture Surface, 800 MPa, TT HT

4.4.2 Specimen Sectioning

The specimens discussed above were sectioned so that the face could be ground down to the first layer of fibers. These sections show the condition of the fibers and matrix directly behind the fracture surface. For this purpose, several specimens were ground down to the second and third layer of fibers to determine the extent of the damage seen in the first layer.

4.4.2.1 Group 1

Very little damage was observed in any of the specimens in Group 1. Minimal fiber cracking was observed in the specimen cycled at 800 MPa as shown in Figure 37. Also, matrix cracking was limited to very short cracks which bridged only a few fibers. Similar matrix damage was observed at 700 MPa but no fiber cracking existed. Also, the

density of matrix cracks at 700 MPa is roughly the same as that observed at 800 MPa. Thus, in Group 1, damage consists of minimal matrix cracking and even less fiber cracking. It should also be noted that even though fiber bridging did occur, the number of fibers bridged by the matrix crack is minimal when compared with that observed in Group 2. The lack of fiber bridging in these specimens suggests that as matrix cracks developed, one of these cracks became dominant. As the dominant crack propagated through the composite, the additional stress carried by the fibers exceeded the fiber's ultimate strength causing them to fail directly behind the advancing crack tip. Thus, crack propagation is rapid and does not allow the other matrix cracks to mature.

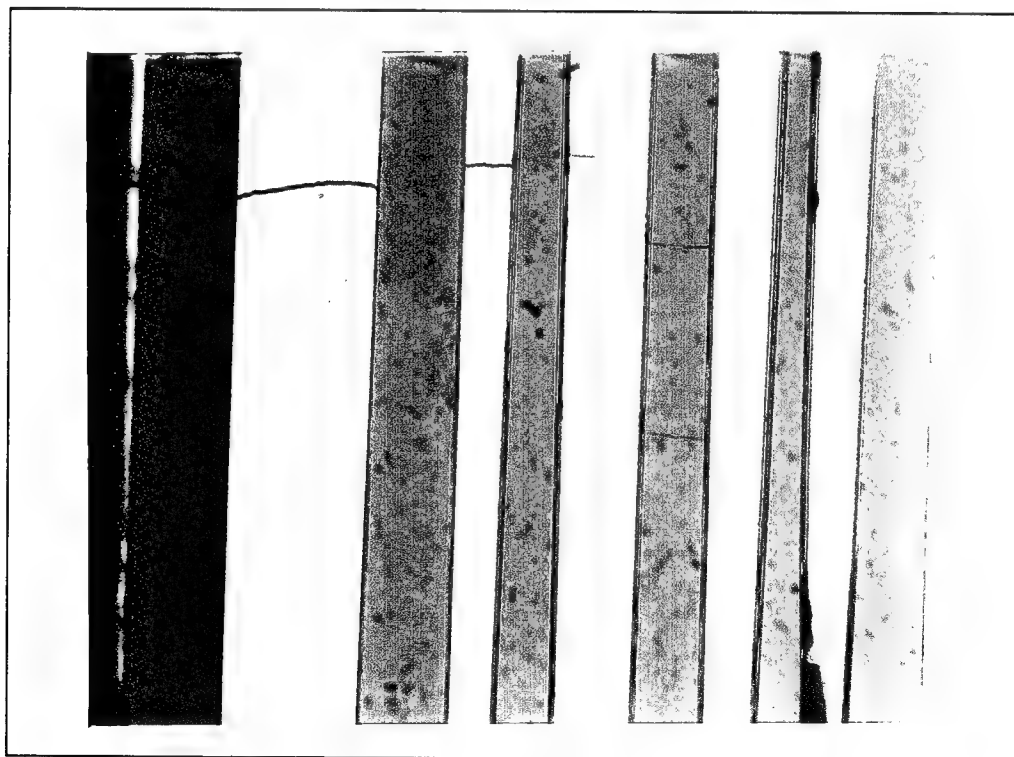


Figure 37. Matrix and fiber cracking, 800 MPa, TC HT

4.4.2.2 Group 2

The damage observed in Group 2 consists of matrix cracking and extensive fiber bridging. As shown in Figures 38-40, the matrix cracks all grow across many lines of fibers without causing fiber failure. This phenomenon, called fiber bridging, was also noted by Sanders in matrix dominated failure modes (33). As cracks grow, they encounter fibers which are much stronger than the matrix in which the cracks are growing. The fiber-matrix interface is relatively weak and rather than progress through the fibers, the cracks progress around them, often causing fiber-matrix debonding. Also seen in Figure 40 are molyweave. Since the molyweave act like precipitates in an alloy, they are strong crack initiation sites. In this specimen, however, cracks did not originate from the molyweave.

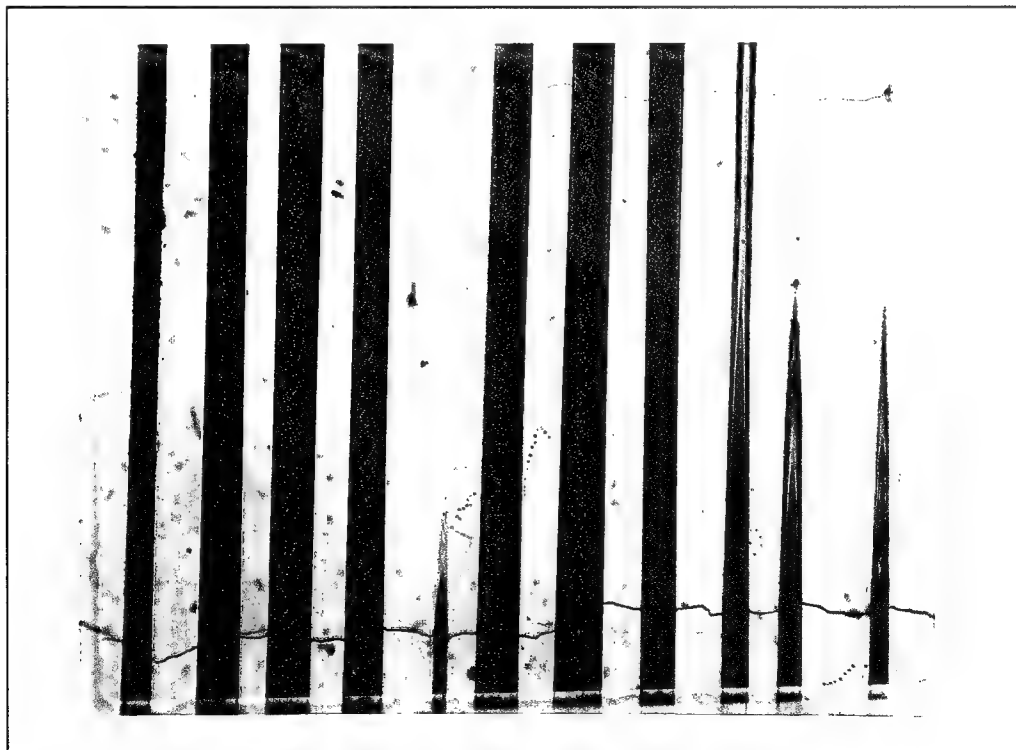


Figure 38. 625 MPa Fiber Bridging

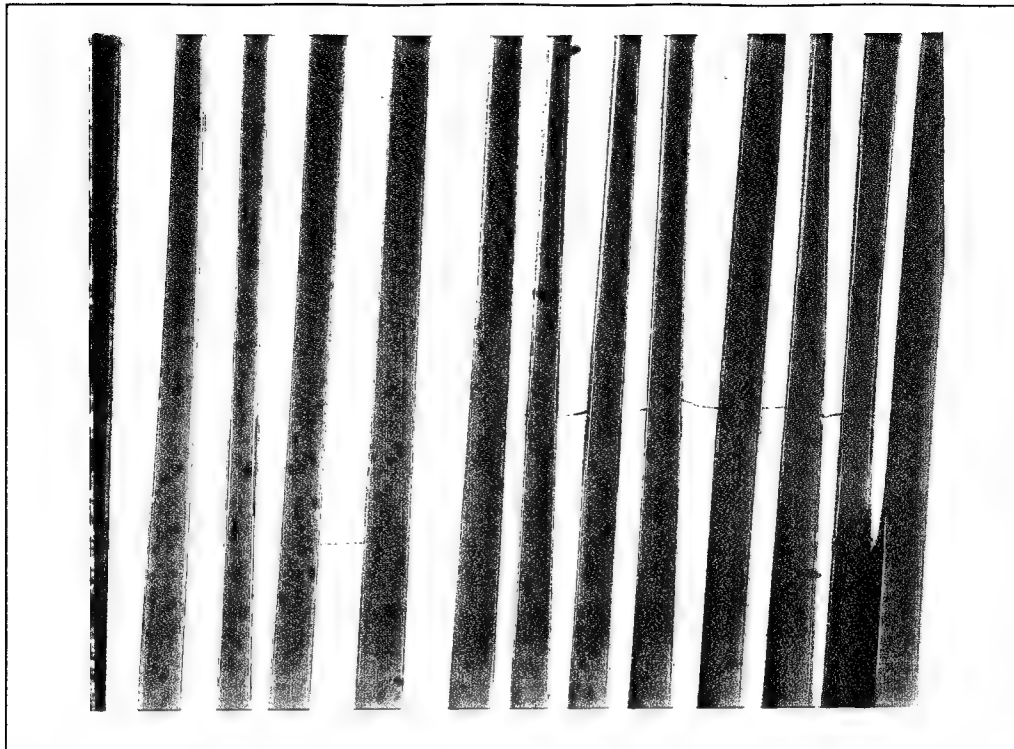


Figure 39. 500 MPa Fiber Bridging, TC HT

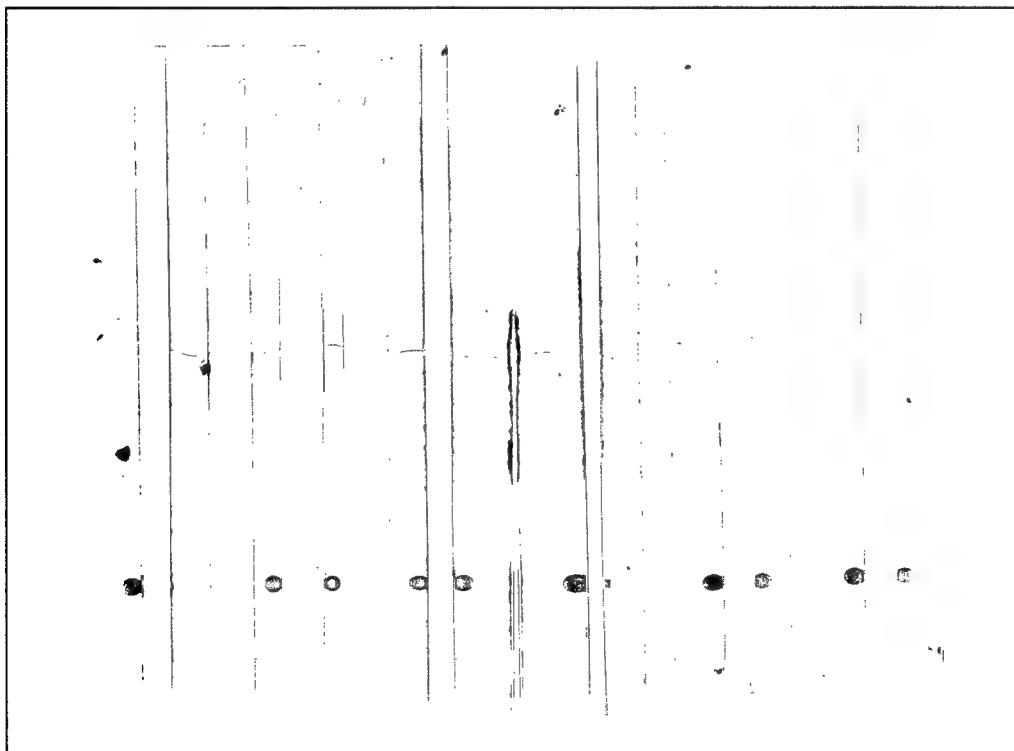


Figure 40. 425 MPa Fiber Bridging and Molyweave

The density of matrix cracks in Group 2 varies with the applied stress. As the stress increases, crack density increases. Although overall crack density is still relatively small even at 625 MPa, it is much greater than that observed at 425 MPa. Increased matrix crack density also explains the increase in the amount of modulus degradation discussed in the macro-mechanic results for Group 2 (Figure 17).

Crack initiation sites were not limited to any particular region of the test specimens. While some cracks initiated on the edge of the specimen, Figure 41, others originated in the middle, Figure 42. This indicates that while the specimen edges are important crack nucleation sites, fatigue cracks can still develop within the material, far from the edge. Cracks that developed within the material initiated from fiber-matrix interface failure, as shown in Figure 42, caused either by other cracks that had bridged the fibers or by interface defects.

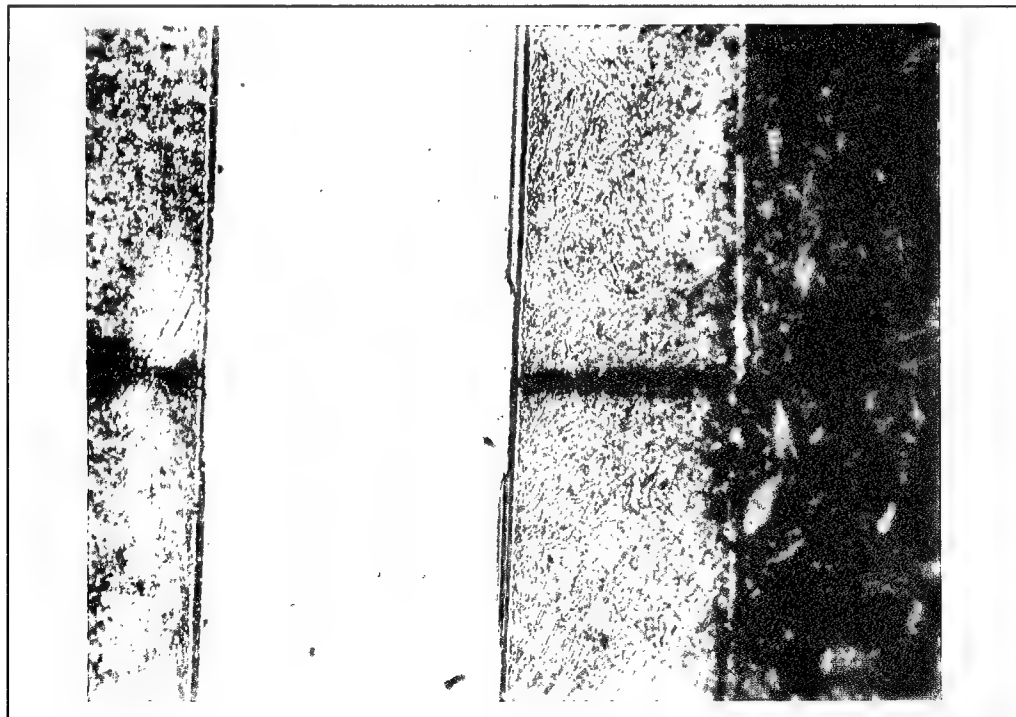


Figure 41. Edge Crack Initiation, 625 MPa, TC HT

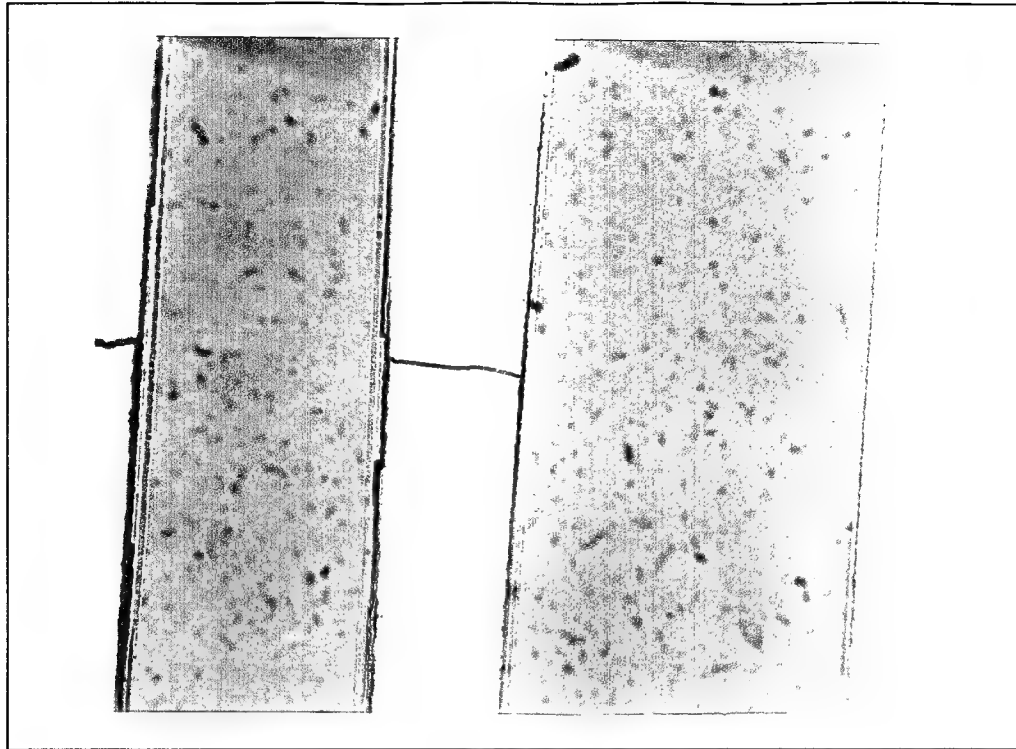


Figure 42. Crack Initiation Within Specimen, 500 MPa, TC HT

Acid etching of the face sections brings out the grain boundaries and plasticity. Grain boundaries do not impede crack growth as can be seen in Figure 43 where cracks grow across grain boundaries. No plasticity was found in the matrix, but slip bands were found surrounding the crack as would be expected. The material in front of the crack tip deforms plastically, resulting in the slip bands seen in Figure 44.

As can be seen from the sectioned samples, no fiber fracture was observed in Group 2. Evidence of matrix cracking was observed in all specimens, both on the fracture surface and in the sectioned samples. The necked regions of the fracture surfaces can now be explained by tensile overload while the flat areas contain strong evidence of fatigue crack growth.



Figure 43. Transgranular crack growth, 425 MPa, TC HT

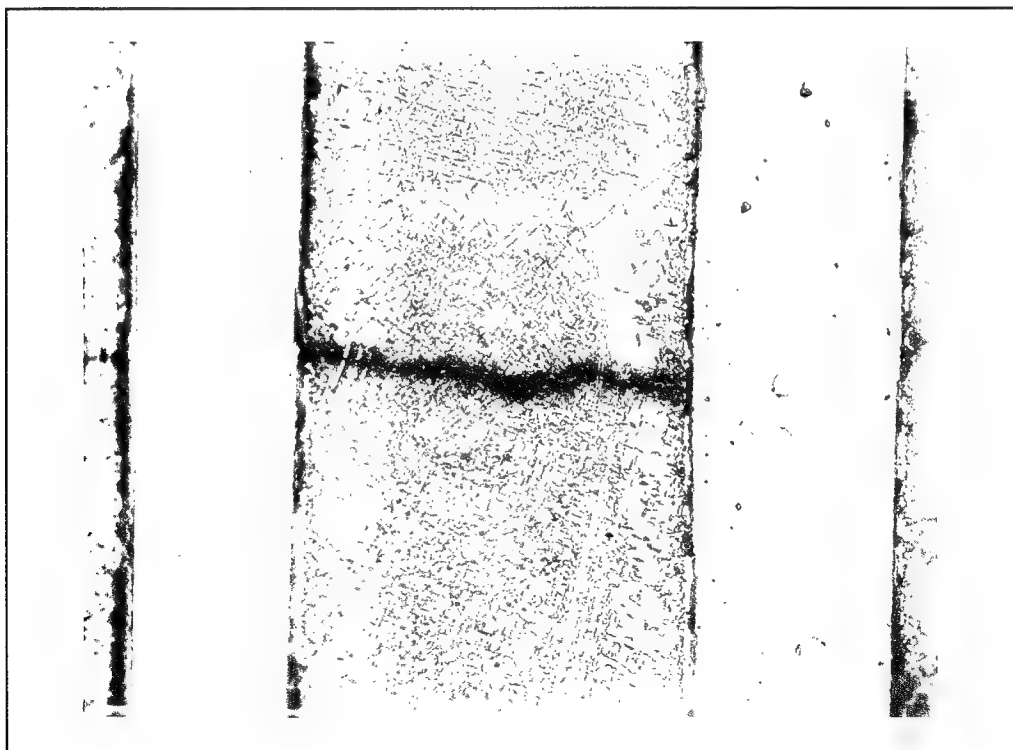


Figure 44. Slip bands around crack, 425 MPa, TC HT

4.4.2.3 Group 3

One specimen in Group 3 was sectioned even though failure had not occurred. Figure 45 shows minimal matrix cracking. In addition, matrix cracks did not progress through the composite indicating they were not detrimental to fatigue life. Even though these specimens have an extremely long fatigue life, failure will eventually occur. Figure 45 indicates that the failure mechanisms associated with these stress levels are most assuredly matrix dominated but further study in this regime of the fatigue life curve is needed to more fully understand the material's behavior at low cyclic stresses.

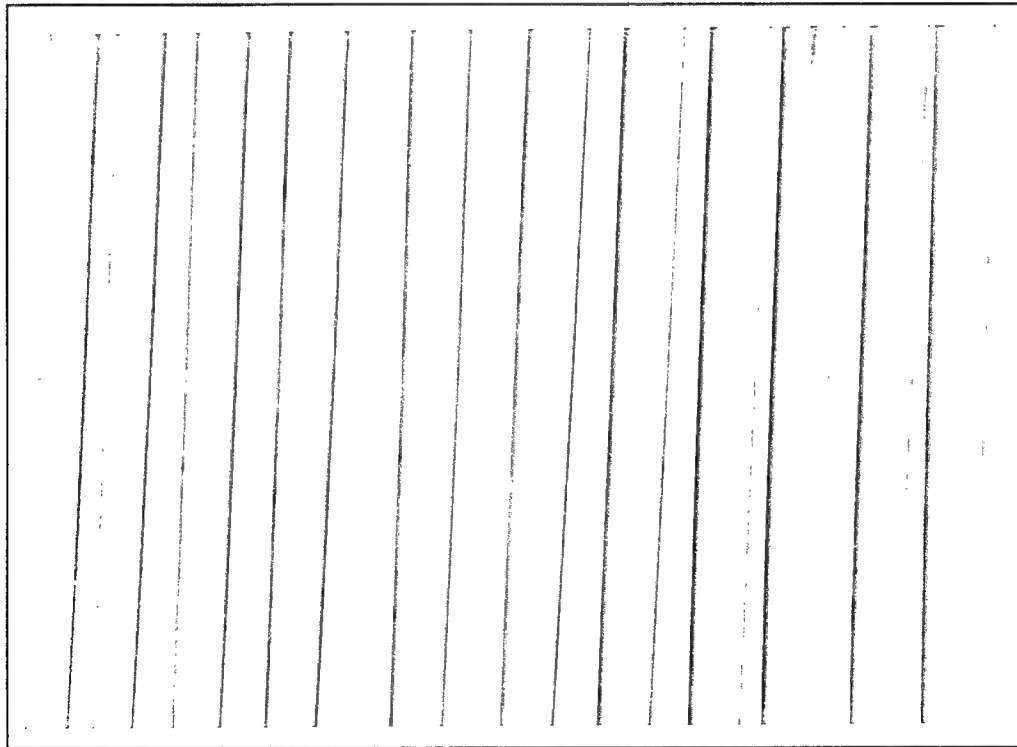


Figure 45. Face Section, 375 MPa, TC HT

4.4.2.4 Tension-Tension Sectioning

Figure 46 shows some fiber fracture with little or no matrix cracking at 800 MPa. Also, very little fiber-matrix debonding was visible. This evidence of fiber cracking

combined with the flat portion of the fracture surface suggest that the specimen failed under a combination of failure mechanisms which include both fiber and matrix fracture. Matrix creep observed in the strain trends previously discussed offers an explanation for fiber cracking. Majumdar and Newaz (24) have suggested that matrix creep results in a drop in matrix stress, forcing the fibers to carry more load, hence causing fiber cracks.

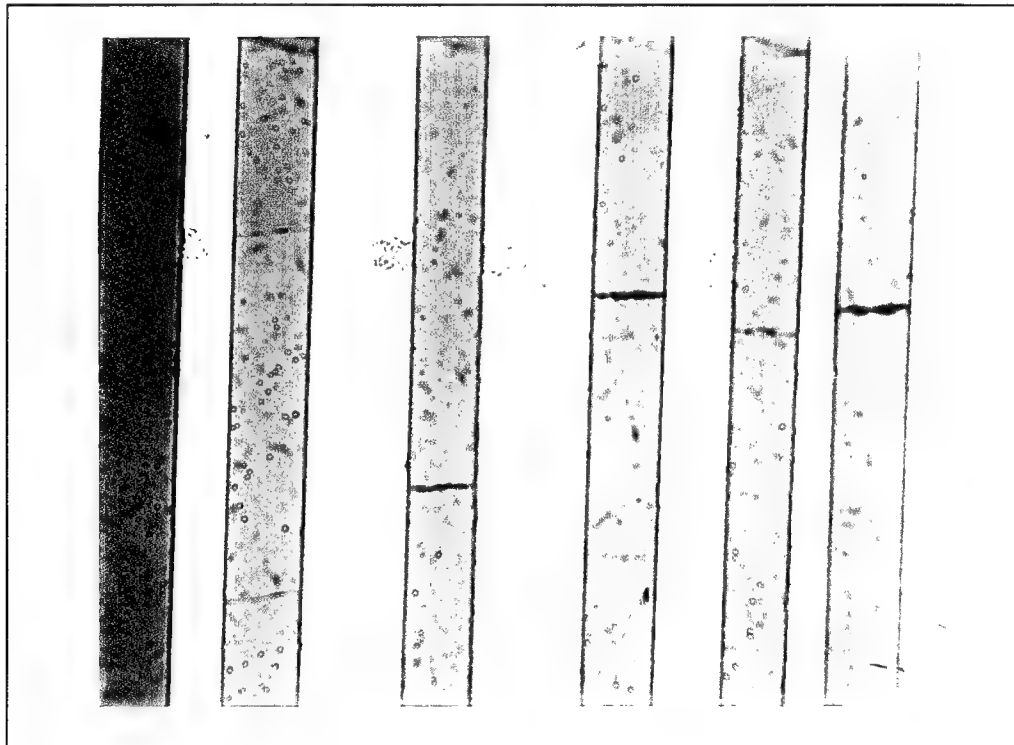


Figure 46. Fiber fracture, 800 MPa, TT HT

4.4.3 Matrix Plasticity

Evidence of matrix plasticity was also absent from all fatigue tests in this study. The specimen cycled at 800 MPa was acid etched to check for slip bands indicating matrix plasticity. No such evidence was found. The etched face section is shown in Figure 47. In a previous study, Sanders found no evidence of matrix plasticity below 0.55% maximum strain, the elastic limit of the matrix material (33). The maximum strain

corresponding to 800 MPa falls well below that limit. Also, a micro-mechanical analysis in Appendix A shows that the matrix stresses at 800 MPa are far below the proportional limit of the matrix material. Therefore, to obtain matrix plasticity, the laminate must be cycled above 0.55% maximum strain regardless of the loading type, e.g. tension-tension vs. tension-compression.

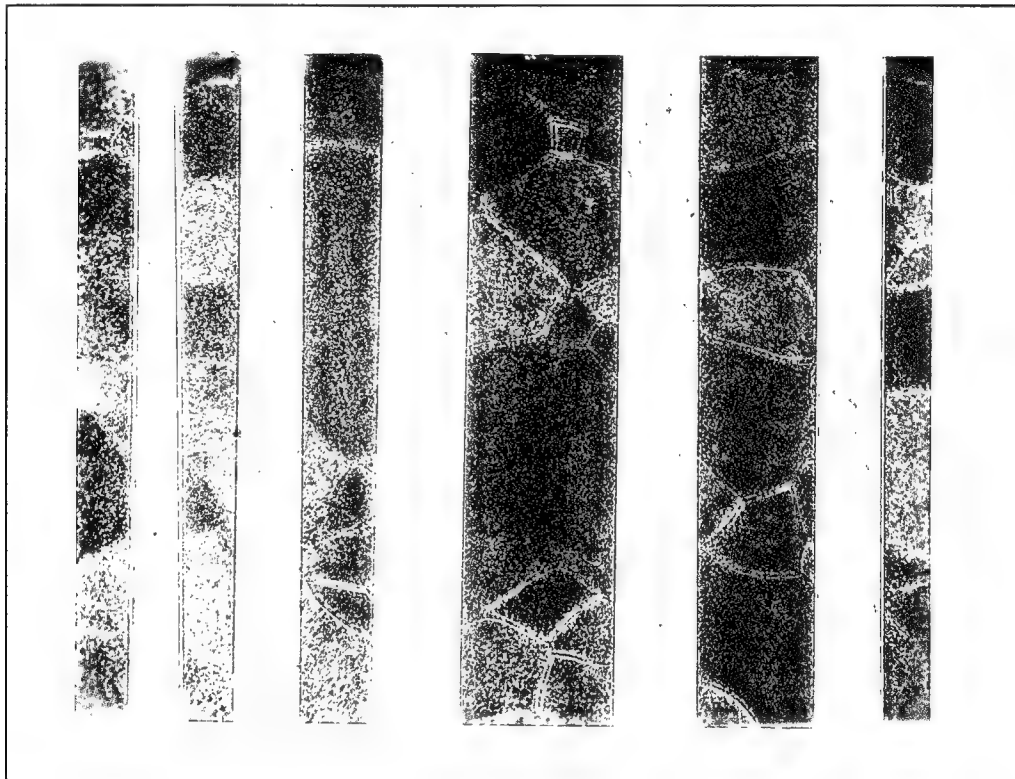


Figure 47. Etched Face Specimen, 800 MPa

4.4.4 Summary of Micro-mechanical Behavior

All of the tension-compression specimens in this study were dominated by matrix failure. The fracture surfaces all show some flat region with fibers intact indicating matrix cracking. Also, fatigue striations are found in this region at all stress levels providing evidence of fatigue crack growth. The uneven, necked region of the fracture surfaces consist of fibers that have pulled out of the matrix and matrix necking. Dimples

indicating ductile failure prove that the matrix in this region failed in tensile overload after the remaining intact fibers failed.

The progression of matrix crack growth differed between groups 1 and 2. In Group 1, very little fiber bridging was found while specimens in Group 2 showed much more fiber bridging. In addition, the crack density in Group 2 increased with increasing stress. Macro-mechanical analysis of Group 2 showed more modulus degradation at higher stresses due to the increased matrix crack density. The lack of fiber bridging in Group 1 and the speed with which matrix cracks progressed through the specimen suggest that fibers failed directly behind the advancing crack tip.

Micro-mechanic comparison of tension-tension and tension-compression fatigue tests shows that for the identical maximum stress level, the failure mechanisms are not the same. The tension-tension fracture surface contained less flat area and the face section contained fiber cracking in the absence of matrix cracking. The presence of creep in tension-tension loading reduces matrix stress, thereby increasing fiber stress and causing fiber cracking. No creep was observed in tension-compression loading where failure was completely dominated by matrix cracking. Thus, failure at 800 MPa TT HT was dominated by a combination of matrix and fiber failure while failure at 800 MPa TC HT was dominated primarily by matrix cracking. Now that both the macro-mechanical and micro-mechanical behavior have been described, an analysis of the fatigue life can be completed. Such analysis, along with some analytical predictions of the stress in the 0° fibers and matrix are presented in Chapter 5.

5. Fatigue Life

The macro-mechanical and micro-mechanical results presented in chapter four described the behavior of the material. The purpose of this chapter is to interpret the observed behavior in an engineering sense. In this chapter an analysis of the fatigue life for the unidirectional metal matrix composite is discussed. In addition, a comparison of fatigue life behavior between a unidirectional, $[0]_8$ and cross-ply, $[0/90]_{2s}$ laminates is given.

5.1 Tension-Compression Fatigue Life

Eight fatigue tests were performed at an elevated temperature of 427 °C to determine the S-N curve for the unidirectional laminate under tension-compression fatigue. Figure 48 shows the S-N curve based on maximum stress for data obtained in this study. Region I is defined by stress levels where the failure mode was dominated by fiber fracture. No data was obtained in this region but existing data from previous studies suggests that this portion of the S-N curve would consist of fiber dominated failure (4,29). Region II is defined by stress levels that cause failure due to matrix cracking and is divided further into Region IIa and IIb. Region IIa contains Group 1 specimens, as discussed in Chapter 4, where failure is dominated by short matrix cracks and minimal fiber bridging. Region IIb contains Group 2 specimens, and is dominated by long matrix cracks with extensive fiber bridging. Region III is designated by stress levels that fall

below the fatigue limit of the matrix material resulting in lives more than 10^6 cycles.

Specimens in Group 3 fall within this region.

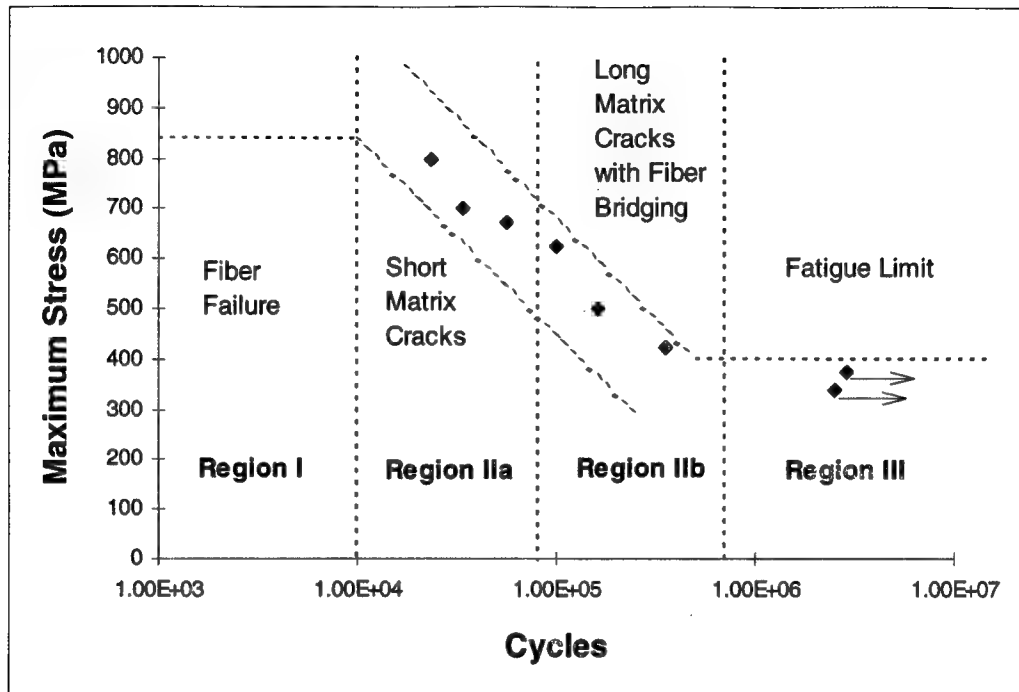


Figure 48. $[0]_8$ Tension-Compression Fatigue Life Curve

5.2 TC vs. TT Fatigue Life Comparison

There are several methods for comparing fatigue data collected under different R-ratios. A Goodman diagram can be useful if there exists data for many R-ratios. Since only two R-ratios ($R=0.1, -1$) were studied in the current research, there is not sufficient data to produce a definitive Goodman diagram. Therefore other comparison methods must be used. Many tension-tension studies have compiled data based on maximum stress or strain (6,9,11,19,21,29,33,34). Comparison based on these maximum values for tension-compression data, however, neglects 50% of the loading cycle and, therefore, must be used with caution. Another method of comparison is strain range. This method

is popular since it is well established that fatigue of metals is strain range controlled (12). Fatigue life comparisons based on all these different parameters will be discussed next.

5.2.1 Maximum Stress/Strain Basis

Figures 49 and 50 show the S-N curves based on maximum stress and strain, respectively, for data obtained in this study and tension-tension data of the same material obtained from other sources (22,29). Maximum strain data was taken to be the strain at the half fatigue life of the specimen. As shown in these figures, the fully-reversed fatigue life based on maximum applied stress or strain is less than that for tension-tension loading. The reduction in fatigue life under tension-compression loading stems from the amount of the matrix stresses. Under tension-tension loading, the stress in the matrix relaxes as the fiber stress increases. Laminate strain is equal to fiber strain for a unidirectional composite. Therefore, as laminate strain increases, fiber strain increases, which also increases fiber stress if there is no change in stiffness. Since laminate stress is constant, an increase in fiber stress must be accompanied by a decrease in matrix stress. Under tension-compression fatigue, no increase in laminate strain was observed without a loss of stiffness. Therefore, fiber and matrix stresses remain constant. The overall effect is that matrix stress under tension-tension fatigue is less than that obtained in tension-compression fatigue. Smaller matrix stresses lead to longer fatigue lives when failure is dominated by matrix cracking.

Another reason for the reduction in fatigue life under tension-compression loading is additional damage resulting from the compressive portion of the loading cycle. Broek states that in metals, compression loading creates intrusions or extrusions that may grow into cracks. In tension-tension, intrusions may still be formed due to the presence of residual compressive stresses (residual tensile strains) during load release, but the mechanism for forming them is much weaker (5:57-59). Since failure in this study was

dominated by matrix cracking, it is reasonable to suggest that these processes were occurring in the titanium matrix material.

A third explanation for the longer life under tension-tension after initiation of damage can be found in the role of the fibers. Compression-induced effects such as fiber buckling and delamination reduce the dominance of the fibers in determining fatigue life. In this situation, the matrix and interface play more important roles (11:489). Previous discussion of the tension-tension failure mechanism at 800 MPa, in Chapter 4, concluded that failure was dominated by a combination of matrix and fiber cracking while failure of the tension-compression specimen at 800 MPa was dominated solely by matrix cracking and fiber bridging. Figure 27 showed that once damage initiated under tension-compression fatigue, it progressed through the laminate much faster than under tension-tension fatigue. The role of fibers in determining failure, the relatively slow speed of damage propagation, and the presence of fiber bridging under tension-compression suggest that fibers play an important role in hindering matrix crack propagation under tension-tension fatigue loading.

Another possible cause of the difference in fatigue life is the effects of compression on the plastic zone surrounding the crack tip. In metals, tensile loading forces the plastic zone size to increase as slip occurs. Work hardening and increasing stress eventually blunt the crack tip. Upon unloading, the elastic material around the plastic zone creates compressive forces that result in reverse slip and sharpen the crack tip. If the cycle continues to apply a compressive stress, the effect may be increased sharpening of the crack tip, resulting in a greater stress concentration. Thus, the compression portion of the loading cycle may make crack growth easier than under purely tensile fatigue.

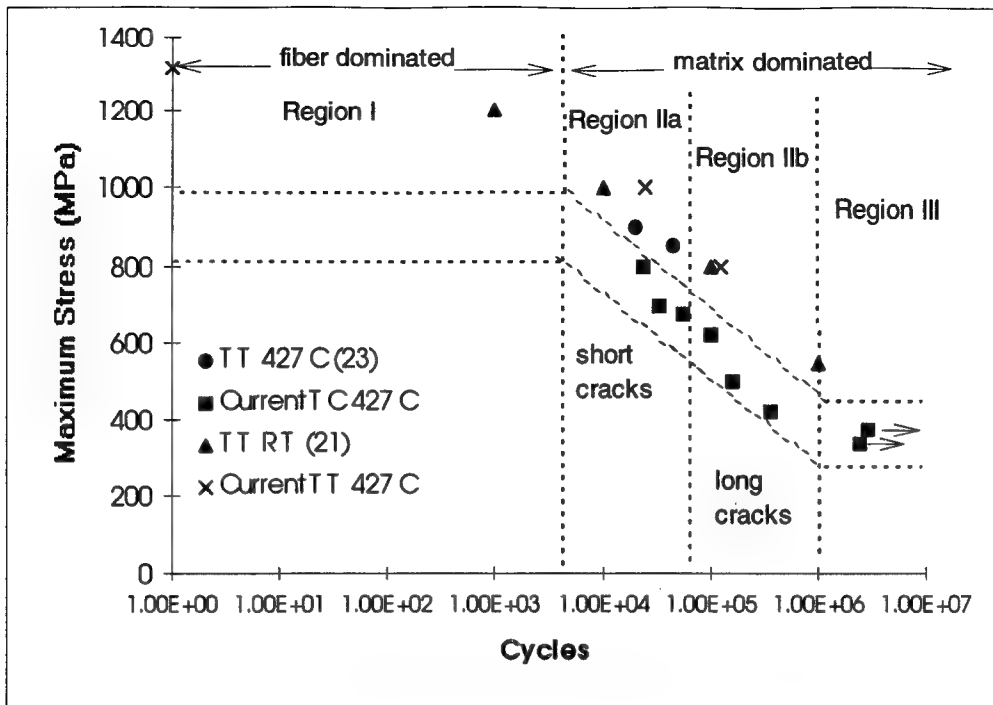


Figure 49. Maximum Stress Fatigue Life Curve

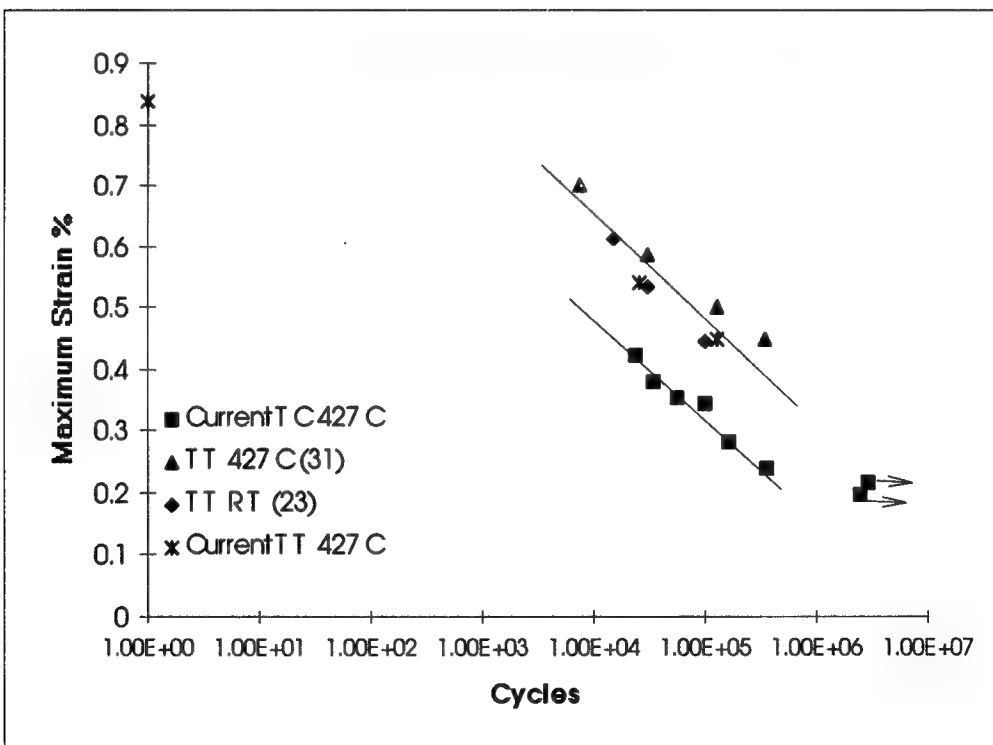


Figure 50. Maximum Strain Fatigue Life Curve

5.2.2 Stress/Strain Range Basis

In contrast to maximum stress and strain comparison, tension-compression fatigue life is actually longer than tension-tension life based on stress or strain range. Figures 51 and 52 show data based on stress and strain ranges for the current study and several other tension-tension studies. Boyum suggested that longer fatigue life based on stress and strain ranges is a result of the mean stress applied throughout the fatigue test (4). Mean stress is defined by:

$$\sigma_m = \frac{\sigma_{\max} + \sigma_{\min}}{2} \quad (2)$$

In the tension-tension test case, $R = 0.1$, the mean stress is greater than zero. Under tension-compression loading, $R = -1$, the mean stress equals zero thereby eliminating any residual strain effects during the loading cycle.

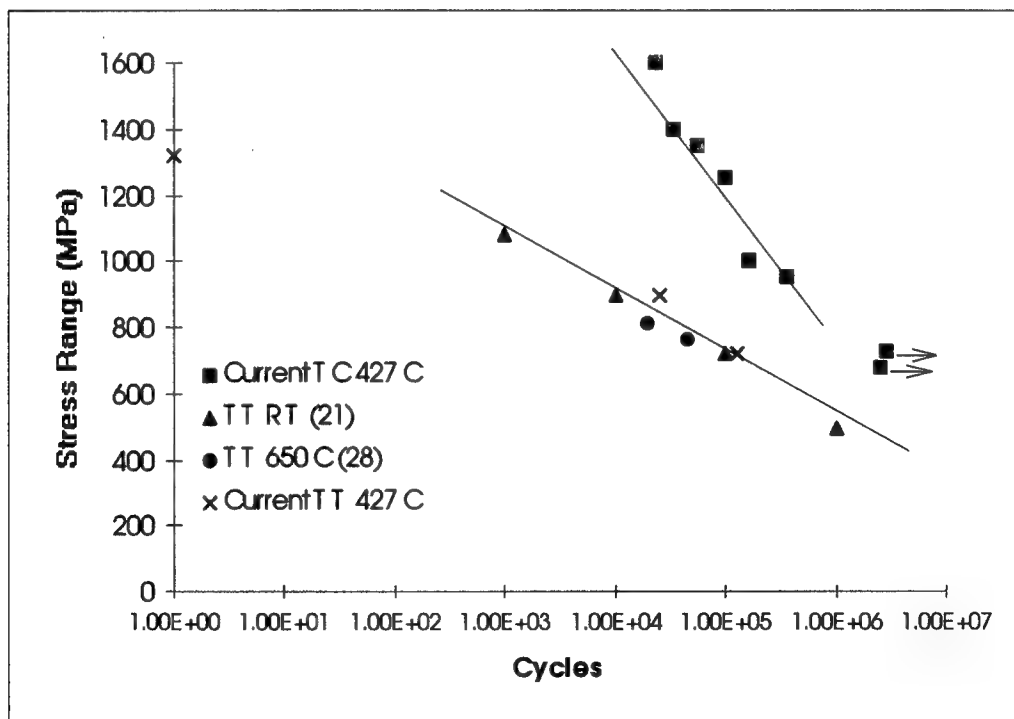


Figure 51. Stress Range Fatigue Life Curve

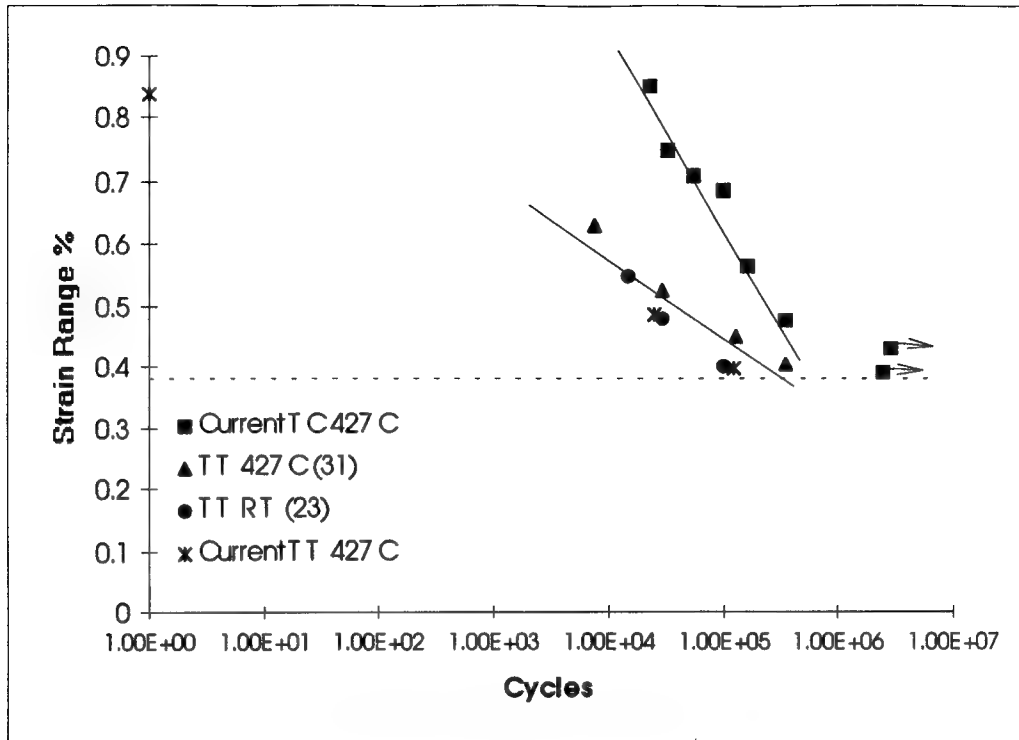


Figure 12. Strain Range Fatigue Life Curve

Further examination of Figure 52 suggests that the fatigue limit is governed by strain range. As shown, the tension-tension and tension-compression data fall together around a strain range of 0.35%, showing that failure is not observed below this point. No such trend occurs based on stress range. Additionally, maximum strains less than 0.35% under tension-compression fatigue loading do produce failure as shown in Figure 50. Thus, strain range may be a material parameter which can be used to identify the fatigue limit for both tension-tension and tension-compression fatigue.

5.3 $[0]_8$ vs. $[0/90]_{2s}$ Fatigue Life Comparison

Figure 53 shows the S-N curves for both the $[0]_8$ and $[0/90]_{2s}$ laminates under tension-compression fatigue loading at 427 °C. The unidirectional laminate has a much

longer fatigue life. Such behavior has been documented previously for tension-tension fatigue in previous studies (15, 20, 26, 29). In these studies, fatigue life became shorter as the percentage of 0° fibers in the laminate decreased. Thus, the fatigue life trend observed under tension-tension fatigue also occurs under tension-compression fatigue. The following sections describe the methods to collapse all of the data onto a single master curve for design purposes.

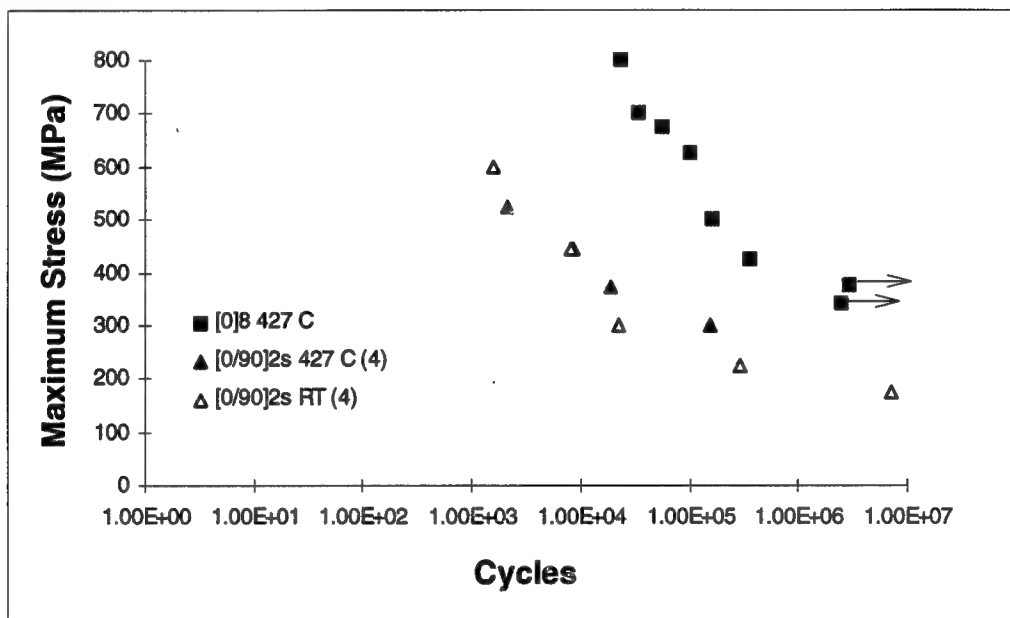


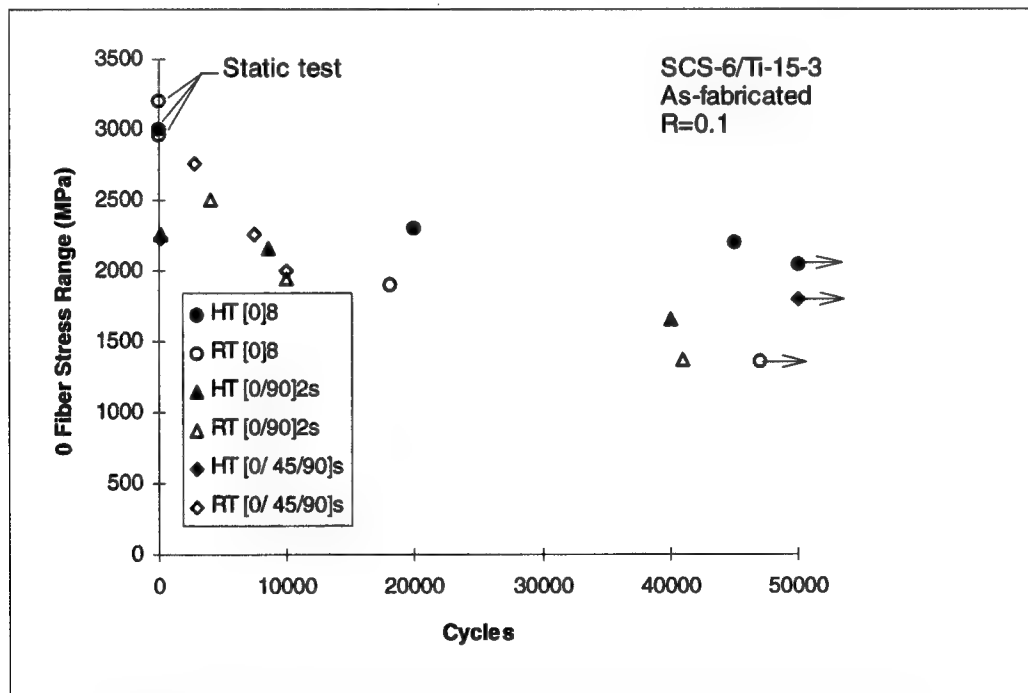
Figure 53. $[0]_8$ vs. $[0/90]_{2s}$ Fatigue Life Comparison

5.4 0° Fiber Stress Analysis

It has been shown that fatigue life increases under fully-reversed fatigue loading based on applied stress or strain ranges (Figures 51 and 52). It has also been shown that the fatigue life for a unidirectional composite under any type of loading is greater than that for a laminate containing off-axis plies subjected to the same type of loading.

Pollock and Johnson tested numerous laminates, including unidirectional, which

contained different percentages of 0° fibers (29). Initially, they found that the 0° fiber stress range plotted against the cycles to failure at room and elevated temperature fell within a single band with more scatter at high temperature. This suggested that 0° fiber stress governed fatigue life. But upon further examination, they concluded that two distinct fatigue life curves are present (Figure 54). The first curve contains all laminates at room temperature and 650°C except the high temperature $[0]_8$ laminate which formed its own curve slightly above the other lay-ups. Although not all data falls within a single band, it is interesting to note that the only exception is the high temperature $[0]_8$ laminate. Subsequent testing under different loading conditions, e.g. TMF, in-phase, out-of-phase, showed that the loading conditions greatly affected the fatigue life curves based on 0° fiber stress. Johnson found that while data falls within a single band for a given loading condition, it does not correlate between loading conditions.



The current data was analyzed in a similar fashion to determine whether tension-tension and tension-compression fatigue loading result in a single or multiple fatigue life curves and also if tension-compression fatigue constitutes a different loading condition from tension-tension fatigue. A simplified approach was used in this study to obtain the stress in the 0° fiber. Perfect bonds are assumed between plies so that the strain exhibited by the composite is the same as the strain exhibited by the 0° fibers. Also, residual thermal stresses are assumed to be small. Knowing the modulus of the 0° fibers (400 GPa), the stress can be easily calculated from Hooke's law (Eq. 1). A micromechanical analysis presented in Appendix A shows that these calculations are accurate.

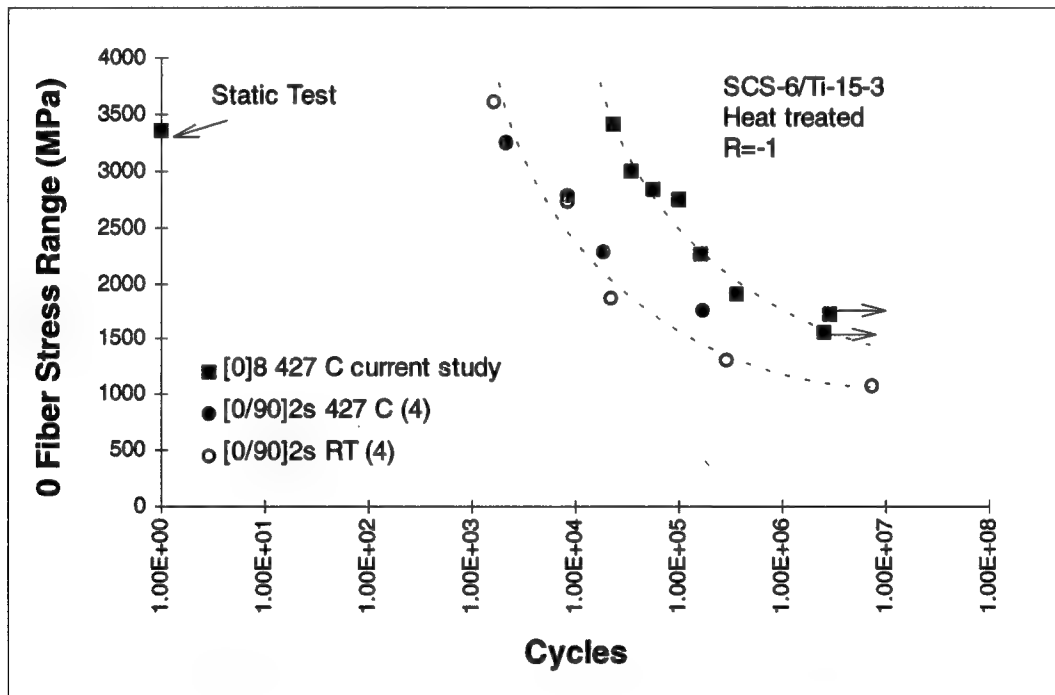


Figure 55. 0° Fiber Stress Fatigue Life Curve, $R = -1$

The 0° fiber stress range for the current study is plotted against cycles to failure in Figure 55. Also plotted are the results of some $[0/90]_{2s}$ fully-reversed fatigue tests conducted at room temperature and 427°C (4). All $[0/90]_{2s}$ data falls along the same line

while the unidirectional high temperature data shows a slightly longer fatigue life. Thus, two lines are formed by the data and a trend similar to that of Johnson is observed under both tension-tension and tension-compression fatigue.

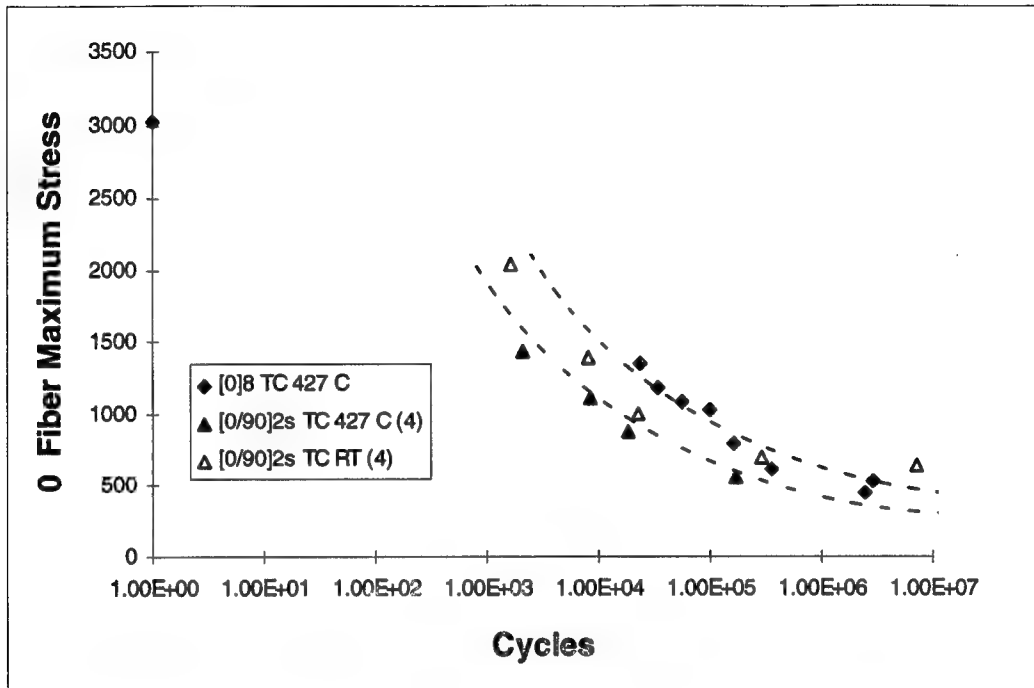


Figure 56. Maximum 0° Fiber Stress Fatigue Life Curve, $R = -1$

Figure 56 plots the maximum 0° fiber stress for the same materials as shown in Figure 55. Unlike the results based on fiber stress range, the fatigue life curves for the different laminates collapse onto a single curve based on maximum fiber stress.

Although there is some scatter in the data, all points fall within a factor of two, the standard band size for interpreting fatigue life data. Since the maximum 0° fiber stress yields a single fatigue life curve, it is likely that the 0° ply stress will produce similar results.

5.5 0° Ply Stress Analysis

Another parameter that may govern fatigue life is the stress in the 0° ply. Such an approach has been suggested by Gao, et.al. (10). They found that the fatigue life curves for tension-tension loading collapsed together based on the 0° ply maximum stress. It is not important to know, in this approach, how the damage is accumulated (i.e., how the specimen failed), therefore all forms of failure may be included in the analysis. Figure 57 shows the fully-reversed fatigue life curves for both the unidirectional and the cross-ply laminates at room temperature and 427 °C based on maximum stress.

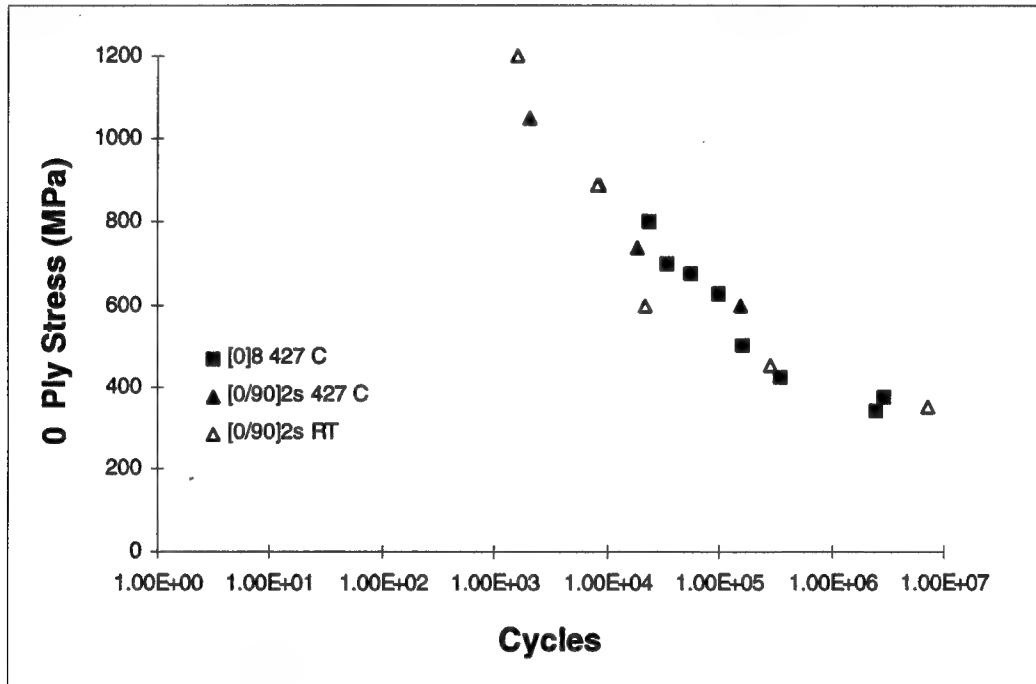


Figure 57. 0° Ply Stress Fatigue Life Curve

For the unidirectional laminate, the 0° ply stress is simply the stress in the laminate. For the cross-ply laminate, [0/90]_{2s}, calculation of the 0° ply stress is also straightforward. The 90° plies are assumed to carry no load, therefore the equivalent area carrying the

applied load is exactly half the area of the laminate. Unlike the two curves produced by 0° fiber stress analysis, all data falls onto a single curve, thereby supporting Gao's hypothesis.

Comparison of this data between tension-tension and tension-compression fatigue does not produce a single fatigue life curve. Rather, the same trends seen in the laminate fatigue life comparison appear in the comparison of 0° ply stress. Based on maximum stress, tension-tension yields longer fatigue life, but based on stress range, tension-compression yields longer fatigue life. Therefore, stress in the 0° ply can only be used to determine fatigue life for a given loading condition (i.e., R-ratio, TMF).

6. Conclusions

In this study, the deformation mechanisms in a unidirectional, $[0]_8$ SCS-6/Ti-15-3, MMC laminate were investigated under tension-compression fatigue at an elevated temperature of 427 °C. Stress-strain data during cycling was used to evaluate the macro-mechanic behavior of the material and microscopic evaluation was performed to characterize the damage on a micro-mechanic level. Fatigue life curves were plotted based on different parameters such as stress or strain. In addition, a comparison of tension-tension and tension-compression failure modes was completed.

The fully-reversed fatigue tests in this study were separated into three groups based on macroscopic trends and failure modes. Groups 1 and 2 were dominated by matrix cracking while Group 3 contained specimens that were cycled below the fatigue limit of the laminate. Fracture surfaces and specimen sectioning revealed that Groups 1 and 2 were both dominated by matrix cracking, yet the propagation of cracks formed a distinct separation between the two groups. In Group 1, which contained specimens between 675 and 800 MPa, specimen sectioning revealed a few short matrix cracks which bridged only a few fibers. In Group 2, which contained specimens cycled between 425 and 625 MPa, matrix cracks were longer, more numerous, and bridged many fibers without causing fiber fracture. Less bridging in Group 1 is caused by the rate of cracks growth at higher stress. Once cracks develop at high stress, a single crack becomes dominant. This crack, then, propagates very rapidly through the matrix. The amount of stress added to the fibers due to matrix cracking causes the fibers to fail directly behind

the advancing crack tip. Other cracks are not allowed to develop given the rate of damage incurred due to the dominant crack.

A comparison was made between tension-tension and tension-compression failure modes. Both specimens were cycled at a maximum stress of 800 MPa. For the fully-reversed case, failure was dominated by matrix cracking. For the tension-tension case, failure was dominated by a combination of fiber and matrix cracking. This difference in failure modes suggests that the fibers play a more important role in determining fatigue life under tension-tension fatigue. On the other hand, compression effects make the matrix and fiber/matrix interface more important under fully-reversed fatigue.

Fatigue life curves were plotted based on maximum stress or strain as well as stress or strain range. Based on maximum stress or strain, the tension-tension fatigue life was greater than that obtained for tension-compression fatigue. The decrease in fatigue life under tension-compression cycling is caused by the relaxation of matrix stresses under tension-tension fatigue due to matrix creep and additional damage sites created by the compressive portion of the loading cycle. These damage sites may consist of intrusions or extrusions which form at a much faster rate under fully-reversed fatigue. Fully-reversed fatigue life based on stress or strain range, however, was longer than tension-tension life. Shorter tension-tension fatigue life is attributed to mean stress effects over the life of the specimen.

The fatigue limit may be governed by the applied strain range. Fatigue life based on strain range for both tension-tension and tension-compression agreed with each other

around 0.4%. Fatigue life curves remain separate based on all other parameters discussed in this study.

Stress range in the 0° fibers does not govern fatigue life but analysis shows that, for a given loading condition, all laminate fatigue lives fall together based on 0° fiber stress range with the exception of elevated temperature unidirectional laminates. Although both tension-tension and tension-compression fatigue tests discussed in this study were conducted under load-controlled conditions, different R-ratios caused 0° fiber stress range fatigue curves to be different. A general increase in fatigue life was noted for the fully-reversed fatigue tests compared to the tension-tension tests based on 0° fiber stress range. Whereas 0° fiber stress range yielded two fatigue life curves, maximum 0° fiber stress yielded a single curve. Although some scatter was observed, all the data points fall within a standard band. Further analysis showed that based on 0° ply stress, fatigue life curves also fall together for a given loading condition, resulting in less scatter than that observed based on maximum 0° fiber stress. This suggests that fatigue life may be governed by stress in the 0° ply.

This study has investigated the fully-reversed fatigue life of a unidirectional MMC at elevated temperature. More compression fatigue data, at the current and other R-ratios, is required to better understand the macroscopic and microscopic behavior of this material under these loading conditions. There is also a significant gap in room temperature fully-reversed fatigue data. Such data is needed to fill in the fatigue curve based on 0° fiber stress. Similar trends between both tension-tension and tension-compression fatigue data suggest that room temperature fully-reversed fatigue data would fall onto the curve created by other laminates leaving the elevated temperature [0]₈ data as

the only exception to the rule. In addition to the areas described above, an investigation of the fatigue limit is important for design purposes. Although the current study contends that the fatigue limit is governed by strain range, more study is required in this area.

Appendix A: LISOL Analysis

There are several micro-mechanically-based tools available for predicting fiber and matrix stress (METCAN, VISCOPLY) under a variety of loading conditions. One such tool, LISOL, was utilized to determine the validity of the 0° fiber stress calculations made in section 5.4. Additionally, matrix stresses were obtained to determine if matrix plasticity should have been observed. A brief discussion of the LISOL program is contained in Chapter 2.

0° Fiber Stress Results

The LISOL model calculates several important parameters including thermal stresses and fiber and matrix stresses. Several cases were completed to analyze the stress in the 0° fibers, both for a unidirectional and a $[0/90]_{2s}$ composite. Table A-1 lists all fiber and thermal fiber stresses calculated for a loading frequency of 10 Hz. When the laminate is cycled above the proportional limit, debonding occurs. For the $[0/90]_{2s}$ case, the tensile yield limit was exceeded but the compressive stress-strain response remained linear. Therefore, additional stress was carried by the fibers in tension while the transfer of stress between the fibers and matrix in compression remained unchanged.

The correlation between the model and the results from the simple procedure presented in section 5.4 is quite good. As shown in Figure A-1, the 0° fiber stress calculations made earlier in this study for both the $[0]_8$ and the $[0/90]_{2s}$ laminates agree with those generated by the model.

Table A-1. LISOL Fiber Stress Calculations

Layup	Laminate Stress	Thermal Stress	Max Fiber Stress	Min Fiber Stress	Max Mech. Stress	Min Mech. Stress	Stress Range
[0] ₈	800	-335.1	1309	-1979	1644	-1643	3288
[0] ₈	700	-335.1	1103	-1773	1438	-1438	2877
[0] ₈	625	-335.1	949	-1619	1284	-1284	2569
[0] ₈	425	-335.1	538	-1208	873	-873	1746
[0/90] _{2s}	575	-508.5	1411	-1951	1920	-1442	3363
[0/90] _{2s}	400	-508.5	792	-1484	1300	-975	2276
[0/90] _{2s}	300	-508.5	447	-1240	955	-731	1687

- All stresses in MPa

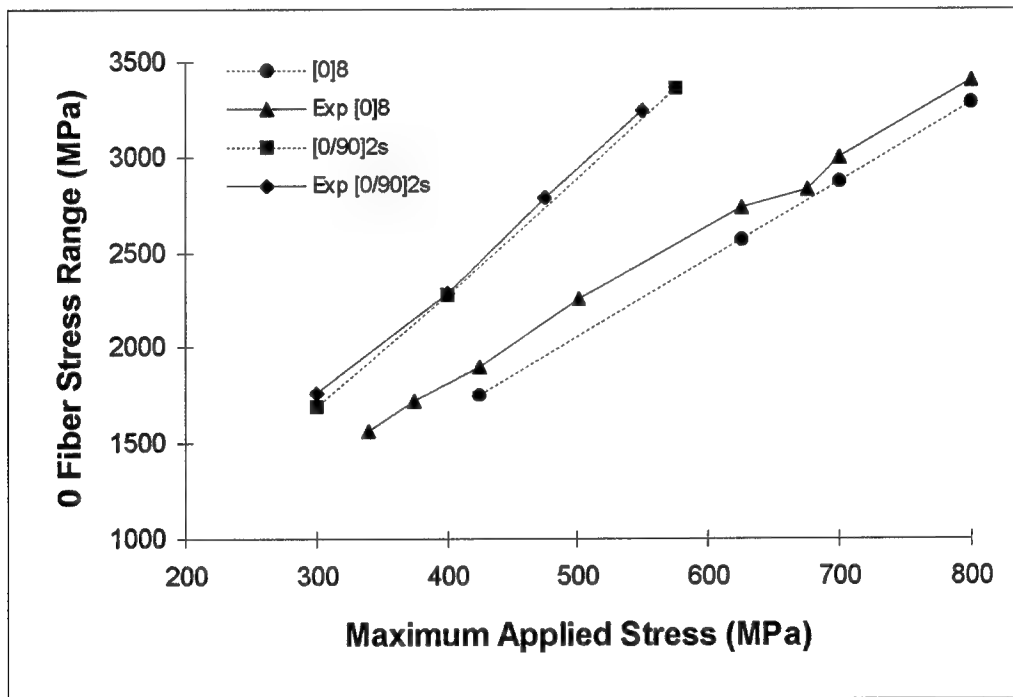


Figure A-1. 0° Fiber Stress Correlation Between LISOL and Approximate Values

Matrix Stress Results

LISOL was also used to calculate matrix stresses at three points around the fiber as shown in Figure 6. These stresses were used to determine if plastic behavior occurred

in the matrix. Earlier it was noted that no plasticity was observed at 800 MPa, the maximum applied load for this study. For comparison purposes, only the element exhibiting the maximum stress (M2) was analyzed.

The results of the model are listed in Table A-2. The maximum matrix stress generated by the model is approximately 604 MPa. At this stress level, minimal plasticity occurs in the titanium matrix at 427 °C. Therefore, the lack of evidence of plasticity is supported by the micro-mechanical model.

Table A-2. LISOL Matrix Stresses

Composite Stress	Thermal Stress	Max Matrix Stress	Min Matrix Stress	Max Mech. Stress	Min Mech. Stress	Stress Range
800	247	604	-110	357	-357	714
700	247	559	-65	312	-312	624
625	247	525	-31	278	-278	557
425	247	436	57	189	-189	379

- All stresses are in MPa

7. Bibliography

1. Agarwal, Bhagwan D. and Lawrence J Broutman. *Analysis and Performance of Fibrous Composites*. New York: John Wiley & Sons, Inc., 1990.
2. Baker, Capt. Robert P. *Investigation of Fatigue Behavior in Notched Cross-Ply Titanium Metal Matrix Composite at Elevated Temperature*. MS Thesis, AFIT/GAE/ENY/92D-03. School of Engineering. Air Force Institute of Technology. Air University. Wright-Patterson AFB OH, December 1992.
3. Bannantine, Julie A. and others. *Fundamentals of Metal Fatigue Analysis*. New Jersey: Prentice Hall, 1990.
4. Boyum, Elizabeth E., *Investigation of Tension-Compression Fatigue of a Cross-Ply [0/90]_{2s} Metal Matrix Composite at Room and Elevated Temperature,* MS Thesis, AFIT/GAE/ENY/93D-06. School of Engineering. Air Force Institute of Technology. Wright-Patterson AFB OH, 1993.
5. Broek, David. *Elementary Engineering Fracture Mechanics*. 4th ed. Boston: Kluwer Academic Publishers, 1991.
6. Castelli, Michael G., J. Rodney Ellis and Paul A. Bartolotta. "Thermomechanical Testing Techniques for High Temperature Composites: TMF Behavior of SiC(SCS-6)/Ti-15-3." NASA Technical Memorandum 103171. NASA Lewis Research Center. Cleveland OH, 1993.
7. Forsyth, P.J.E., *The Physical Basis of Metal Fatigue*. New York: American Elsevier Publishing Company, Inc., 1969.
8. Fuchs, Henry O., and R.I. Stephens, *Metal Fatigue in Engineering*. New York: John Wiley & Sons, Inc., 1980.
9. Gabb, T.P., J. Gayda, B.A. Lerch, and G.R. Halford. "The Effect of Matrix Mechanical Properties on [0]8 Unidirectional SiC/Ti Composite Fatigue Resistance." NASA Lewis Research Center. Cleveland OH, 1991.
10. Gao, Zhanjun, Hulixia Zhao, and Brian P. Sanders. "Damage and Fatigue Failure of Titanium Matrix Composite Laminates." Submitted for Publication. ASME Winter Annual Meeting, 1994.
11. Gayda, John Jr., Timothy P. Gabb, and Alan D. Freed. "The Isothermal Fatigue Behavior of a Unidirectional SiC/Ti Composite and the Ti Alloy Matrix." NASA Technical Memorandum 101984. NASA Lewis Research Center. Cleveland OH, 1989.

12. Hertzberg, Richard W., *Deformation and Fracture Mechanics of Engineering Materials*. 3rd Ed., John Wiley & Sons, Inc.: New York, 1989.
13. Harmon, D.M., and C.R. Saff, "Damage Initiation and Growth in Fiber Reinforced Metal Matrix Composites," *Metal Matrix Composites: Testing, Analysis, and Failure Modes, ASTM STP 1032*, W.S. Johnson, Ed., American Society for Testing and Materials, Philadelphia, 1989, pp 237-250.
14. Johnson, W.S., "Fatigue Testing and Damage Development in Continuous Fiber Reinforced Metal Matrix Composites," *Metal Matrix Composites: Testing, Analysis, and Failure Modes, ASTM STP 1032*, W.S. Johnson, Ed., American Society for Testing and Materials, Philadelphia, 1989, pp. 194-221.
15. Johnson, W.S., M. Mirdamadi, and J.G. Bakuckas, Jr. "Fatigue of Continuous Fiber Reinforced Metallic Materials." NASA Langely Research Center, 1993.
16. Kennedy, J.M., "Tension and Compression Testing of Metal Matrix Composites," *Metal Matrix Composites: Testing, Analysis, and Failure Modes, ASTM STP 1032*, W.S. Johnson, Ed., American Society for Testing and Materials, Philadelphia, 1989, pp. 7-18.
17. Konitzer, D.G., and M.H. Loretto, "Interfacial Interactions in Titanium-based Metal Matrix Composites," *Interfacial Phenomena in Composites: Processing, Characterization and Mechanical Properties*. Suresh, S. and A. Needleman Eds., Elsevier Applied Science: New York, 1989.
18. Lerch, Bradley A. "Fatigue Behavior of SiC/Ti-15-3 Laminates." NASA Lewis Research Center, Cleveland OH.
19. Lerch, Bradley A., Michael J. Verrilli, and Gary R. Halford. "Fully-Reversed Fatigue of a Ti-MMC." Conference Proceedings. ASC 8th Technical Conference on Composite Materials, October 1993, Cleveland OH.
20. Lerch, Bradley A. "Matrix Plasticity in SiC/Ti-15-3 Composite." NASA TM 102760, July 1991.
21. Majumdar, B.S., and Bradley A. Lerch. "Fatigue Mechanisms in a Ti-Based Fiber-Reinforced MMC and Approaches to Life Prediction." Submitted to Titanium Composites Workshop, La Jolla, California, June 1993.
22. Majumdar, B.S., and G.M. Newaz. "Fatigue of a SCS-6/Ti-15-3 Metal Matrix Composite," Battelle Memorial Institute, Columbus, OH, 1993.

23. Majumdar, B.S., and G.M. Newaz. "Inelastic Deformation of Metal Matrix Composites: Compression and Fatigue." Submitted for publication. Batelle Memorial Institute, Columbus OH, 43201.
24. Majumdar, B.S., and G.M. Newaz. "Isothermal Fatigue Mechanisms in Ti-Based Metal Matrix Composites." NASA Contractor Report 191181, 1993.
25. Mirdamadi, M., Johnson, W.S., Bahei-El-Din, Y.A., and Castelli, M.G., "Analysis of Thermomechanical Fatigue of Unidirectional Titanium Metal Matrix Composites." *Composite Materials: Fatigue and Fracture*. 4th Vol., Stinchcomb, Wayne W. and Noel E. Ashbaugh eds., ASTM Publication, STP 1156, 1993.
26. Naik, R.A., and W.S. Johnson. "Observations of Fatigue Crack Initiation and Damage Growth in Notched Titanium Matrix Composites." NASA Langley Research Center. Hampton, Virginia.
27. Nicholas, T., and J. Ahmad. "Modeling Fiber Breakage in a Metal-Matrix Composite." submitted for publication, *Composites Science and Technology*, 1994.
28. Park, H.S., G.S. Zong, L.D. Brown, L. Radenberg, and H.L. Marcus. "Fiber-Matrix Interface Failures." *Metal Matrix Composites: Testing, Analysis, and Failure Modes*, ASTM STP 1032, W.S. Johnson, Ed., American Society for Testing and Materials, Philadelphia, 1989, pp. 270-279.
29. Pollock, W.D. and W. Steven Johnson. "Characterization of Unnotched SCS-6/Ti-15-3 Metal Matrix Composite at 650 °C." NASA Technical Memorandum 102699, Langley Research Center, 1990.
30. Portner, Capt. Barry D. "Investigation of Fatigue Damage Mechanisms in a Metal Matrix Composite Under Elevated Temperature." MS Thesis. School of Engineering. Air Force Institute of Technology, Air University. Wright-Patterson AFB OH, AFIT/ENY/GAE-90D-20.
31. Rich, Daniel L., R.E. Pinckert, and T.F. Christian, Jr. "Fatigue and Fracture Mechanics Analysis of Compression Loaded Aircraft Structure," *Case Histories Involving Fatigue & Fracture Mechanics*. Hudson, C. Michael and Rich, Thomas P. Eds., ASTM Special Technical Publication 918, 1986.
32. Robertson, David D., and S. Mall. "A Non-Linear Micromechanics-Based Analysis of Metal-Matrix Composite Laminates," *Composite Science and Technology*, Elsevier Science Limited, 1994.
33. Sanders, Capt. B.P. "Characterization of Fatigue Damage in a Metal Matrix Composite (SCS-6/Ti-15-3) at Elevated Temperature." Ph.D. Dissertation. School

of Engineering. Air Force Institute of Technology, Air University. Wright-Patterson AFB OH, AFIT/DS/AA/93-4.

34. Sanders, B.P., and S. Mall. "Longitudinal Fatigue Response of a Metal Matrix Composite Under Strain Controlled More at Elevated Temperature," Department of Aeronautics and Astronautics, Air Force Institute of Technology, Wright-Patterson Air Force Base, OH, 1993.
35. Schubbe, Capt Joel J. *Investigation of Damage Mechanisms in a Cross-Ply Metal Matrix Composite with Circular Holes*. MS Thesis, AFIT/GAE/ENY/91D-24. School of Engineering. Air Force Institute of Technology. Air University, Wright-Patterson AFB OH, December 1991 (AD-A243894).
36. Skelton, R.P. *Fatigue at High Temperature*. New York: Applied Science Publishers, 1983.
37. Stinchcomb, W.W., K.L. ReifS-Nider, L.A. Marcus, and R.S. Williams. "Effects of Frequency on the Mechanical Response of Two Composite Materials to Fatigue Loads," *Fatigue of Composite Materials*. ASTM Special Technical Publication 569, 1973.
38. Talreja, Ramesh. *Fatigue of Composite Materials*. Lancaster: Technomic Publishing Company, 1987.
39. Taya, Minoru, and Richard J. Arsenault. *Metal Matrix Composites: Thermomechanical Behavior*. Oxford: Pergamon Press, 1989.
40. Worthem, P.W. "Flat Tensile Specimen Design for Advanced Composites." Nasa Contractor Report No. 185261, 1990.

Vita

Second Lieutenant Darren L. Kraabel was born 06 October 1970 in Brainerd, Minnesota. He graduated from Menahga High School in Menahga, MN in 1989. That summer he entered the United States Air Force Academy where he majored in Engineering Mechanics, specializing in structures. Upon his graduation from USAFA in June, 1993, he entered the Air Force Institute of Technology School of Engineering in July 1993.

Permanent Address: P.O. Box 953
Watertown, MN 55388